C.P. No. 1243

C.P. No. 1243

PROCUREMENT EXECUTIVE, MINISTRY OF DEFENCE

AERONAUTICAL RESEARCH COUNCIL

CURRENT PAPERS

Measurement of the Internal Performance of a Rectangular Air Intake with Variable Geometry at Mach Numbers from 1.7 to 2.5

Part I

by

C. S. Brown and E. L Goldsmith

Aerodynamics Dept., R.A.E., Bedford

LONDON: HER MAJESTY'S STATIONERY OFFICE

1973

PRICE *£1·10* NET

UDC 533.697.2 : 533.6.015 : 533.6.011.5

CP No.1243 *
August 1971

MEASUREMENT OF THE INTERNAL PERFORMANCE OF A RECTANGULAR AIR INTAKE WITH VARIABLE GEOMETRY AT MACH NUMBERS FROM 1.7 TO 2.5

Part I

by

C. S. Brown
E. L. Goldsmith

SUMMARY

Measurements have been made of the internal performance of a rectangular intake having variable geometry compression surfaces. The measurements have been made over a range of Mach numbers from 1.70 to 2.46. The Reynolds number based on intake height was between 1.27 and 1.54 $\times 10^6$. Pressure recoveries at zero bleed are well below those predicted from simple shock patterns, but there is a substantial gain with increase of bleed flow particularly at Mach numbers above 2. Subcritical stable flow range correlated quite well with the Ferri instability criterion.

* Replaces RAE Technical Report 71159 - ARC 33681

CONTENTS

1 INTRODUCTION

Many strike fighter aircraft designs feature twin engines mounted in the fuselage and fed by air from intakes on the fuselage side. Several different designs of intakes have been used in this position, e.g., on the Phantom, Jaguar, F104, Mirage and Viggen aircraft; and before making relative assessments of the various types of intake, data on the aerodynamic performance of each is required. The model described in this report was originally part of an investigation aimed at the assessment of the relative merits of a rectangular and a half axisymmetric intake related to the same project. However the model has now become absorbed into a larger and much broader programme of wind tunnel tests carried out at RAE Bedford, the aim of which is the investigation, for several different intake designs both rectangular and half axisymmetric, of

(a) the basic internal performance in a uniform flow field of an intake over a wide range of conditions, e.g., compression surface position, bleed geometry, cowl shape and endwall shape[1],

(b) the effect on the internal performance of mounting an air intake, whose characteristics in uniform flow are known, on a fuselage and operating over a wide range of Mach number and attitude[2],

(c) the external spillage, cowl, bleed and diverter drag and interference effects when mounted on a fuselage[3].

This Report fulfills the aims of (a) above for a rectangular intake with a particular shape of duct,having one fixed compression surface followed by one variable angle compression surface and with a particular geometry of endwalls, cowl and boundary layer bleed. Subsequent reports will deal with changes in endwall shape, cowl and compression surface geometries.

2 DESCRIPTION OF THE TEST RIG

Fig.1 shows the intake and duct assembled on the General Intake Test Rig (GERTI) used in the 3ft × 4ft supersonic wind tunnel at RAE Bedford. This rig has been described in detail in Ref.4. It consists of a sting support, a calibrated mass flow control and measuring unit, a system of hydraulics for actuating the compression surface ramps and an instrumented duct with interchangeable exit plugs for controlling and measuring intake bleed flow.

Because the minimum Mach number in the 3ft × 4ft tunnel is 2.5, the test rig incorporates a shock plate ahead of the intake. The local Mach number in front of the intake is thus controlled by pitching the whole assembly relative to the tunnel freestream. Photographs of the installed rig, including the shock plate, and of the intake are reproduced in Figs.2a and 2b.

3 DETAILS OF THE MODEL

The model has two wedge compression surfaces, the first fixed and the second variable in angle. The design of model incorporates a considerable degree of flexibility and interchangeability with regard to cowl shape, endwall shape, location of front hinge and size and position of bleed. However this Report is concerned only with a particular configuration of the model for which the geometry of the intake is as shown in Fig.3. The nomenclature used throughout this Report is shown in Fig.4.

The first wedge angle δ_1 is 10° and the shock from its leading edge theoretically falls on the cowl lip at a freestream Mach number M_∞ of 2.43. The second compression surface is movable and is linked to the rear ramp so that a single hydraulic actuator moves both these surfaces interdependently. The maximum value of δ_2, the angle between the first and second ramps, is 14°, imposed by a limitation in movement of the hydraulic actuator. The gap between the second and rear ramps forms a slot for bleeding the boundary layer from the compression surfaces and this extends over the whole width of the intake. The geometry of the bleed exit and details of the interchangeable exit plugs which are used to vary the bleed flow, are shown in Fig.5.

The leading edge of the endwalls joins the front edge of the first compression surface to the cowl lip and is chamfered at an angle of 10° in the direction normal to the entry plane of the intake. Externally the intake is not representative of an actual installation. It was designed to be tested at stagnation pressures up to 4 atmospheres and the endwall thickness and leading edge chamfer were largely dictated by considerations of strength and ease of manufacture.

The shape of the subsonic diffuser is such as might be encountered in an aircraft with wings of variable sweep angle, with the intake leading edge vertical and the duct from the intake to the compressor face having to avoid a wing pivot. The area distribution through the intake and duct for various values of δ_2 is shown in Fig.6. Two factors dominate the choice of area distribution; the length of the rear ramp as dictated by the position of the rear hinge, and the initial rate of diffusion. In this case the short rear ramp was dictated by the same reason which determined the shape of the subsonic duct. The initial rate of diffusion was kept very conservative within the design range of δ_2 because of the unfavourable shape of the duct. However this has produced an area distribution with some undesirable features, such as excessive internal contraction when the intake is operated at low values of second ramp angle.

The ratio of engine face cross-sectional area to maximum capture area is 0.881 and the distance from the cowl lip to the engine face is 9.89 times the intake height. The height to width ratio at the intake entry plane is 1.54.

3.1 Instrumentation

The standard mass flow control and measuring unit[4] is fitted with a cruciform rake having a total of 24 pitot tubes for measuring total pressure at the engine face station. The tubes are disposed for area-weighted averaging and the rake is rotatable to enable pressure surveys to be made in greater detail. Static pressure at the engine face is measured using four holes equispaced round the circumference. Additionally the static pressure is measured in the venturi section of the mass flow measuring unit, downstream of the engine face rake.

The bleed duct contains 12 pitot tubes for measuring total pressure and three equispaced static holes. Three rakes each containing six pitot tubes are used to measure the pressure distribution in the intake at the entrance to the fixed portion of the subsonic diffuser. These rakes are located in the cowl at the rear ramp hinge position and can be seen clearly in Fig.2b.

All pressures were measured by means of self-balancing capsule type manometers[5].

4 CALIBRATION OF THE SHOCK PLATE

In order to determine the local flow conditions ahead of the intake the shock plate was calibrated against θ, the angle of the shock plate relative to the wind tunnel centre line. Using a rake of pitot tubes in conjunction with a rake of static probes as indicated in Fig.7, pressure measurements were made in the plane of the intake leading edge. Local Mach numbers were calculated using individual pitot pressures and an average static pressure and local total pressures were obtained from these local

Mach numbers and their corresponding pitot pressures. The average of these local values, M_∞ and $\left(\frac{P_\infty}{P_0}\right)$, covering the area occupied by the intake in its test position, was used as the effective Mach number and non-dimensional total pressure ahead of the intake. The variation of M_∞ and $\frac{P_\infty}{P_0}$, with shock plate incidence is shown in Figs.8a and 8b.

5 TEST CONDITIONS

The tests were done in the 3ft × 4ft supersonic wind tunnel at RAE, Bedford between 1967 and 1969. The tunnel stagnation pressure was 2 atmospheres and the total temperature was $40^\circ C$. The humidity of the air was at all times less than 150 parts per million. The Reynolds number based on intake height was between 1.27 and 1.54×10^6.

6 TEST TECHNIQUE AND REDUCTION OF RESULTS

The only model variable not controllable while the tunnel was in operation was bleed exit area. Consequently performance characteristics were obtained for a range of values of second ramp angle δ_2 for each Mach number, with a particular bleed exit plug. This series was then repeated, using in all five different bleed exit plugs.

Main duct or engine flow was controlled by the translating plug in the mass flow measuring unit. During the tests the bleed total pressure and the static pressure in the venturi section of the mass flow measuring unit were monitored and used, in conjunction with the shock plate and translating plug calibrations, to compute the engine face and bleed mass flows and pressure recoveries. Performance characteristics could thus be drawn on-line.

The technique was to withdraw the main duct exit plug until a constant bleed pressure was obtained. Starting at this point the plug was closed in a series of nine or ten steps until the point was reached at which the intake was seen on the Schlieren optical system to be obviously in 'big buzz'. Bleed and engine face pressure recoveries and mass flows were plotted at each position of the main duct plug and where necessary points were added in order to define precisely the shape of the intake characteristic especially in the region of the critical point, i.e., the point at which the total mass flow just departs from its maximum value. At the majority of positions of the main duct plug, pressure measurements were made at the engine face with the cruciform rake in one fixed position. In general, however, for at least two positions of the

the exit plug in every characteristic, usually near the critical point, the rake was rotated through 30° intervals to cover the complete engine face annulus. This 72 point measurement, termed a comprehensive engine face survey enables any distribution parameter such as DC_{60}, $\frac{V_{max} - V_{min}}{V_{mean}}$, $\frac{V_{max}}{V_{mean}}$ etc., to be calculated.

Area mean pressure recovery is defined as:-

$$\frac{P_f}{P_\infty} = \frac{1}{n\, P_\infty} \sum_1^n P_j$$

where P_∞ is the freestream total pressure

P_j is the pitot pressure at the jth tube in the rake

and n is the number of pressure points in the survey.

Mass flow ratio, $\frac{A_\infty}{A_{en}}$, in both main and bleed ducts was calculated assuming the exit flows to be choked:-

$$\frac{A_\infty}{A_{en}} = \frac{P}{P_\infty} \frac{A_{ex}}{A_{en}} \left(\frac{A}{A^*}\right)_\infty$$

where A_{en} is the intake entry area, and

A_{ex} is the effective choked exit area as determined by calibration in the case of the main duct. In the case of the bleed duct the exit was not calibrated and A_{ex} was taken to be the geometric area.

$\frac{P}{P_\infty}$ is either the engine duct pressure recovery $\frac{P_f}{P_\infty}$ or the bleed duct pressure recovery $\frac{P_B}{P_\infty}$.

7 ACCURACIES

Errors in the direct measurement of engine face and bleed duct total pressure are thought to be very small, certainly better than 0.1 per cent. The major causes of uncertainty in the calculation of pressure recovery and mass flow are the use of M_∞ and P_∞, obtained from the shock plate calibration and the use of A_{ex}, obtained from the calibration of the mass flow measuring unit. A_{ex} also depends critically on the accuracy to which the translating plug can be re-aligned from test to test. Overall, it is thought that quantitatively the values of pressure recovery $\frac{P_f}{P_\infty}$ are subject to errors of about ± 0.0025 throughout the Mach number range, while the values of mass flow $\frac{A_\infty}{A_{en}}$ are subject to errors of ± 0.0025 at $M_\infty = 1.7$ increasing to ± 0.006 at M_∞ = 2.5. However because the Mach number is determined by the pitch setting of the shock plate which is repeatable to better than 0.01 degree, the consistency of the results for any given Mach number should be better than these values.

The accuracy of setting of the second ramp angle δ_2 is about 0.1 degree.

8 DISCUSSION OF RESULTS

Some of the basic characteristics of the intake are shown in Figs.9 to 23 where main and bleed duct pressure recovery, and bleed mass flow are plotted against total intake flow i.e., main duct plus bleed duct flows. These characteristics are for bleed exit plugs 0, 4 and 8 whose exit areas result in relative bleed mass flows $\left(\frac{A_\infty}{A_{en}}\right)_B$ at critical flow conditions of zero, 0.03 to 0.04 and 0.06 to 0.08 respectively. The critical flow condition is defined as the point on the pressure recovery-mass flow characteristic where the total mass flow just departs from the maximum value.

From these characteristics and those for bleed exit plugs 1 and 2, (which have not been reproduced) variations of maximum total intake flow, maximum main duct flow and pressure recovery at critical flow conditions have been derived. In Figs.24 to 29 these quantities are shown as functions of bleed mass flow and of second ramp angle δ_2. Sketches of the theoretical shock patterns in front of the intake, drawn for the geometric value of δ_1, and a number of values of δ_2, are also shown in these Figures.

These theoretical shock patterns and hence the corresponding values of shock recovery and maximum mass flow, will be affected by a number of the geometric properties of the intake. The area distribution of the duct downstream of the cowl lip and the initial inclination of both internal and external surfaces of the cowl all affect the shock pattern by determining whether or not the cowl lip shock is attached at full flow. The general behaviour of the intake will also be affected by the position of the hinge point on the compression surface, which for a given δ_2 and M_∞, determines whether the second oblique shock falls inside or outside the cowl lip. In this case however the influence on the pressure recovery and mass flow is generally predictable from the shock patterns. The regions of influence of these various factors are summarised for this particular intake in Fig.36. For a given value of M_∞ and the particular value of δ_1 for this intake, δ_2 defines the Mach number approaching the cowl lip

(M_2 in Fig.3). From this Mach number the one dimensional area ratio required to start the duct flow can be calculated i.e., the area ratio $\frac{A_t}{A_i}$ required to accelerate the subsonic flow behind a normal shock occurring at $M = M_2$, to sonic velocity. This area ratio is shown plotted against δ_2 for the values of M_∞ at which the intake has been tested.

Superimposed on these curves are the curves A, B_1, B_2 and B_3. Curve A shows the geometric contraction ratio $\frac{A_t}{A_i}$ for the internal duct for this particular intake. It indicates that with zero bleed the internal duct is quite severely over-contracted at all values of δ_2 for Mach numbers 1.7, 1.8 and 1.9 and that there is only a small range of δ_2 (2° to 5°) where this is not also the case at $M_\infty = 2.01$. Under this condition the maximum flow is determined by choking at the minimum area in the duct. This maximum flow will be smaller than that determined by the position of the external oblique shocks from the compression surface and will cause the cowl lip shock to detach in order that the excess flow may be spilled. The location of the minimum area varies, depending upon the value of δ_2, but in general it is downstream of the bleed, and the effect of increasing bleed flow will be to reduce progressively the excessive contraction. Curves B_1, B_2 and B_3 show what is effectively the internal contraction of the main duct when 2, 4 and 6 per cent respectively of the total capture flow is removed through the bleed slot. At 6 per cent bleed flow for example the intake should not be over-contracted anywhere throughout the entire Mach number range except for values of δ_2 between 0° and 2° at $M_\infty = 1.7$ and in the vicinity of $\delta_2 = 0^\circ$ at $M_\infty = 1.8$.

It is convenient to add to Fig.36 curves which delineate two other features which affect the intake shock patterns. These are the boundary which indicates whether, due to the inclination of either the cowl outer or inner surface, the cowl lip shock is theoretically attached or detached, and the boundary which indicates whether the second oblique shock is inside or outside the cowl lip.

From Fig.36 it can be seen that detailed discussion of the results will tend to fall into two groups of Mach numbers: (a) Mach numbers of 2.22 and 2.46 where the intake shock patterns should be independent of bleed for nearly all values of δ_2 and shocks everywhere should be attached and as predicted - and (b) Mach numbers of 2.01 and below where in general the shock patterns will be much affected by the amount of bleed flow and where for zero bleed the cowl lip shock will be detached at nearly all values of δ_2.

8.1 Maximum mass flow

At $M_\infty = 2.46$ the first wedge shock should be theoretically inside the cowl lip, so that for all values of δ_2 less than 11° when the second oblique shock should also be inside the cowl lip, the maximum mass flow ratio should be unity. However as Fig.25 illustrates, the measured value of maximum mass flow is 0.988; which agrees with the value derived theoretically for a first wedge angle of 11° rather than 10°. A test with a local Mach number in front of the intake of $M_\infty = 2.52$ gave a measured maximum mass flow ratio of 1.000 ($\pm$ 0.001) which is again consistent with an effective δ_1 of 11° as this would place the first wedge shock theoretically just on the cowl lip at this Mach number. At Mach numbers of 2.22 and 2.01, where some sideways spillage will occur between the first and second wedge shocks and the swept endwalls, the relation between calculated and measured maximum mass flow ratios suggests that δ_1 is effectively a little less than 11°. (Figs. 27 and 29). In Ref.6 this effective increase in wedge angle is postulated as being the effect of transition of the boundary layer to turbulent flow conditions a short distance downstream of the wedge tip.

At Mach numbers of 2.46 and 2.22, except in the presence of shock detachment due to excessive flow turning at the cowl undersurface, maximum total flow is unaffected by the amount of bleed flow and with increasing bleed flow the engine duct flow falls by the amount the bleed flow increases. (Figs. 24 and 26). At a Mach number of 2.01 the total mass flow is independent of bleed flow only for bleed flows above about 2 per cent; below this value both the maximum total flow and the engine duct flow increase. This is in reasonable agreement with Fig.36 which indicates that at zero bleed the internal contraction will be too large to allow starting of the duct at M_∞ of 2.01; but by removing some 2 per cent of flow through the bleed duct, full flow without shock detachment will be attainable at the inlet. The fact that engine duct flow also increases initially with bleed, especially at the lower values of δ_2, suggests a reduction in duct throat area at zero bleed due to viscous effects.

At Mach numbers below M_∞ of 2.01 the situation becomes more complicated. In this region the duct is overcontracted throughout the whole range of applicable values of δ_2. For a given bleed flow the value of δ_2 below which the mass flow is determined by the minimum area of the duct according to the predictions of Fig.36 is shown in Table 1 compared with the observed values.

Because of the spacing of the experimental points the values of δ_2 are accurate to only about half a degree, but in general the observed values are greater than the predicted values, which is consistent with viscous effects causing a reduction in duct throat area.

Table 1

M_∞	Bleed flow %	Second ramp angle below which flow is controlled by duct minimum area	
		δ_2 predicted	δ_2 observed
1.9	2	1.7	3.5
	4	0.3	1.3
1.8	4	2	3
	6	0.4	3
1.7	6	1.5	2

The choking flow based on the duct minimum area as given by Curve A of Fig.36 has been calculated for the Mach numbers 1.7, 1.8, 1.9 and 2.01, where the measured flow departs from that predicted by the external shock pattern. These are shown on Figs.37a and 37b, together with the mass flow measured at zero bleed and at 2 per cent of bleed flow. Comparison at M_∞ = 1.7, 1.8 and 1.9 indicates that for values of δ_2 netween 0^o and 2^o there is agreement between the calculated flow and the flow measured at 2 per cent of bleed while for δ_2 above about 5^o the agreement is between the calculated flow and that measured at zero bleed. In the case of M_∞ of 2.01 the agreement between calculated flow and that measured at zero bleed is at a slightly higher value of δ_2 and the overall impression is that viscous effects within the duct produce an apparent internal contraction at zero bleed as indicated by curve C of Fig.36. The pressure distributions at the rear hinge position shown in Figs.38 to 43 indicate the presence of a large low pressure region adjacent to the rear ramp at this position for all Mach numbers and at all values of δ_2. At values of δ_2 between 0^o and 5^o the intake throat is at the rear hinge, well downstream of the inlet plane and large viscous effects might be expected. The effect of this, together with the possibility of some separation on the rear ramp, on a contraction ratio which is already high probably accounts for the significant reduction in effective choking area.

At values of δ_2 of about 5^o the throat moves upstream to the leading edge of the rear ramp so that for this and higher values of δ_2, with a more favourable contraction ratio, the viscous effects no longer influence the choking area to the same extent.

8.2 Pressure recovery

Referring again to Figs.24, 26 and 28 it can be seen that at Mach numbers of 2.46, 2.22 and 2.01 critical point pressure recovery $\left(\frac{P_f}{P_\infty}\right)$ increases rapidly with bleed flow up to bleed flows of about 0.05. $d\left(\frac{P_f}{P_\infty}\right)\Big/d\left(\frac{A_\infty}{A_{en}}\right)_B$ is equal to approximately 1.8 independent of M_∞ and δ_2. Figs.38 to 40 show total pressure distributions at three stations across the duct at the rear hinge position for bleed plugs 0, 4 and 8. These show a consistent pattern of a large low pressure region adjacent to the rear hinge which although not fully eliminated is considerably diminished by increasing bleed flow.

Another feature of these profiles which is particularly noticeable at the rake station adjacent to the duct endwall is the high peak values of recovery in the middle of the flow. In general these values are equal to or are slightly below a calculated shock recovery based on two oblique shocks only. This indicates that this rake is in the region outside of the separated flow associated with the interaction of the normal shock with the endwall boundary layer but in the region of local distortion of the normal shock associated with this separation. In this region the shock compression is through a 'fan' of oblique shocks which effectively gives isentropic compression.

The increase in pressure recovery with increased bleed flow is less pronounced at the lower Mach numbers. (Figs.30, 32 and 34.) The slope of the curve reduces from 1.3 at M_∞ = 1.90 to about 0.8 at M_∞ = 1.7 and the slope decreases considerably below these values at bleed flows greater than about 0.03 to 0.04. Pressure recovery at critical flow conditions for bleed flows of zero, 0.02, 0.04 and 0.06, is shown plotted against δ_2 in Figs.25, 27, 29, 31, 33 and 35. Shock recoveries calculated for both $\delta_1 = 10^o$ and $\delta_1 = 11^o$ are included for comparison. Pressure recovery is much less sensitive than mass flow to this order of change in δ_1, but it is noticeable from the pressure distributions at the position of the rear hinge, that mean recovery measured in the middle of the flow agrees more closely with that calculated for δ_1 of 11^o.

At zero bleed flow losses other than shock losses can be calculated by the method of Ref.7. A comparison of calculated and measured pressure recoveries at the critical flow condition is shown in Figs.44a and 44b. Measured recoveries are always lower than the calculated values, but this is not too surprising as the method of Ref.7 was derived for intakes which have no turning of the flow in the region of the inlet plane. It is probable that some of the discrepancy is due to inadequacies in estimating the components that go to make up the losses other than shock losses when the method of Ref.7 is applied in this situation. It is known for instance from tests on axisymmetric intakes[8] that losses other than shock losses are affected by the flow deflection imposed at the cowl lip and the amount of internal contraction, neither of which factors are included in the method of Ref.7. Nevertheless the discrepancy between calculated and measured recoveries can be attributed loosely to an additional loss due to 'flow turning'.

At Mach numbers of 1.7, 1.8 and 1.9 the measured pressure recoveries, at all bleed flows, vary with δ_2 in the same manner as the calculated shock recoveries. At Mach numbers of 2.01 and 2.22 this regular pattern is not followed and the losses other than shock losses appear to increase sharply at the higher values of δ_2. At $M_\infty = 2.46$ this pattern of increasing extra-to-shock losses as δ_2 increases is present for all the δ_2 values tested (i.e. 7^o to 14^o) and is increased in magnitude relative to the lower Mach numbers. From the pressure distributions at the position of the rear ramp hinge this behaviour appears to be caused by the failure of the boundary layer control to remove the low total head air adjacent to the rear ramp surface even at high bleed flows. (Figs.38, 39 and 40). It should be noted that in these conditions of higher values of δ_2 and higher freestream Mach number all the geometric and flow conditions are becoming more adverse, i.e., normal shock pressure rise, change of angle between front and rear moving ramps, and initial rate of diffusion in the duct downstream of the position of minimum area, are all increasing. (Fig.45). A crude correlation of these factors with the losses ascribed to 'flow turning', for the zero bleed case, is shown in Fig.46.

8.3 Stable flow range and flow distortion at the engine face

Stable flow range is defined as the fraction by which the maximum mass flow can be reduced before the onset of buzz. Buzz in this case is simply 'big buzz' as seen using the schlieren optical system and is therefore not a precise measurement.

The variation of stable flow range with δ_2 for zero bleed and for a bleed flow of 0.04 is shown in Fig.47. Also indicated in this Figure are theoretical predictions of stable flow range derived from a method proposed in Ref.9. which uses the Ferri instability criterion[10]. Despite the inexactness of the measurements, the correlation is good, confirming that for this intake the instability arises from the vortex sheet which originates at the intersection of the terminal normal shock and the second oblique shock.

It is also interesting to note that agreement between predicted and measured onset of buzz is much better for $\delta_1 = 11^\circ$ than for $\delta_1 = 10^\circ$, which further reinforces the evidence of 8.1.

During each intake characteristic, one or two comprehensive pressure surveys were made at the engine face. The flow distortion parameter DC_{60} has been derived from these surveys and is shown in Fig.48, plotted against bleed flow. Whilst no very clear trend emerges it is apparent that despite the maldistribution at the rear hinge position, the distortion level at the engine face is reasonably low, DC_{60} being of the order of -0.20 throughout. This is no doubt due to the long duct which allows mixing to take place. There is little apparent difference between zero and low bleed flows, but there is some evidence that high bleed flows $\left[\left(\frac{A_\infty}{A_{en}}\right)_B > 0.04\right]$ have a detrimental effect. This is probably due to the adverse pressure gradient imposed on the flow on the wall opposite to the region where the bleed flow is being removed i.e., the cowl undersurface, which will thicken or maybe separate the boundary layer on this surface when the bleed flow is high.

9 CONCLUSIONS

Measurements have been made of the internal performance of a rectangular intake having variable geometry compression surfaces. The measurements have been made over a range of Mach numbers from 1.70 to 2.46. The Reynolds number based on intake entry height was between 1.27 and 1.54×10^6.

The results indicate that simple shock patterns can be used to predict maximum mass flow and pressure recovery. The effective initial compression angle may be larger than its geometric value due to transition to turbulent flow on the first compression surface and this will have an appreciable effect on the maximum values of mass flow.

In using the method of Ref.7 to estimate losses other than shock losses some refinement is needed to take account of flow turning, particularly between the front and rear movable ramps. There is a substantial gain in pressure recovery with increase of bleed flow at the higher Mach numbers but this falls off sharply at Mach numbers below 2.

At the higher Mach numbers a large low pressure region adjacent to the surface of the rear ramp is not greatly diminished even by large bleed flows. This may be the penalty for large turning angles between the front and rear movable ramps, which is a result of the short length of the rear ramp.

NOTATION

(See also Fig.4)

A	cross sectional area
DC_{60}	distortion parameter = $\dfrac{\left(P_f\right)\text{minimum} - \left(P_f\right)\text{mean}}{\left(\frac{1}{2}\rho V^2\right)_f}$ taken over the worst 60° sector
M	Mach number
P	total pressure
p	static pressure
SFR	stable flow range
T	stagnation temperature
V	velocity
w	width of intake
X	distance downstream of cowl lip
Z	lateral distance from duct sidewall
δ_1	angle between first compression surface and freestream ahead of intake
δ_2	angle between first and second compression surfaces
θ	angle of incidence of shock plate relative to wind tunnel centre line
ω	angle between front and rear movable ramps

Subscripts

c	at critical flow conditions
B	in the bleed
en	in the entry plane
ex	in the duct exit plane
f	at the engine face
i	at the cowl lip
O	in the wind tunnel freestream
t	at the section of duct minimum area
T	total (i.e. engine plus bleed)
X	at station X
∞	in the freestream ahead of the intake
1	in the region behind the first oblique shock
2	behind the second oblique shock
3	behind the terminal normal shock

REFERENCES

No.	Author	Title, etc.
1	E.L. Goldsmith C.S. Brown	Some measurements of the internal performance of two half axisymmetric air intakes with conical compression surfaces at Mach numbers between 1.8 and 2.5. RAE Technical Report 71058 (ARC 33115) (1971)
2	C.S. Brown E.L. Goldsmith	Measurement of the internal performance of a rectangular air intake with variable geometry. Part II. Effect of angle of attack. RAE Technical Report 71236 (ARC 33891) (1971)
3	M.D. Dobson E.L. Goldsmith	The external drag at subsonic and supersonic speeds of fuselage-side air intakes for strike-fighter aircraft. Unpublished MOD (PE) material
4	E.L. Goldsmith	Variable geometry intakes at supersonic speeds. Some techniques and some test results. Agard Conference Proceedings No.34 (1958)
5	G.F. Midwood R.W. Hayward	An automatic self-balancing capsule manometer. ARC CP No.231 (1955)
6	J.D. Bryce B.J. Cocking	Unpublished MOD (PE) material (1971)
7	J. Seddon	Boundary layer interaction effects in intakes with particular reference to those designed for dual subsonic and supersonic performance. ARC R & M 3565 (1966)
8	E.L. Goldsmith	The effect of internal contraction, initial rate of subsonic diffusion, and cowl and centrebody shape on the pressure recovery of a conical centrebody intake at supersonic speeds. ARC R & M 3204 (1956)

REFERENCES (Contd.)

No.	Author	Title, etc.
9	I. McGregor	Some theoretical parameters relevant to the performance at supersonic speeds of rectangular air intakes with double ramp compression surfaces. RAE Report (to be published).
10	A. Ferri L.M. Nucci	The origin of aerodynamic instability of supersonic inlets at subcritical conditions. NACA RM L50K30 (1957)

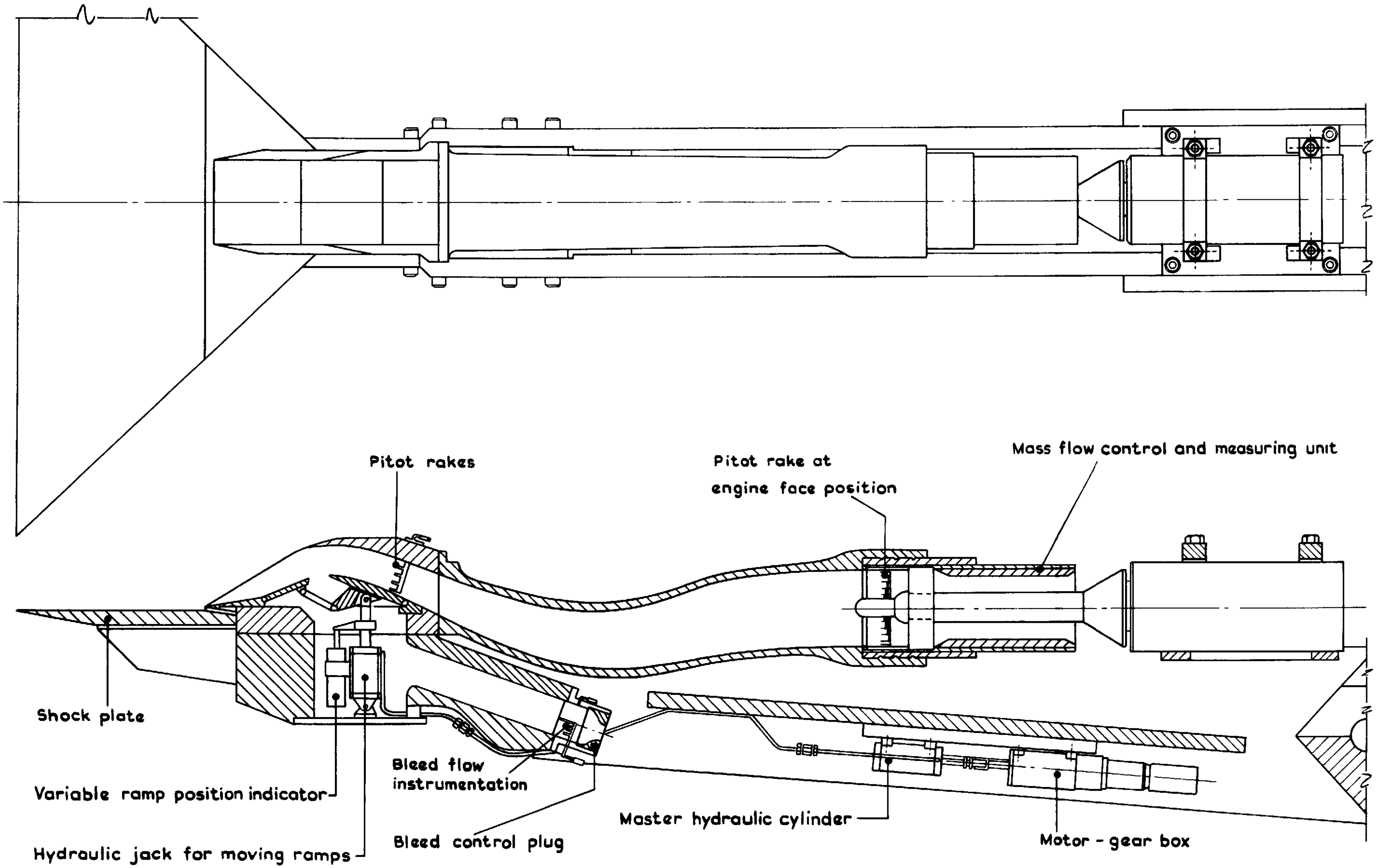

Fig.1 Arrangement of variable geometry rectangular intake on 4 ft x 3 ft tunnel support

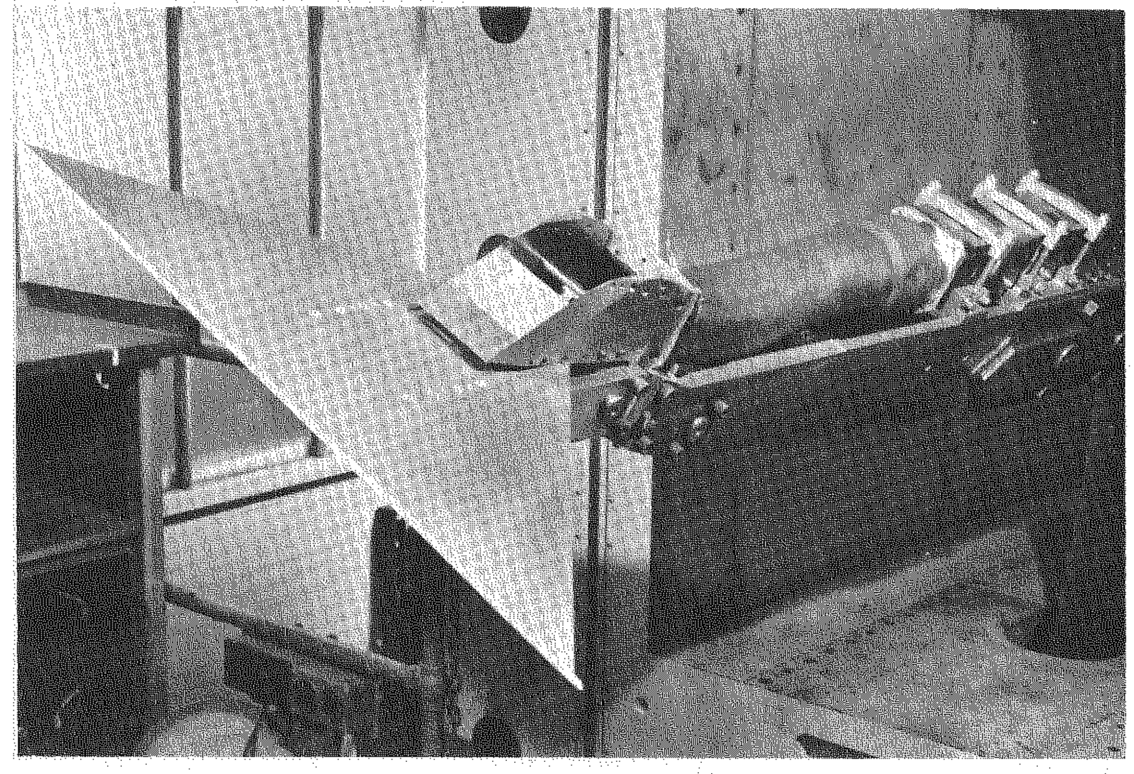

Fig.2(a). Intake (cowl removed) on test rig

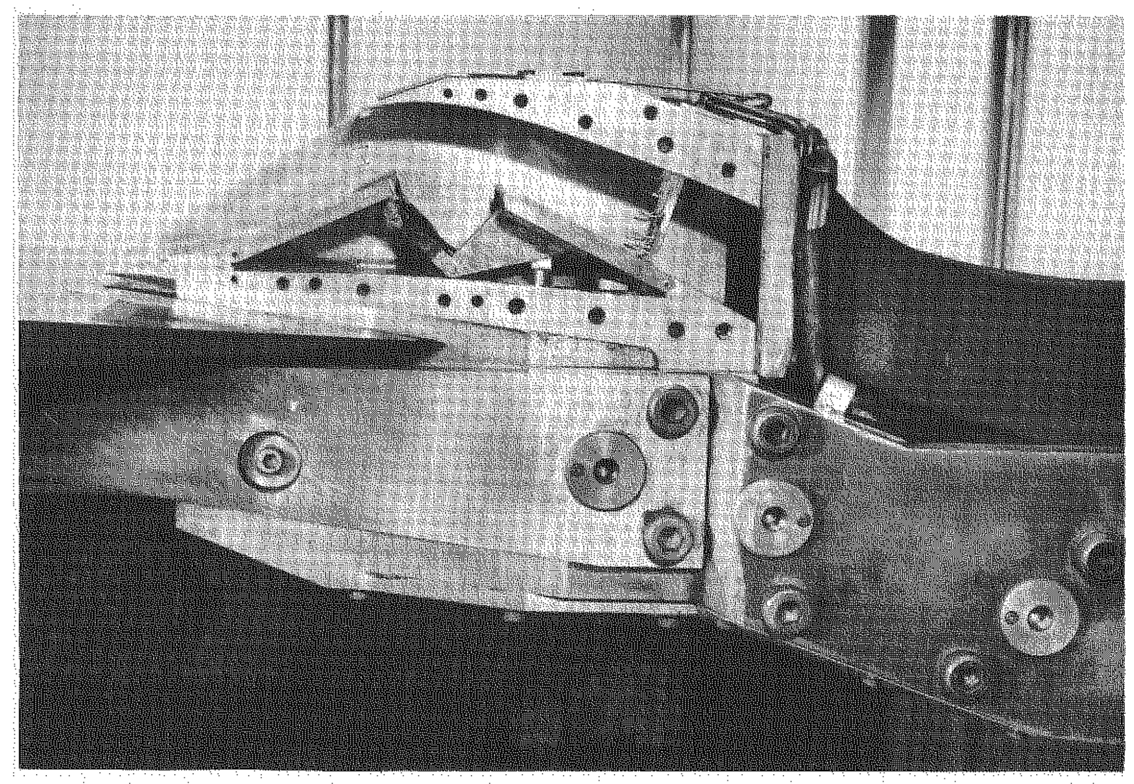

Fig.2(b). Intake with one endwall removed

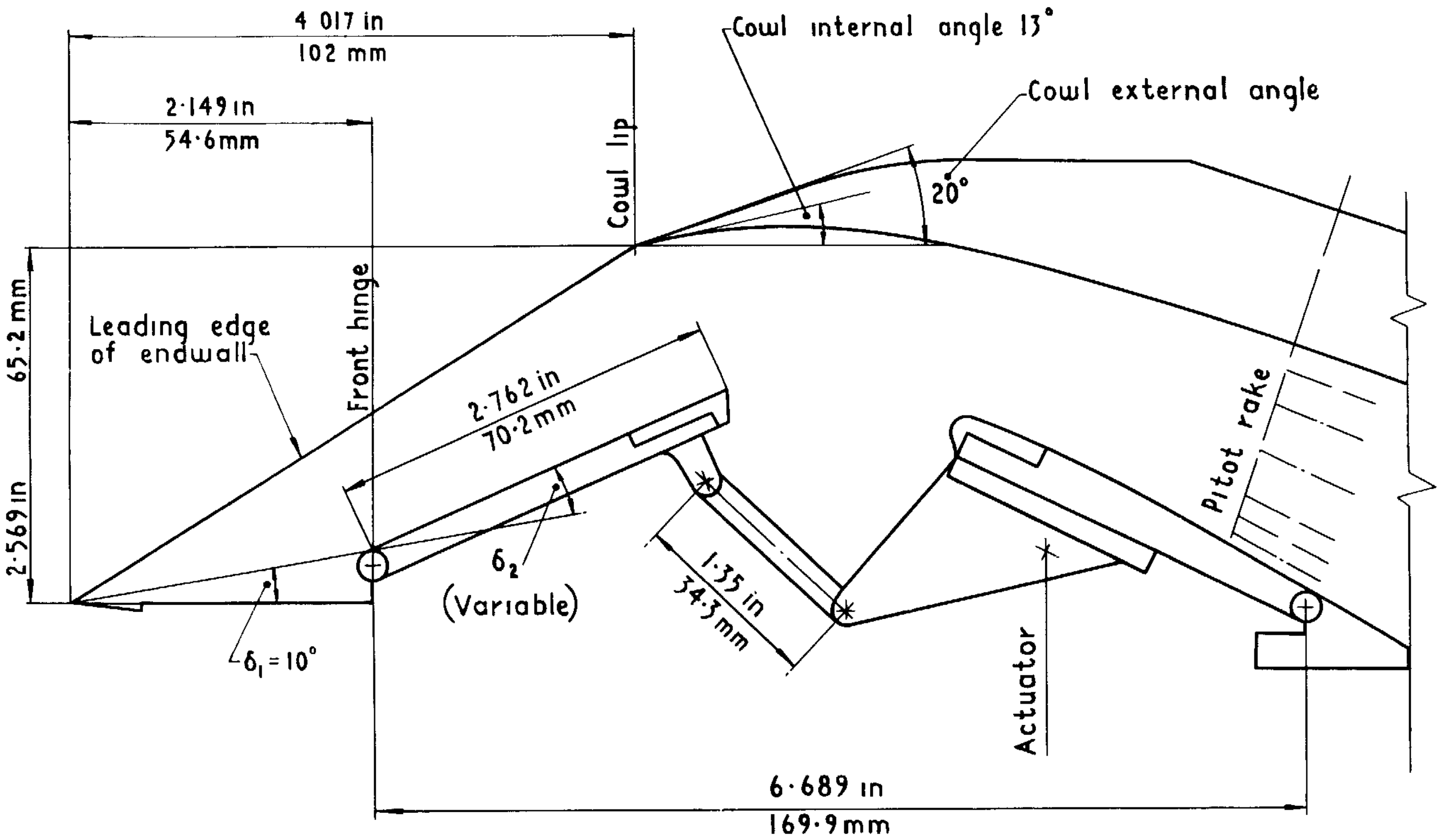

Fig 3 Geometry of compression surface ramps, cowl and bleed

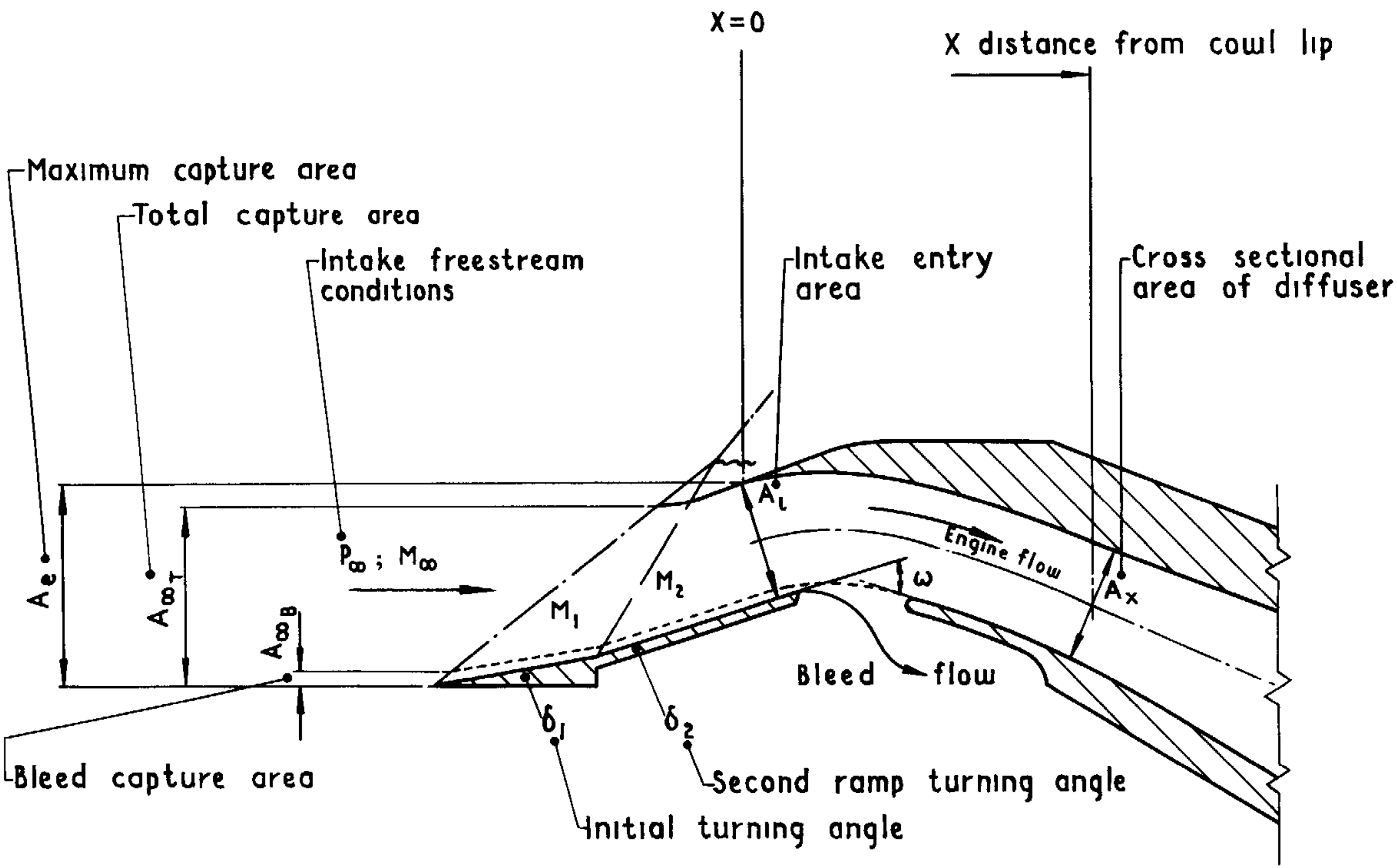

Fig 4 Definition of terms used throughout text

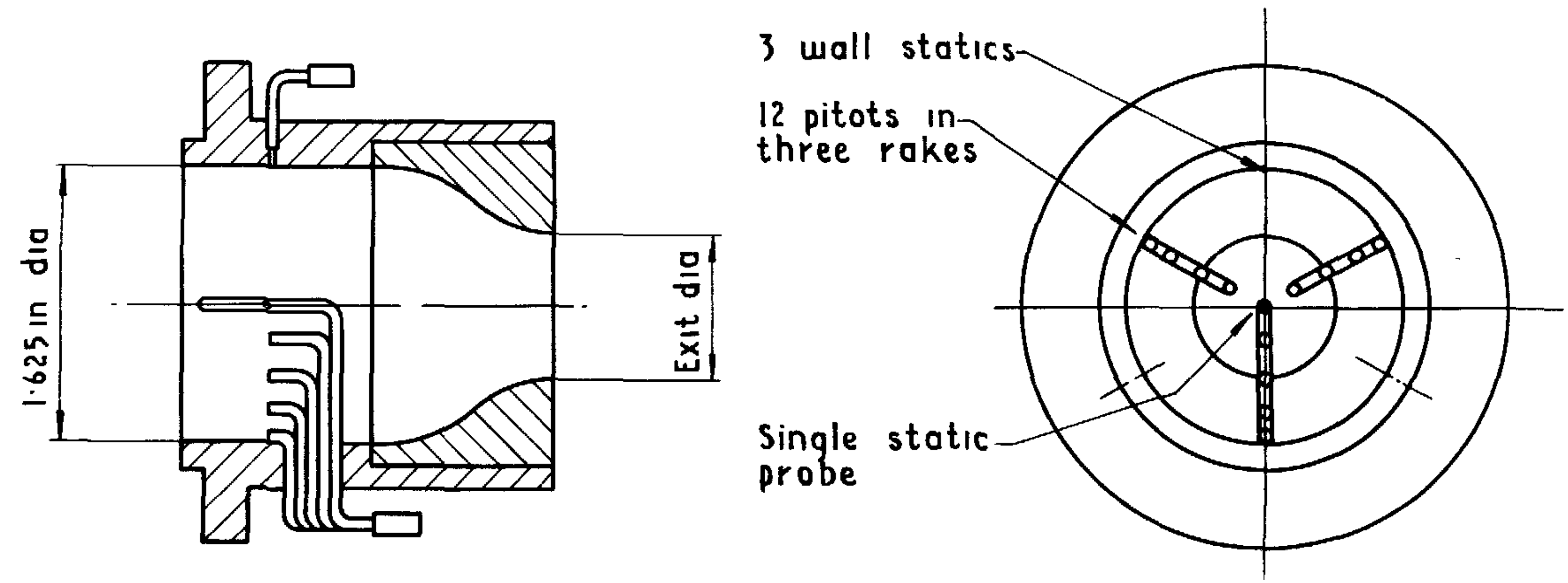

Plug No	0	1	2	4	8
Exit dia (inches)	0	0·412	0·609	0·803	1·1435

Fig.5 Details of bleed instrumentation and bleed exit plugs

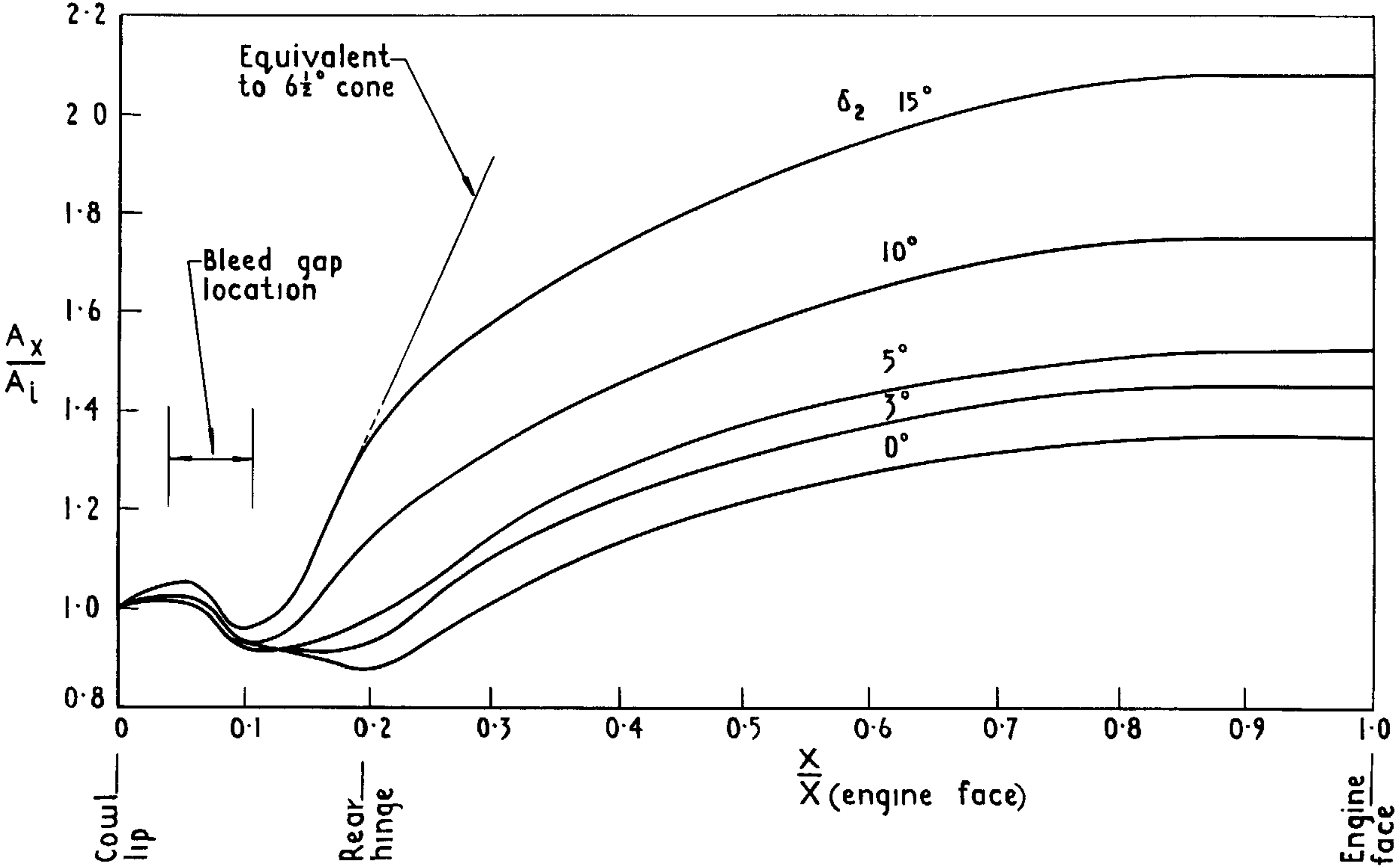

Fig 6 Area distribution through intake and duct

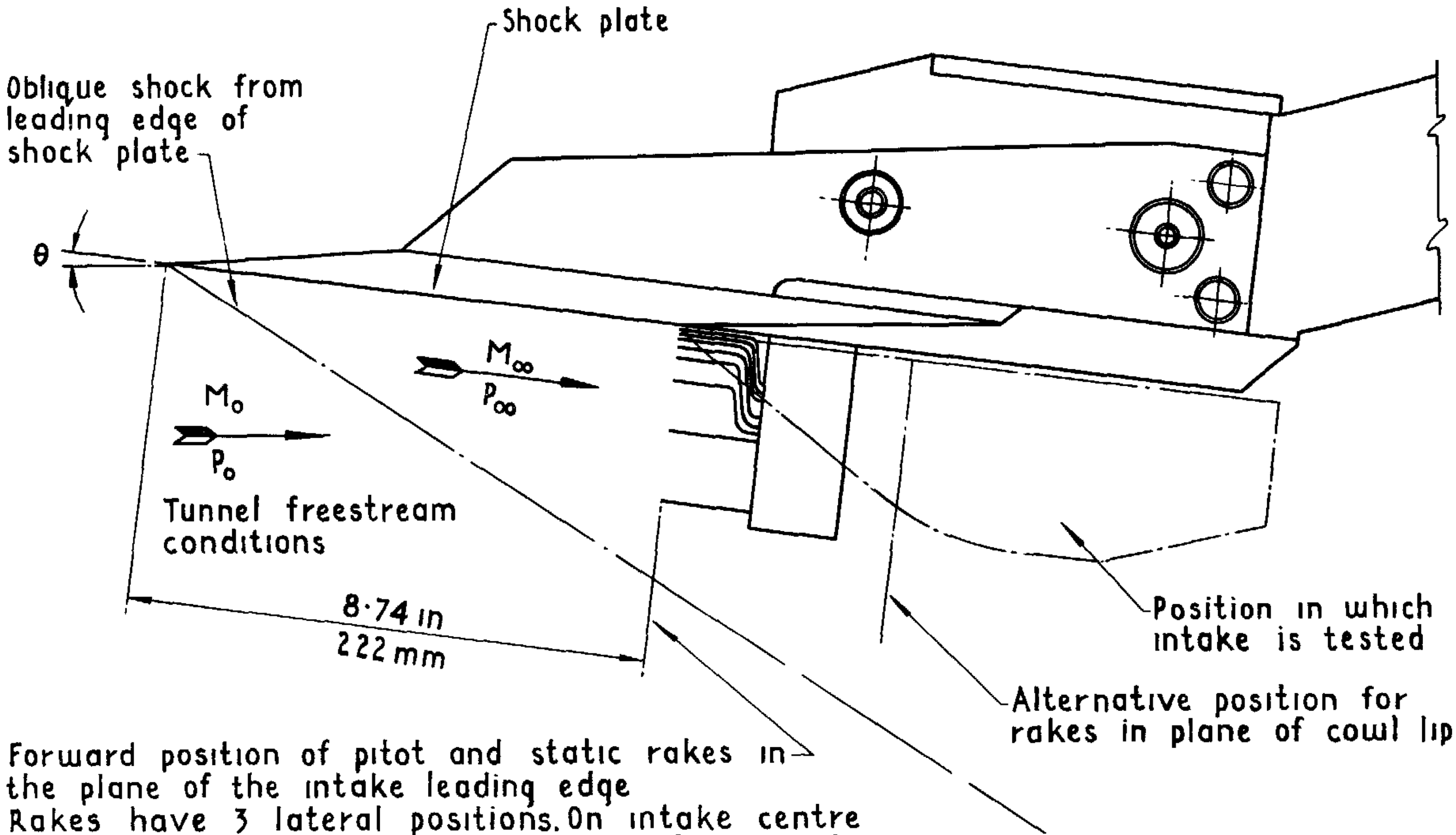

Fig 7 Diagram of shock plate indicating location of calibration rakes

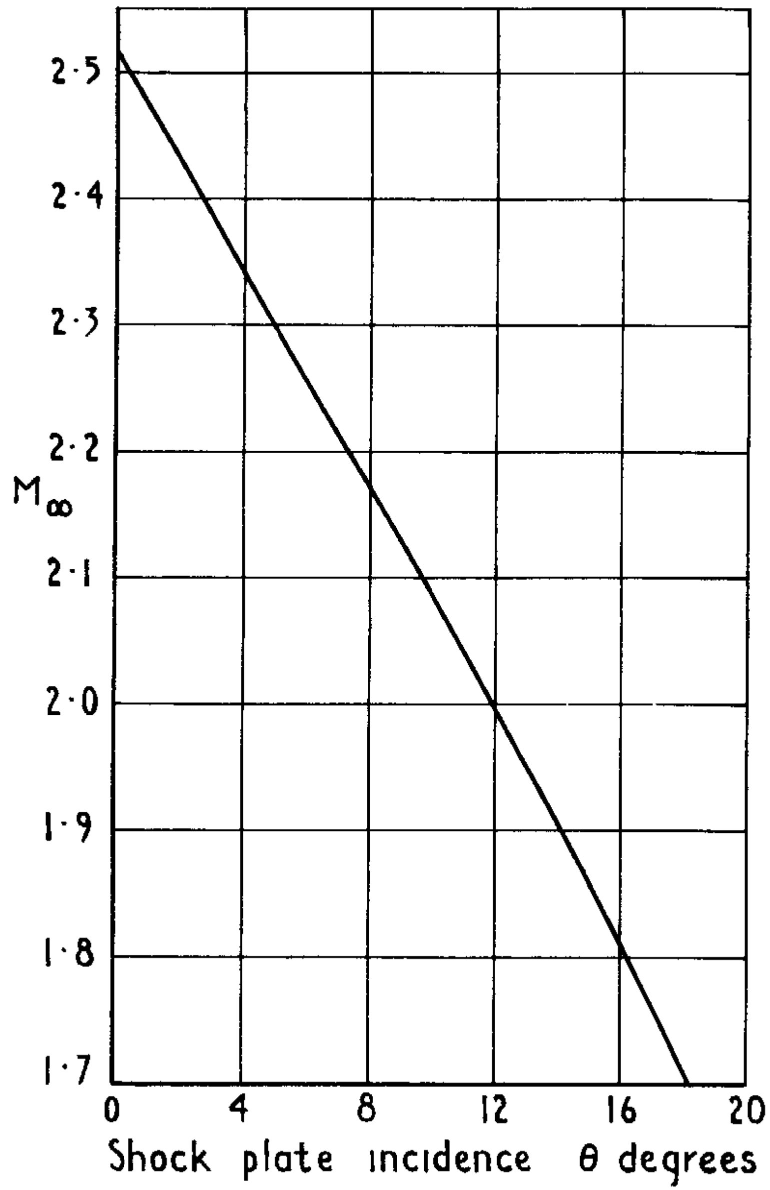

Fig 8a Mach number in freestream ahead of intake

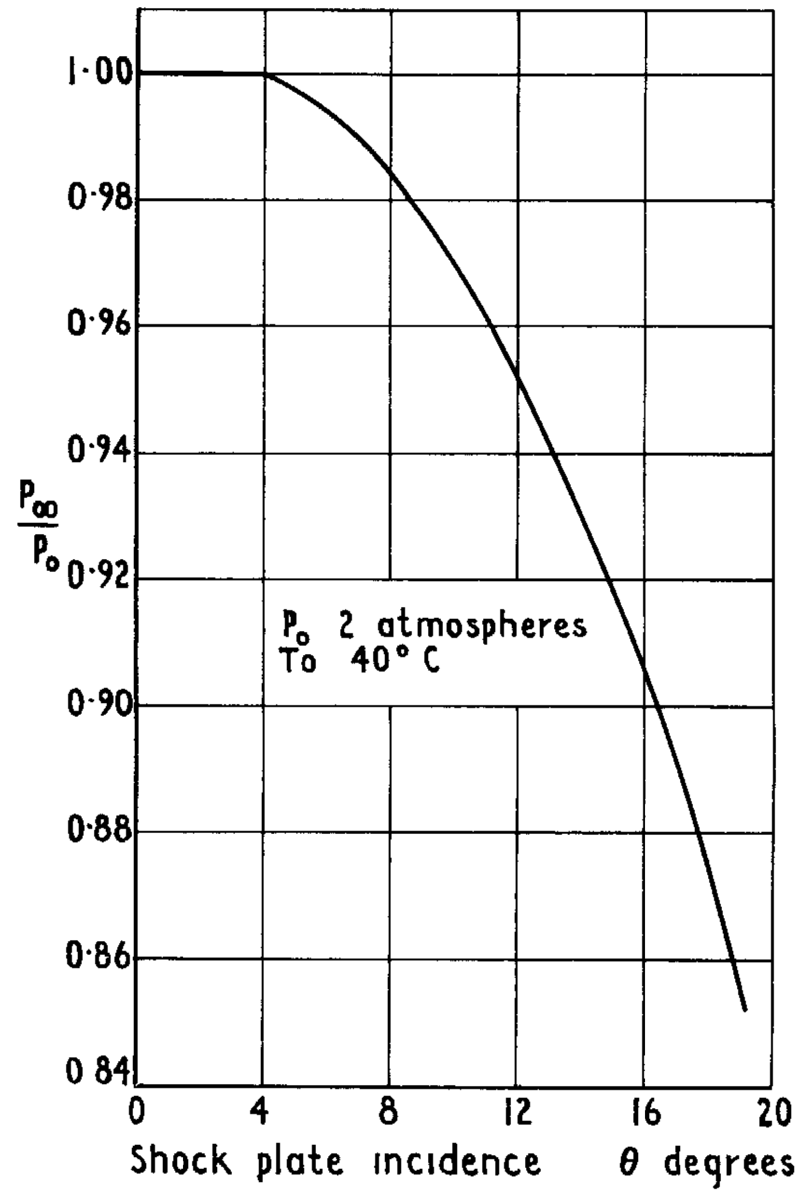

Fig.8b Ratio of intake freestream total pressure to tunnel stagnation pressure

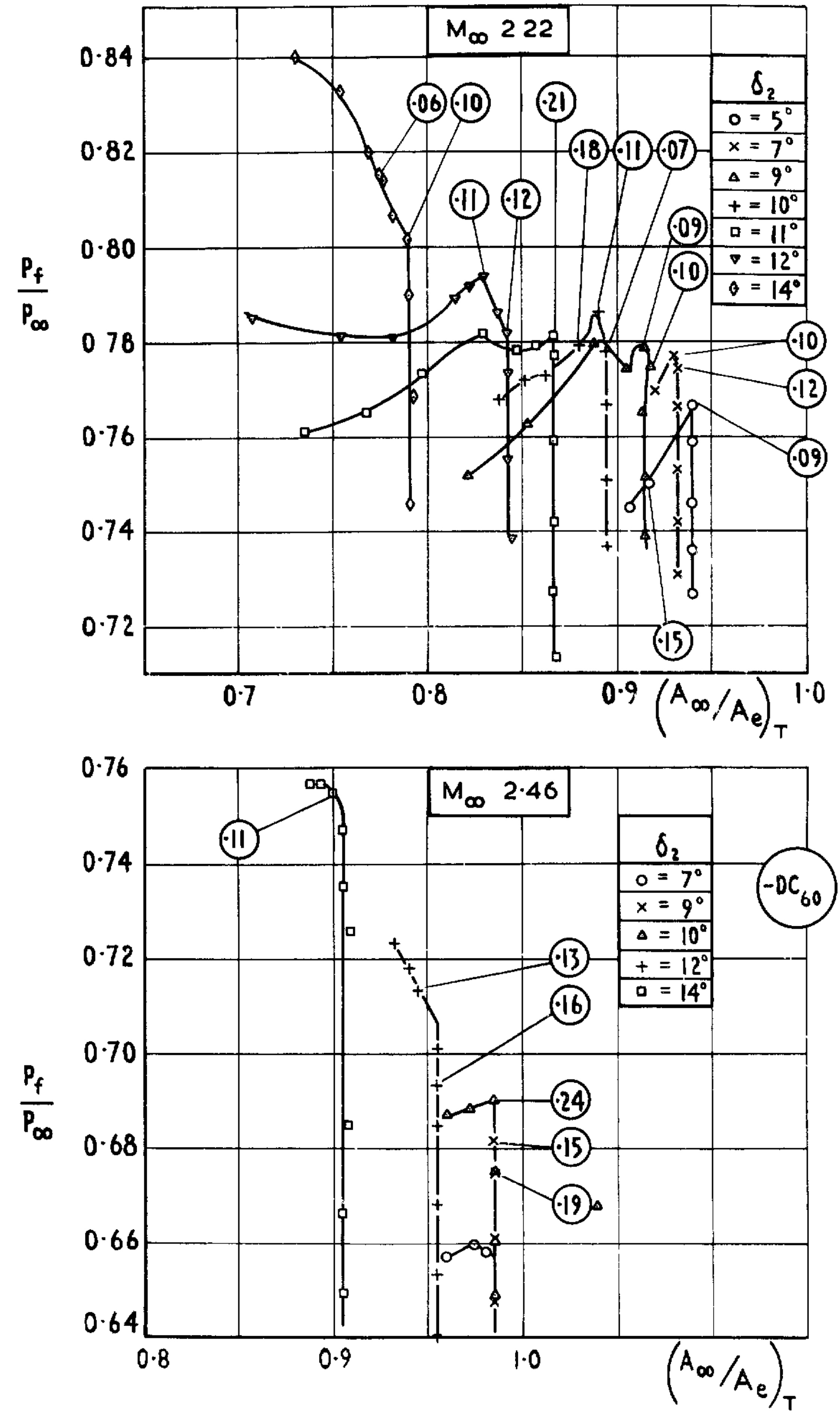

Fig 9 Variation of pressure recovery with mass flow. Zero bleed. M_∞ 2 22 and 2·46

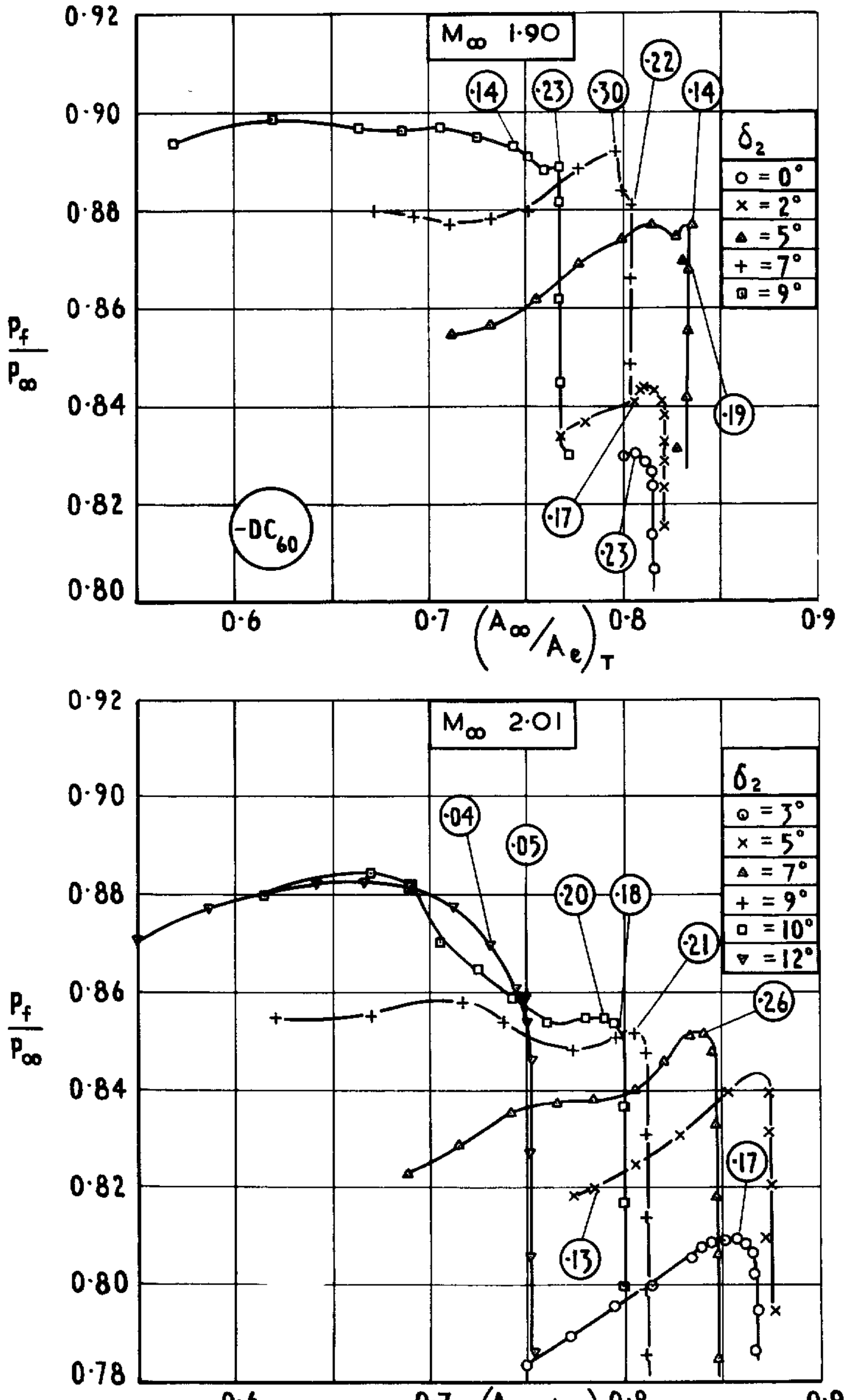

Fig.10 Variation of pressure recovery with mass flow.
Zero bleed. M_∞ 1·90 and 2·01

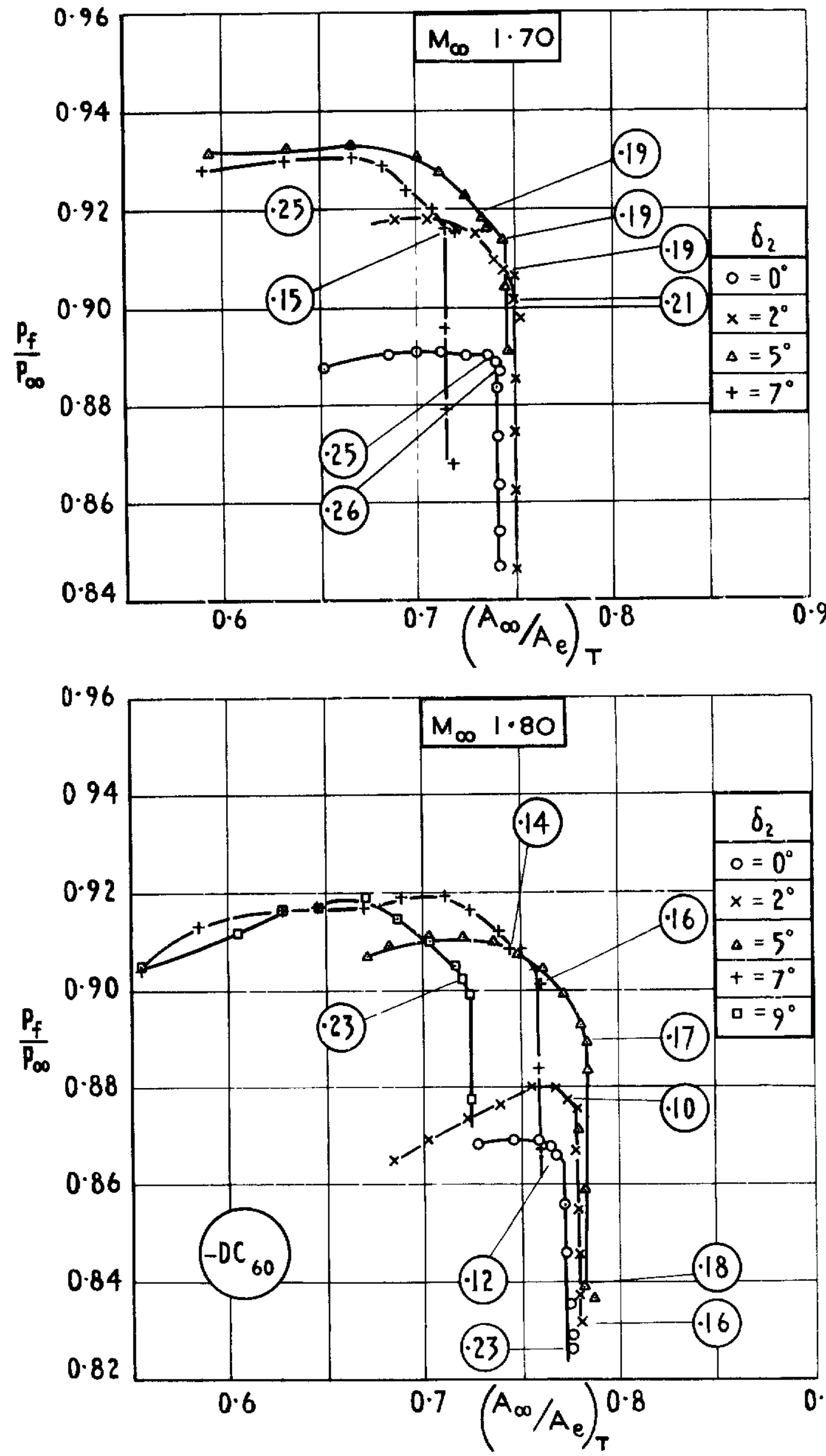

Fig.11 Variation of pressure recovery with mass flow
Zero bleed. M_∞ 1·70 and 1·80

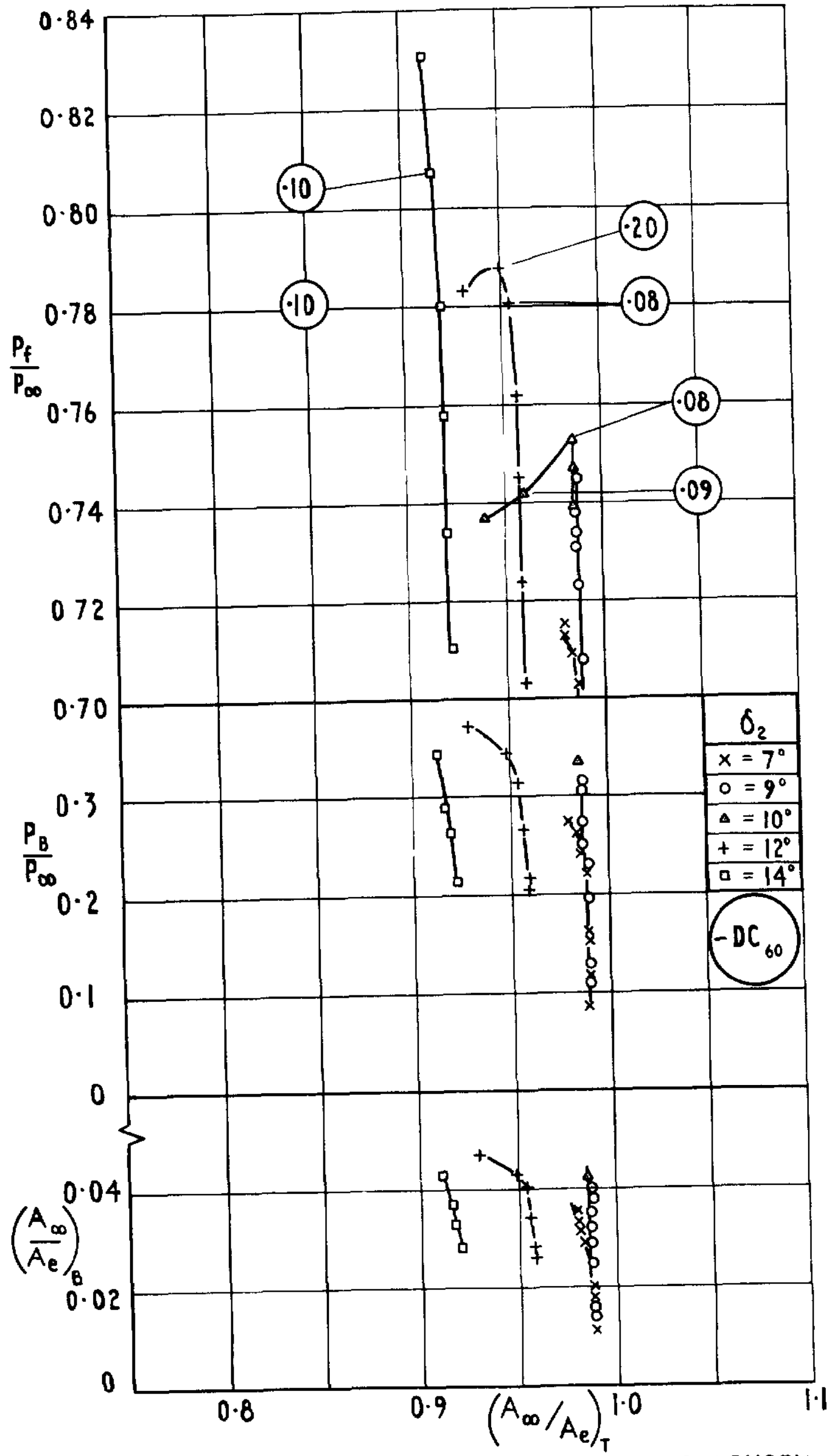

Fig 12 Variation of engine face pressure recovery, bleed pressure recovery and bleed mass flow with total mass flow. Bleed exit plug 4. M_∞ 2·46

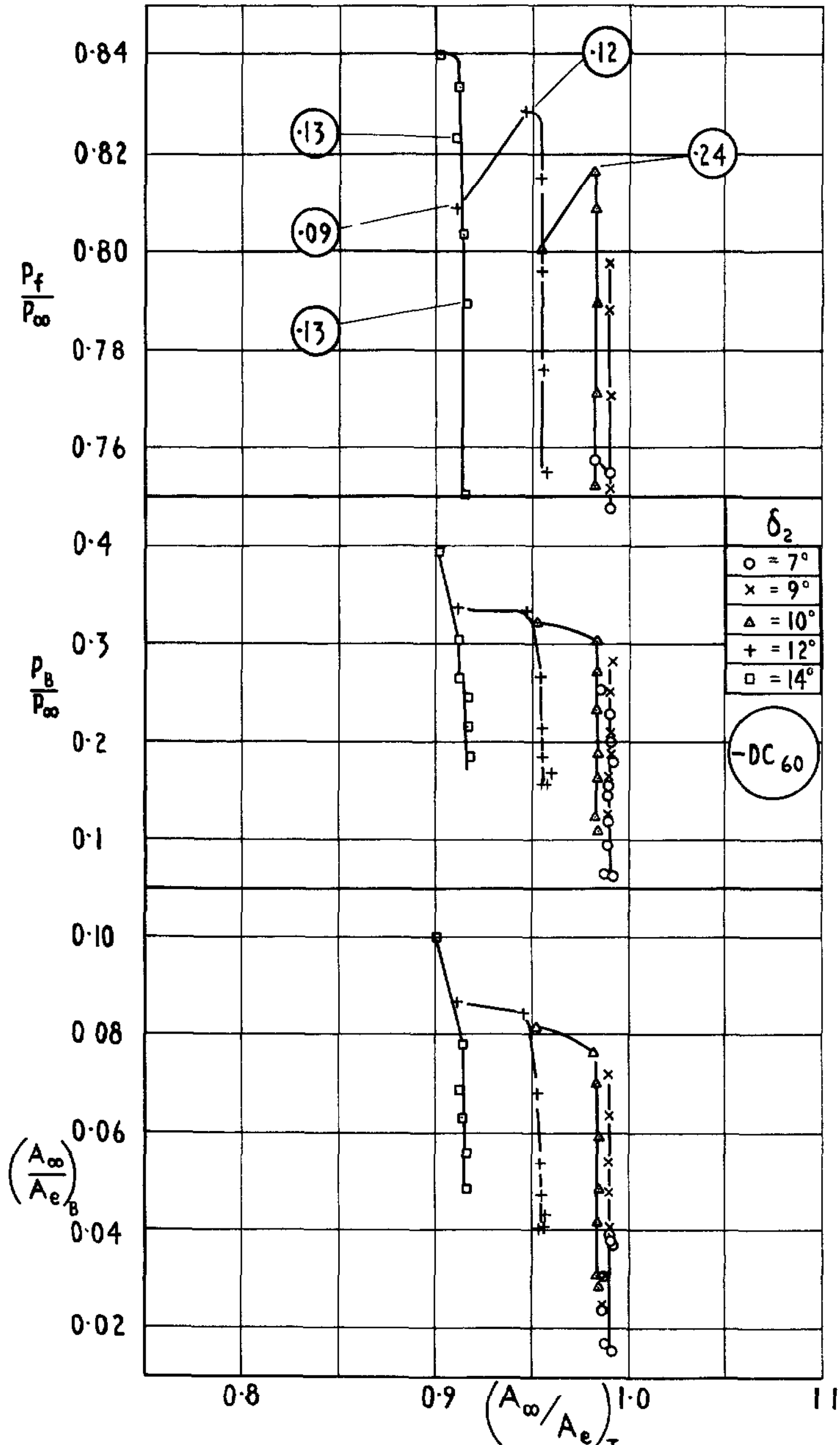

Fig 13 Variation of engine face pressure recovery, bleed pressure recovery and bleed mass flow with total mass flow. Bleed exit plug 8. M_∞ 2·46

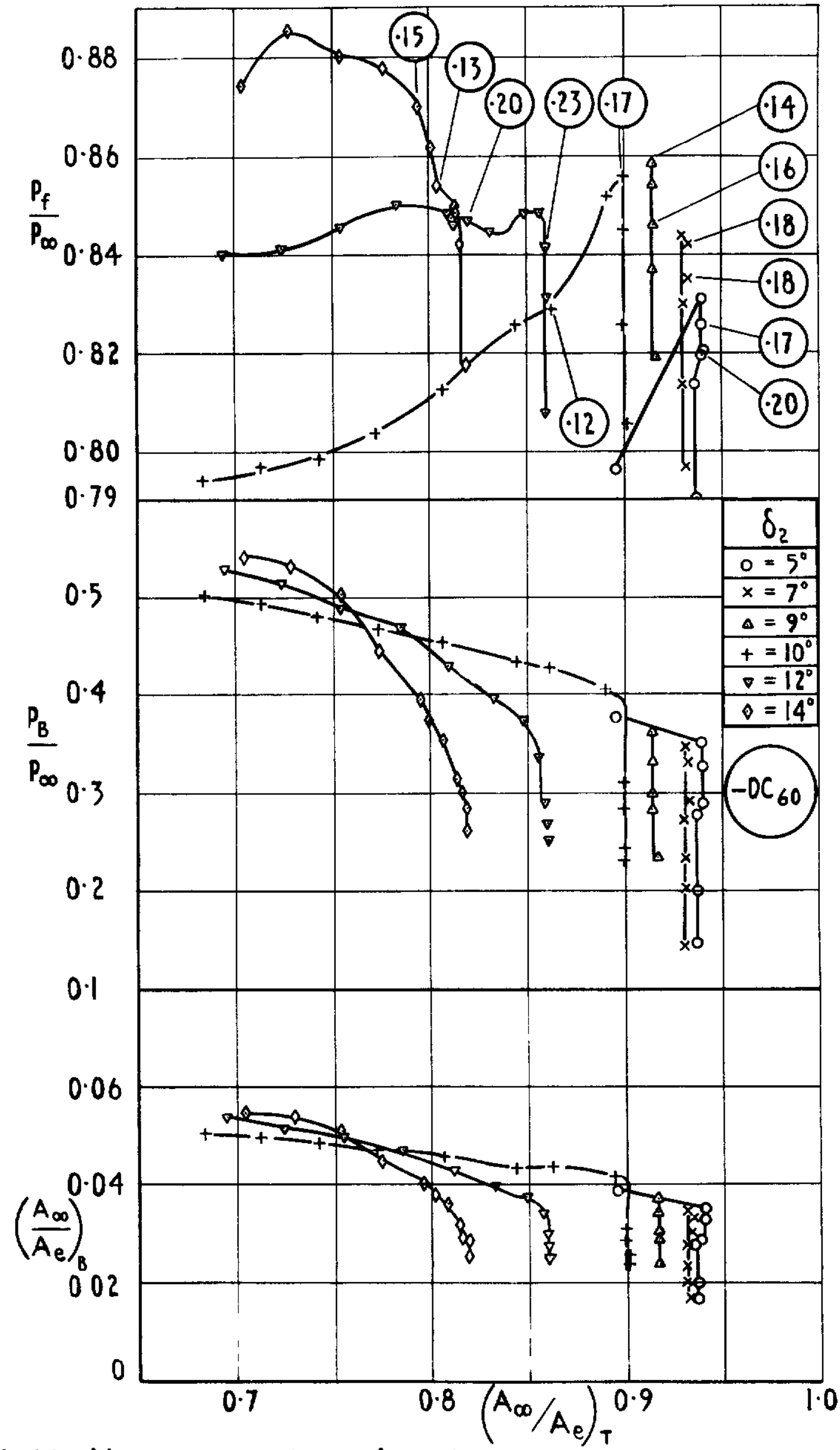

Fig 14 Variation of engine face pressure recovery, bleed pressure recovery and bleed mass flow with total mass flow. Bleed exit plug 4. M_∞ 2·22

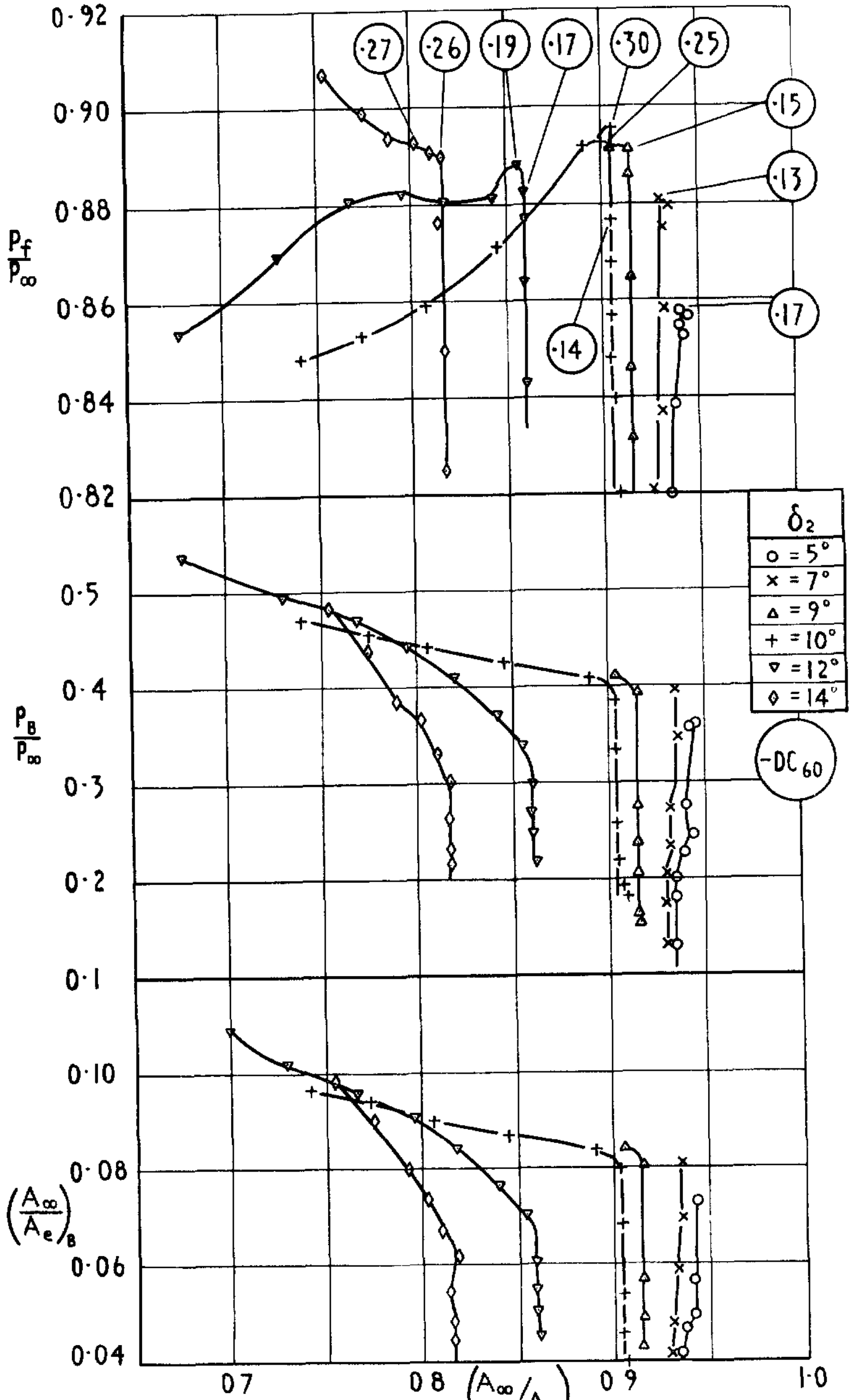

Fig 15 Variation of engine face pressure recovery, bleed pressure recovery and bleed mass flow with total mass flow. Bleed exit plug 8. M_∞ 2·22

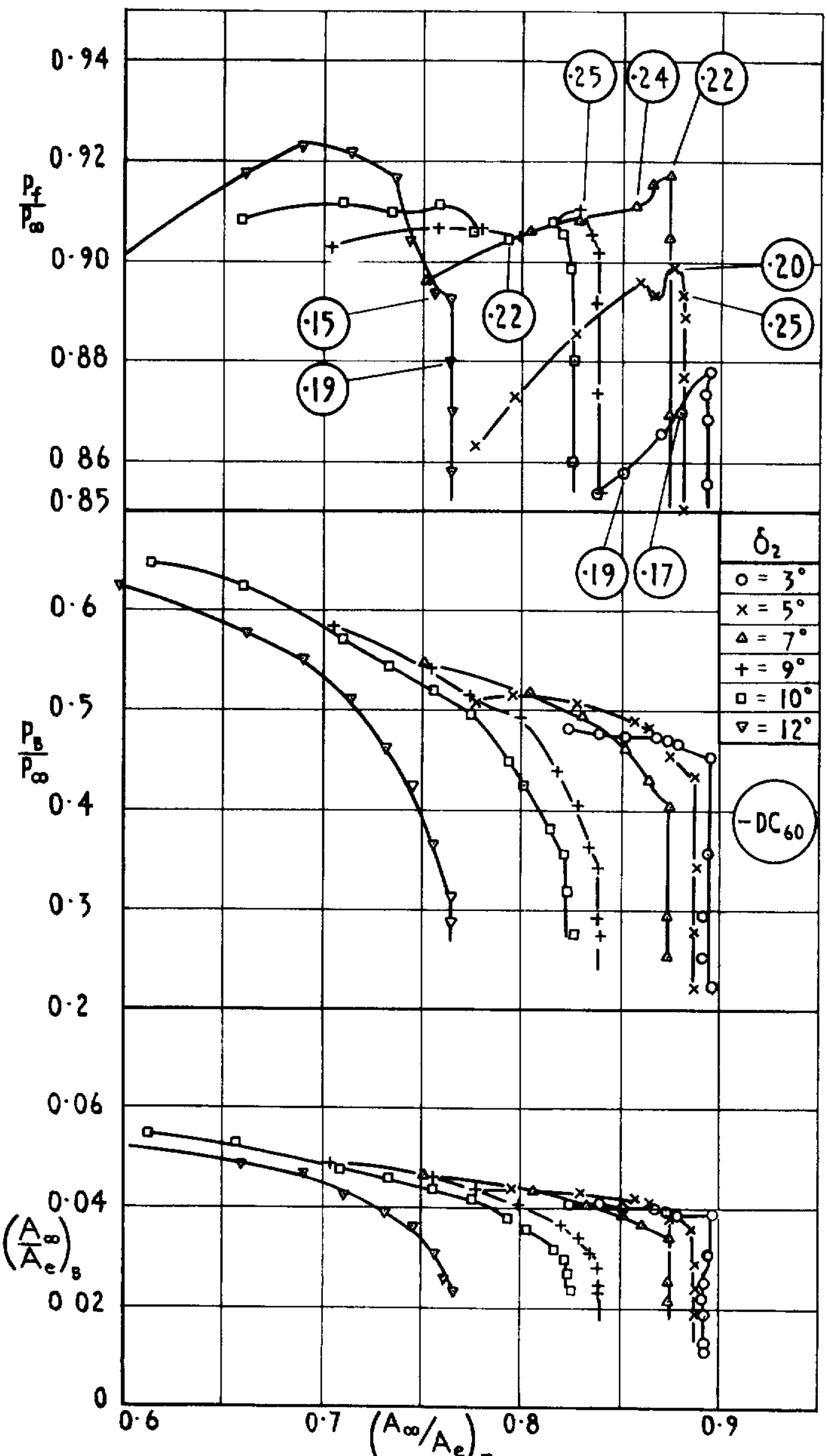

Fig. 16 Variation of engine face pressure recovery, bleed pressure recovery and bleed mass flow with total mass flow. Bleed exit plug 4. M_∞ 2·01

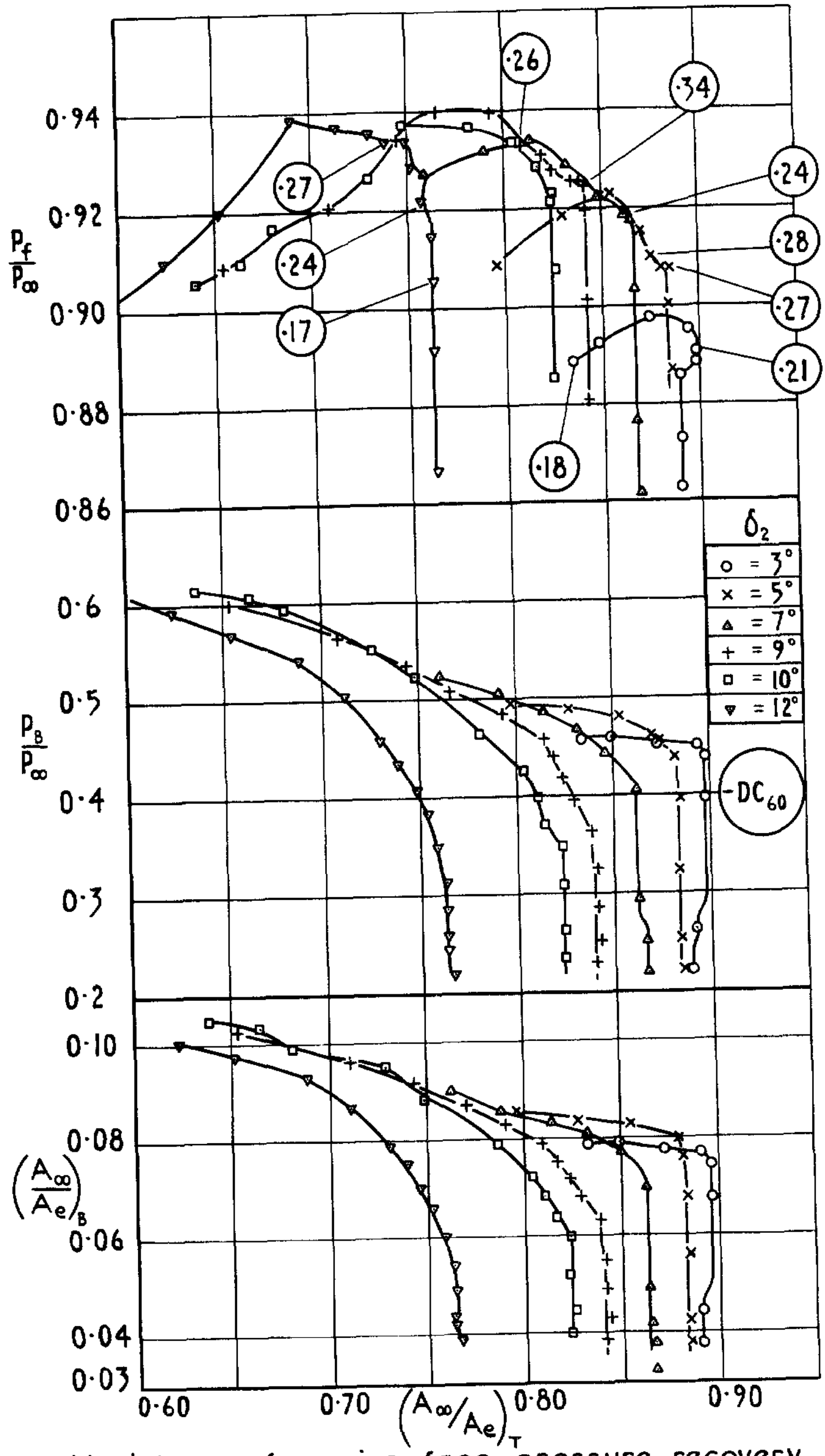

Fig. 17 Variation of engine face pressure recovery, bleed pressure recovery and bleed mass flow with total mass flow. Bleed exit plug 8. M_∞ 2·01

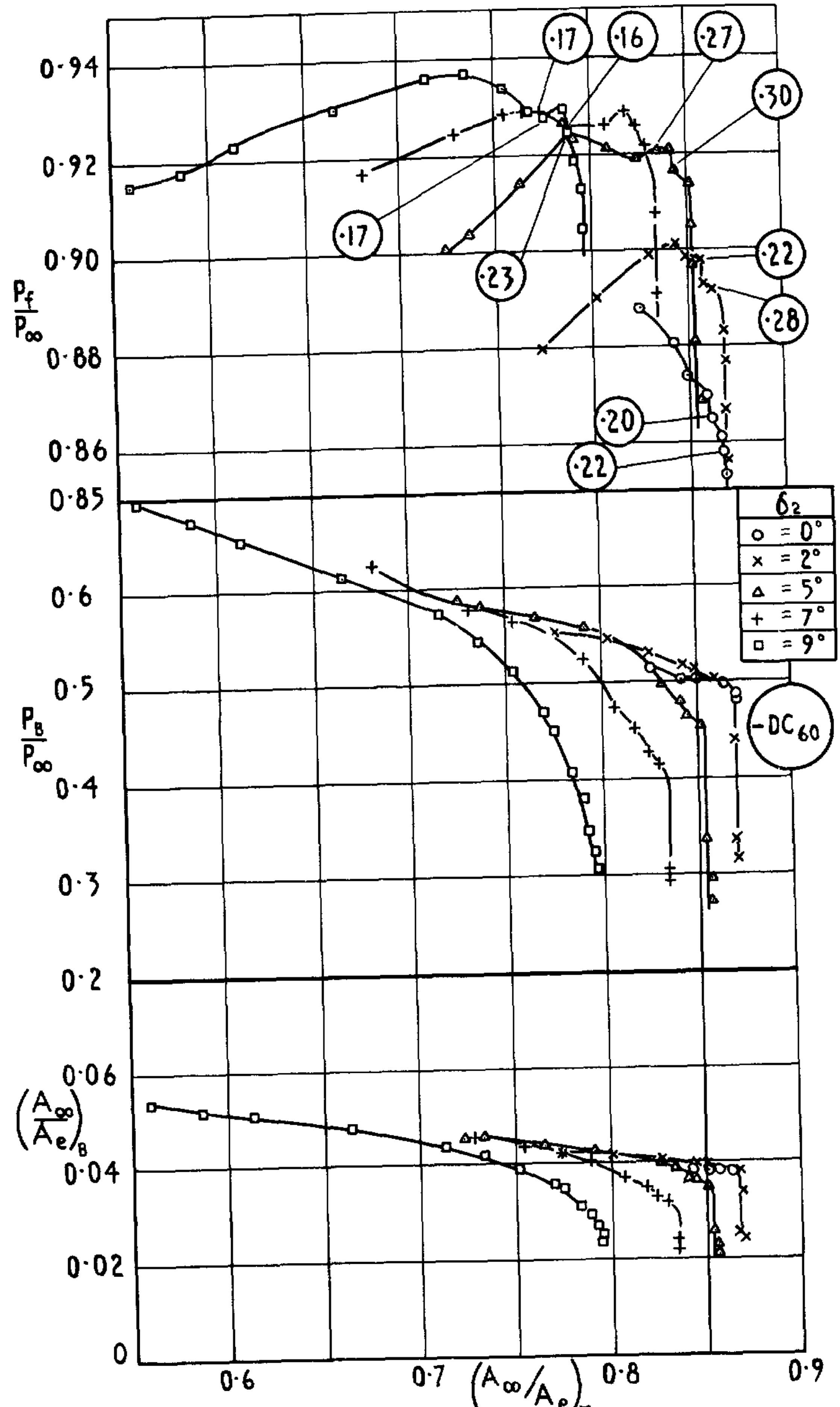

Fig 18 Variation of engine face pressure recovery, bleed pressure recovery and bleed mass flow with total mass flow. Bleed exit plug 4. M_∞ 1·90

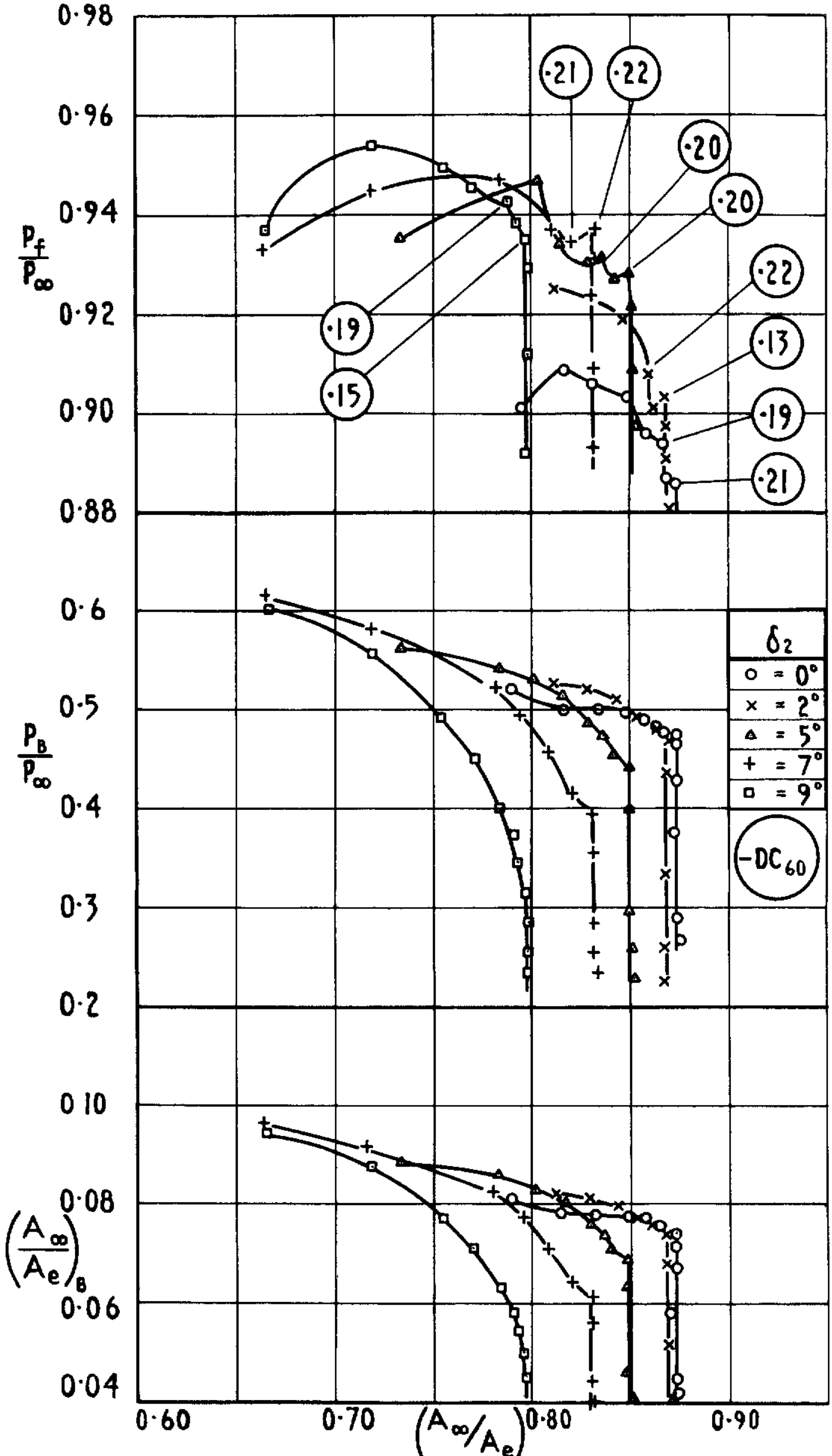

Fig 19 Variation of engine face pressure recovery, bleed pressure recovery and bleed mass flow with total mass flow. Bleed exit plug 8. M_∞ 1·90

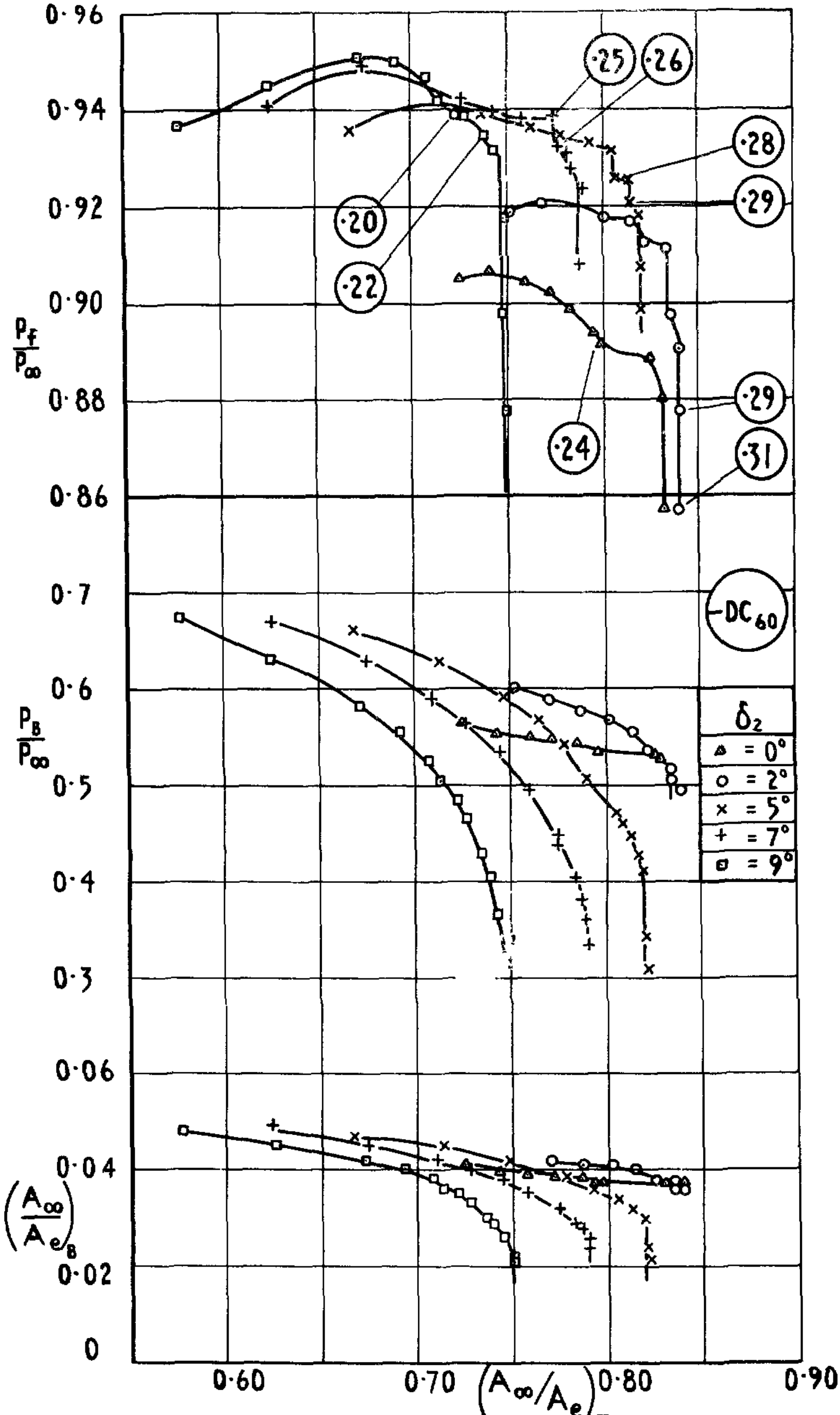

Fig. 20 Variation of engine face pressure recovery, bleed pressure recovery and bleed mass flow with total mass flow. Bleed exit plug 4. M_∞ 1·80

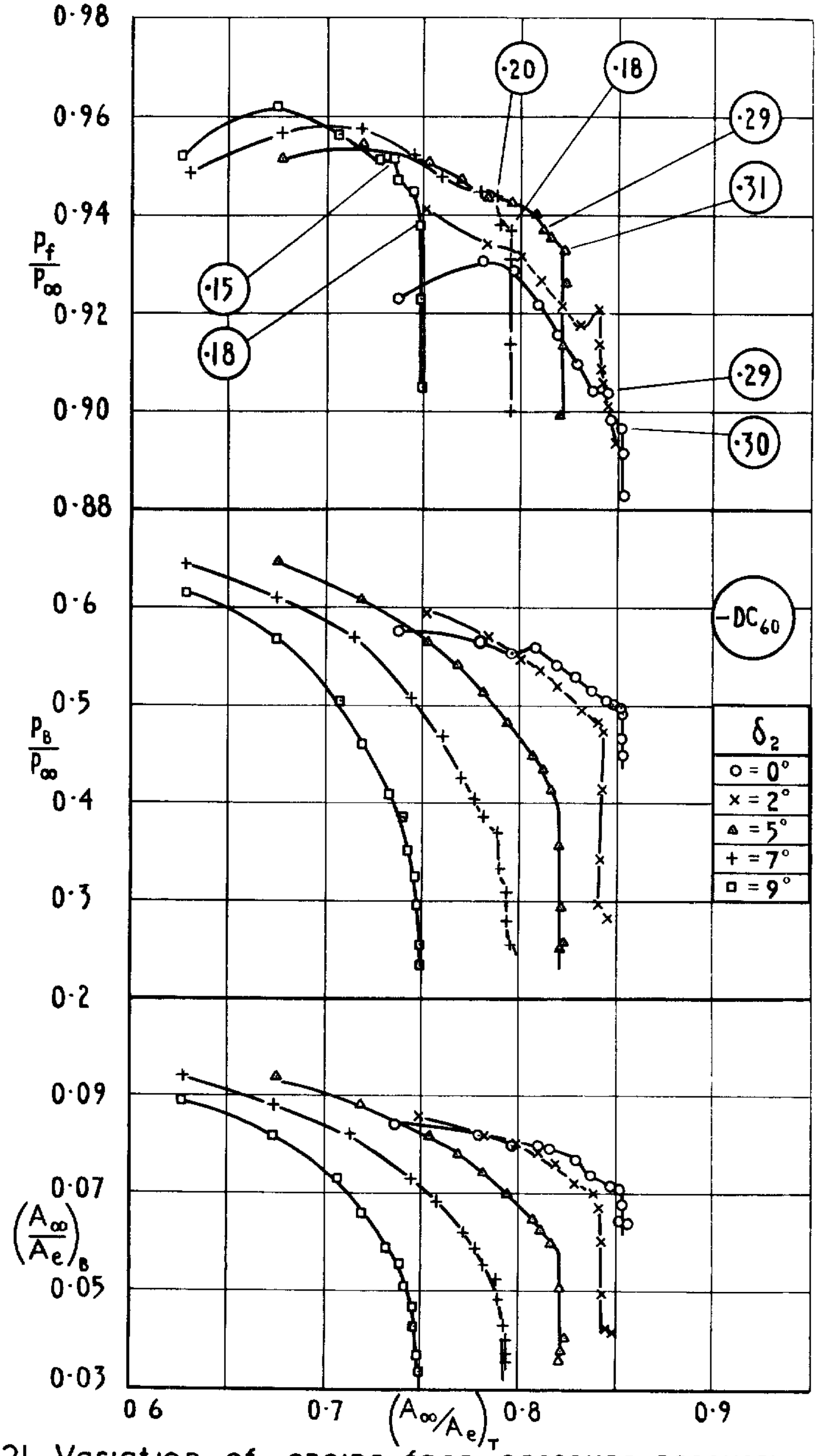

Fig 21 Variation of engine face pressure recovery, bleed pressure recovery and bleed mass flow with total mass flow. Bleed exit plug 8. M_∞ 1·80

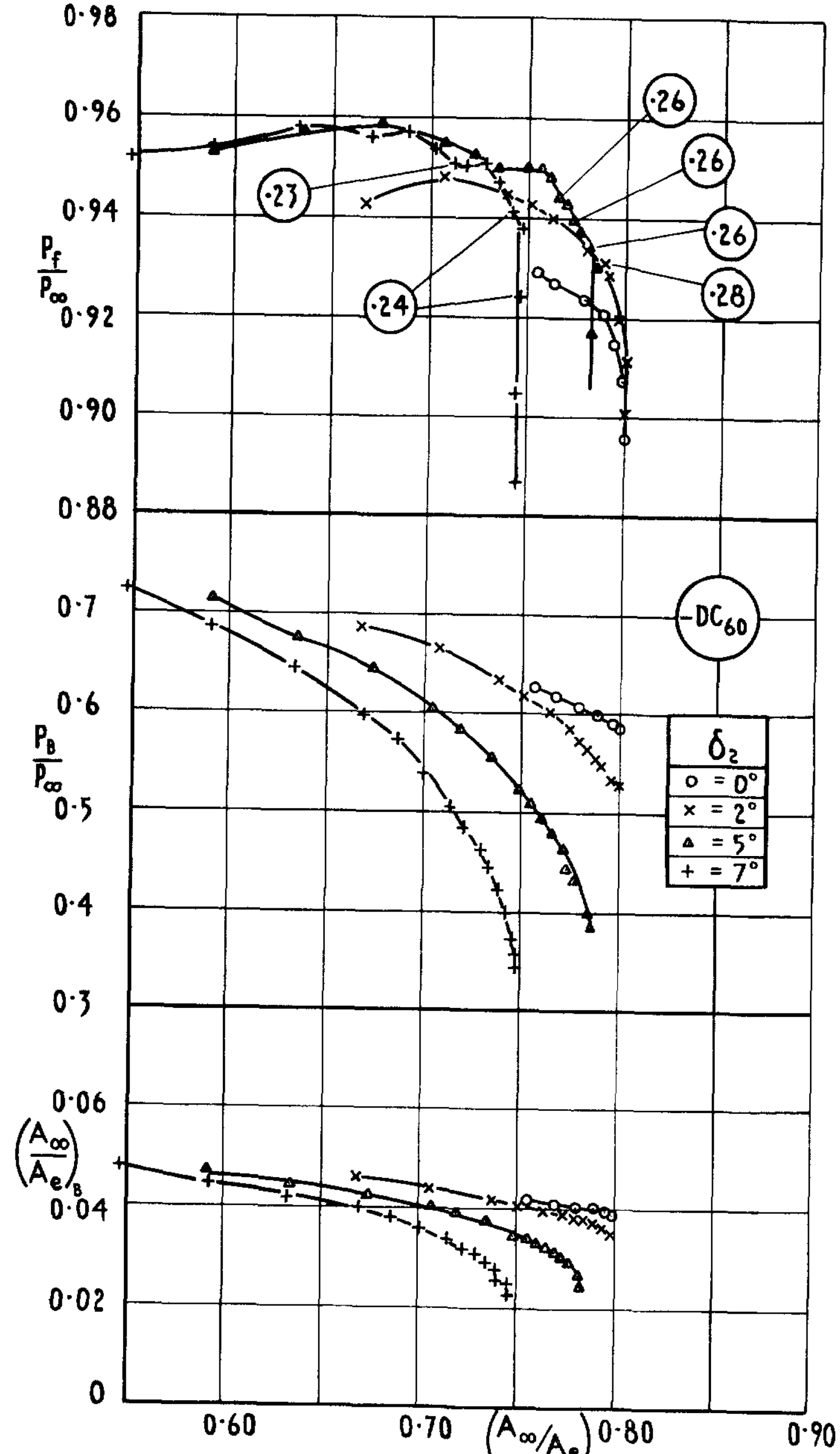

Fig.22 Variation of engine face pressure recovery, bleed pressure recovery and bleed mass flow with total mass flow. Bleed exit plug 4. M_∞ 1·70

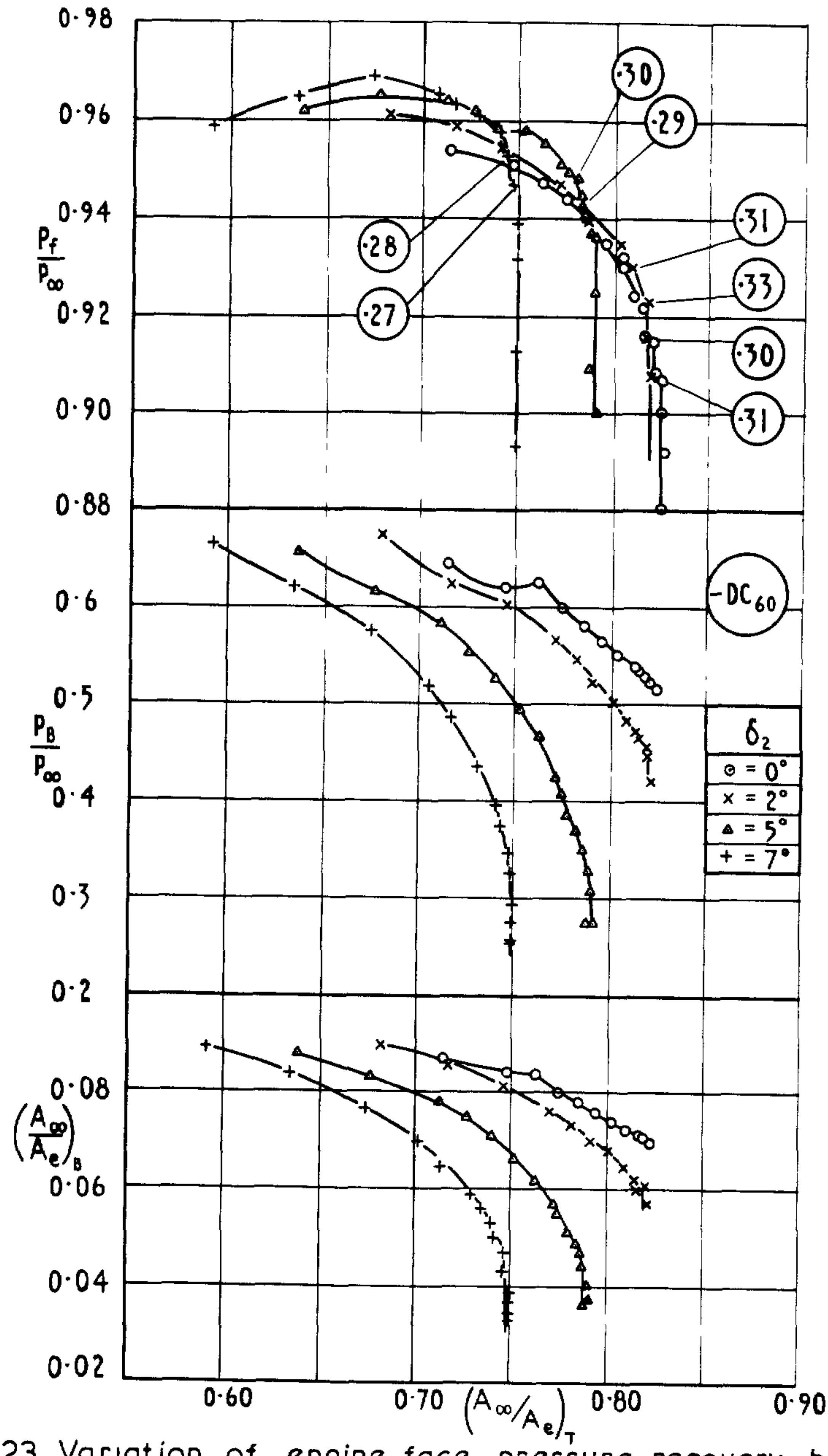

Fig 23 Variation of engine face pressure recovery, bleed pressure recovery and bleed mass flow with total mass flow. Bleed exit plug 8. M_∞ 1·70

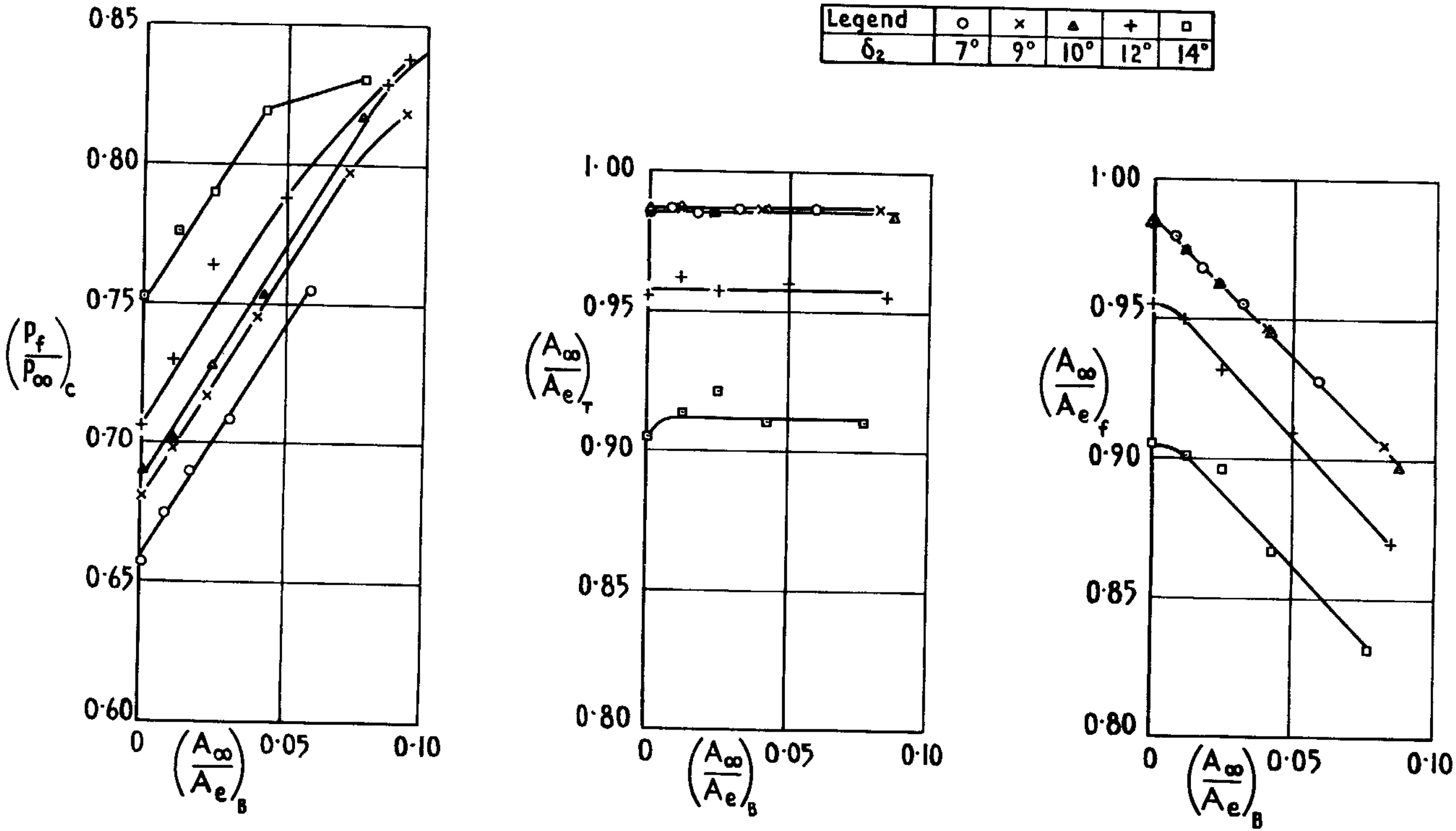

Fig. 24 Effect of bleed on critical pressure recovery, total mass flow and mass flow at engine face. M_∞ 2·46

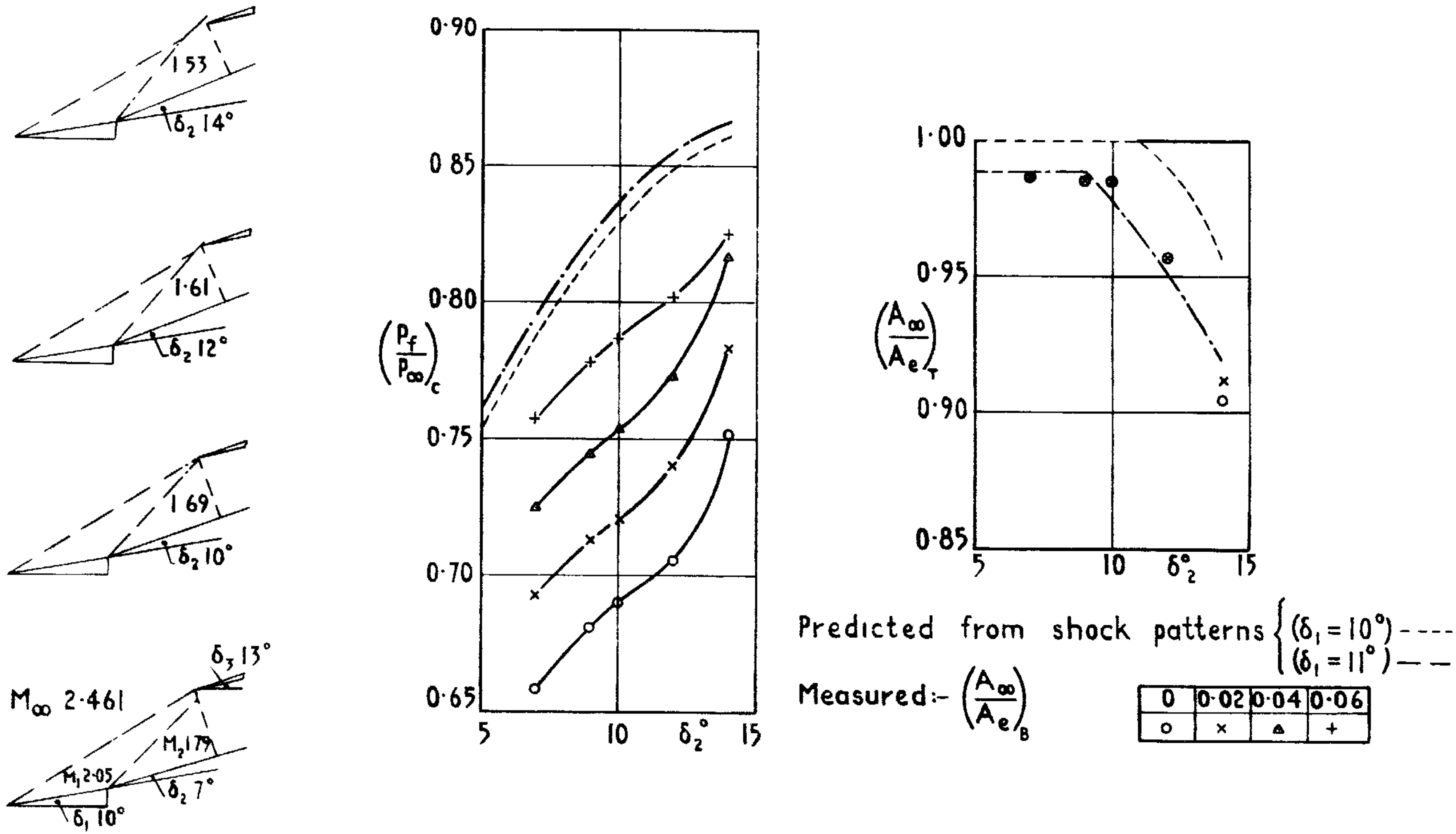

Fig 25 Variation of critical pressure recovery and maximum mass flow with δ_2 at constant bleed flow. M_∞ 2·46

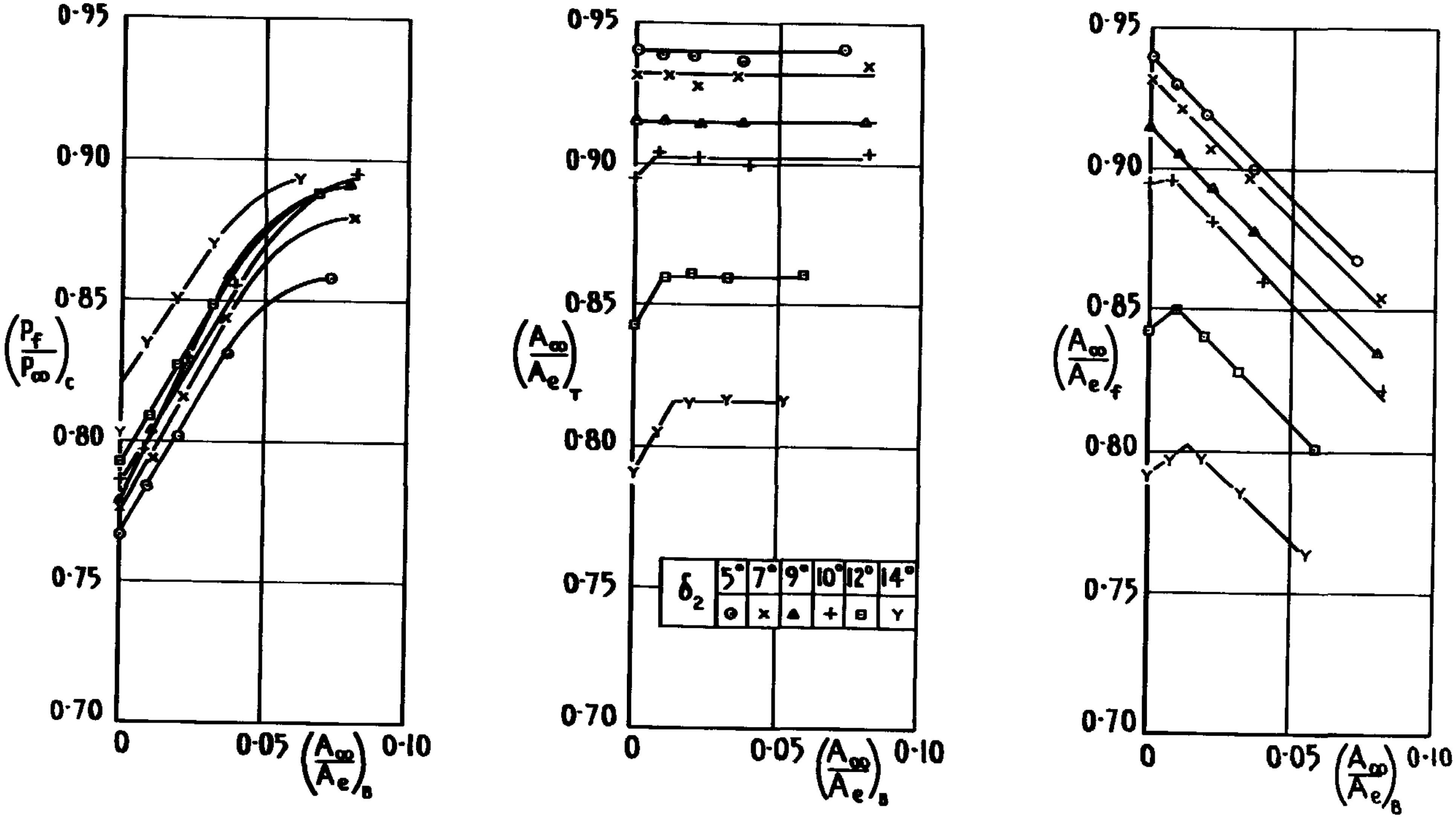

Fig. 26 Effect of bleed on critical pressure recovery, total mass flow and mass flow at engine face. M_∞ 2·22

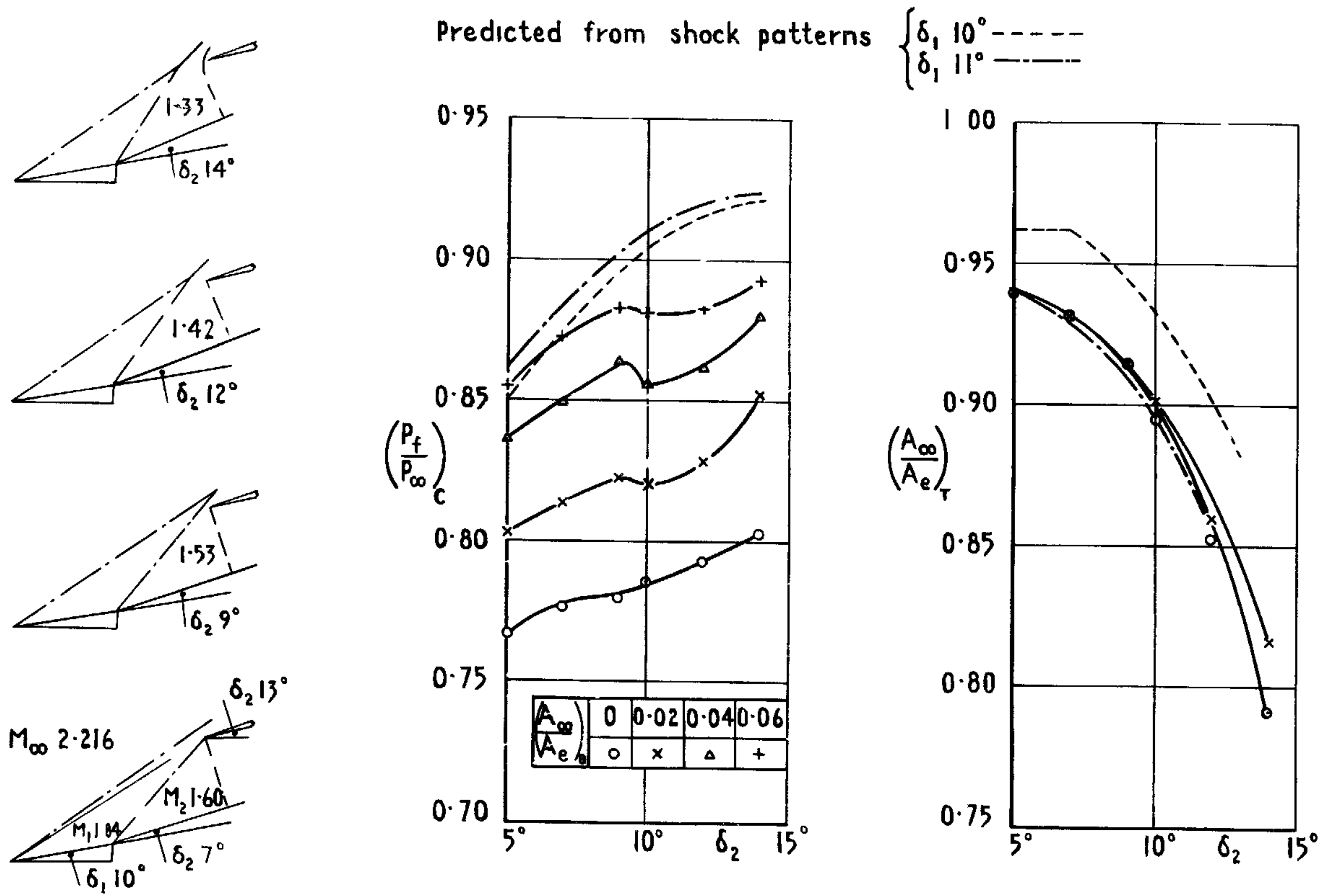

Fig. 27 Variation of critical pressure recovery and maximum mass flow with δ_2 at constant bleed flow. M_∞ 2·22

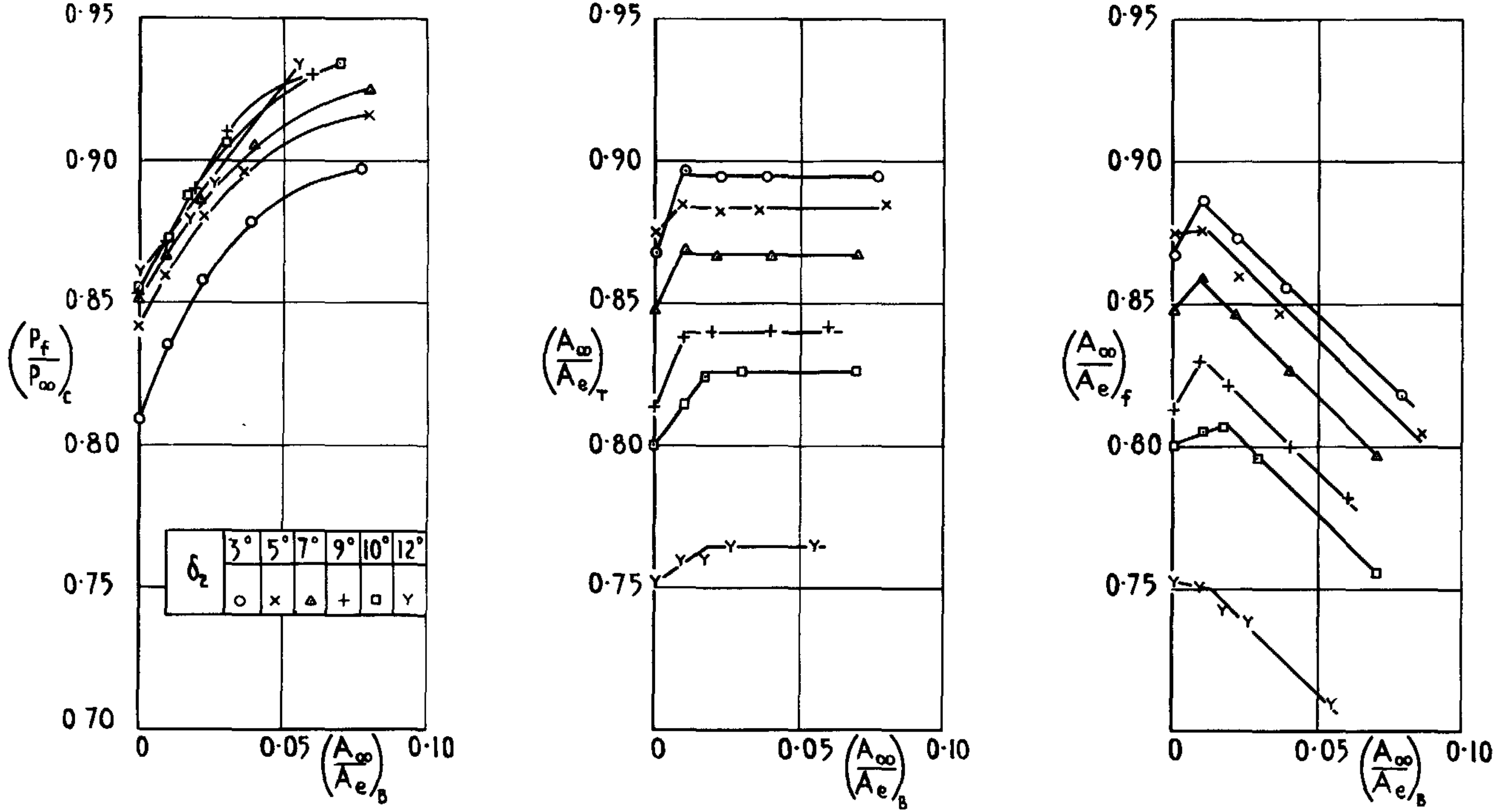

Fig. 28 Effect of bleed on critical pressure recovery, total mass flow and mass flow at engine face M_∞ 2·01

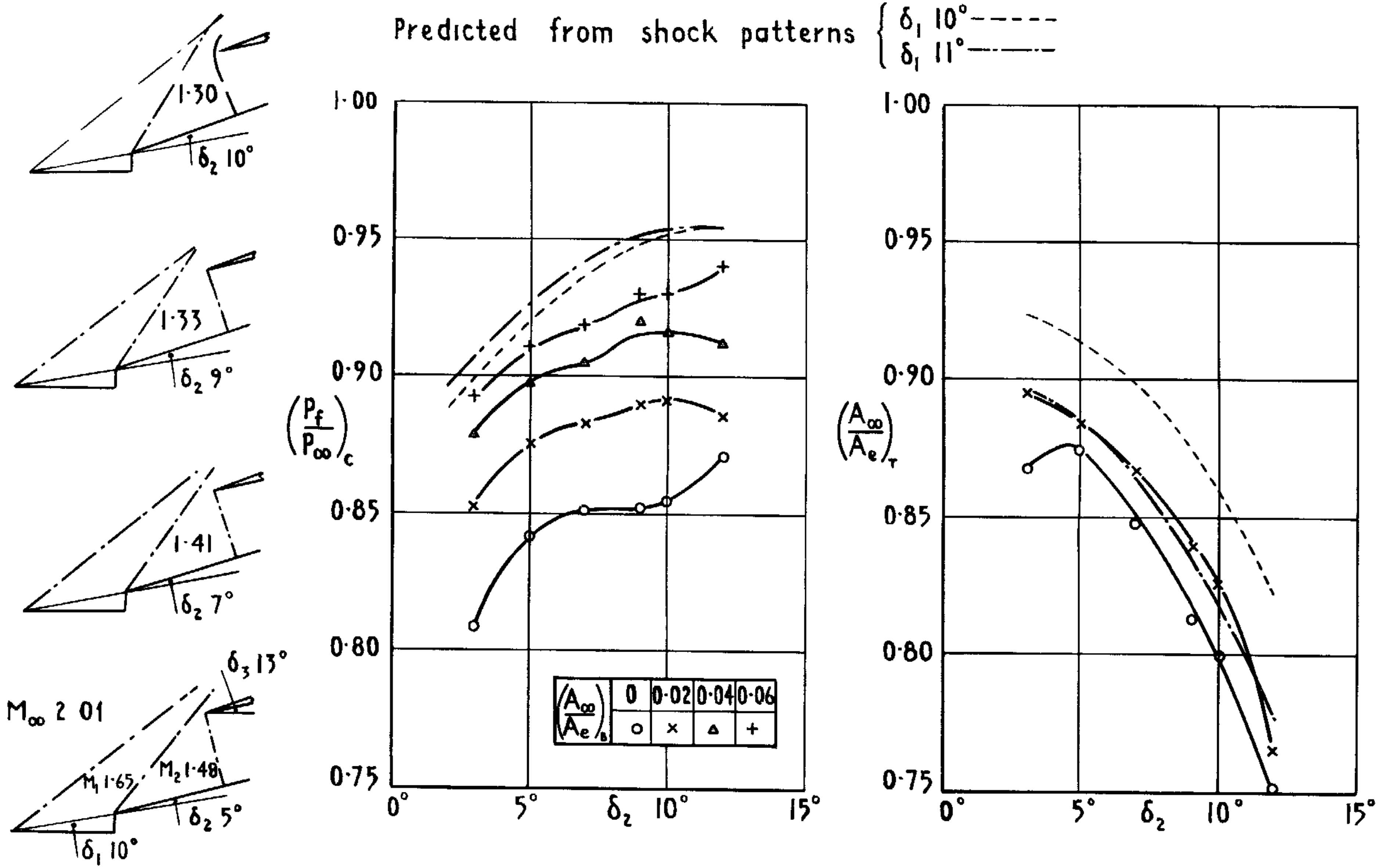

Fig 29 Variation of critical pressure recovery and maximum mass flow with δ_2 at constant bleed flow. M_∞ 2·01

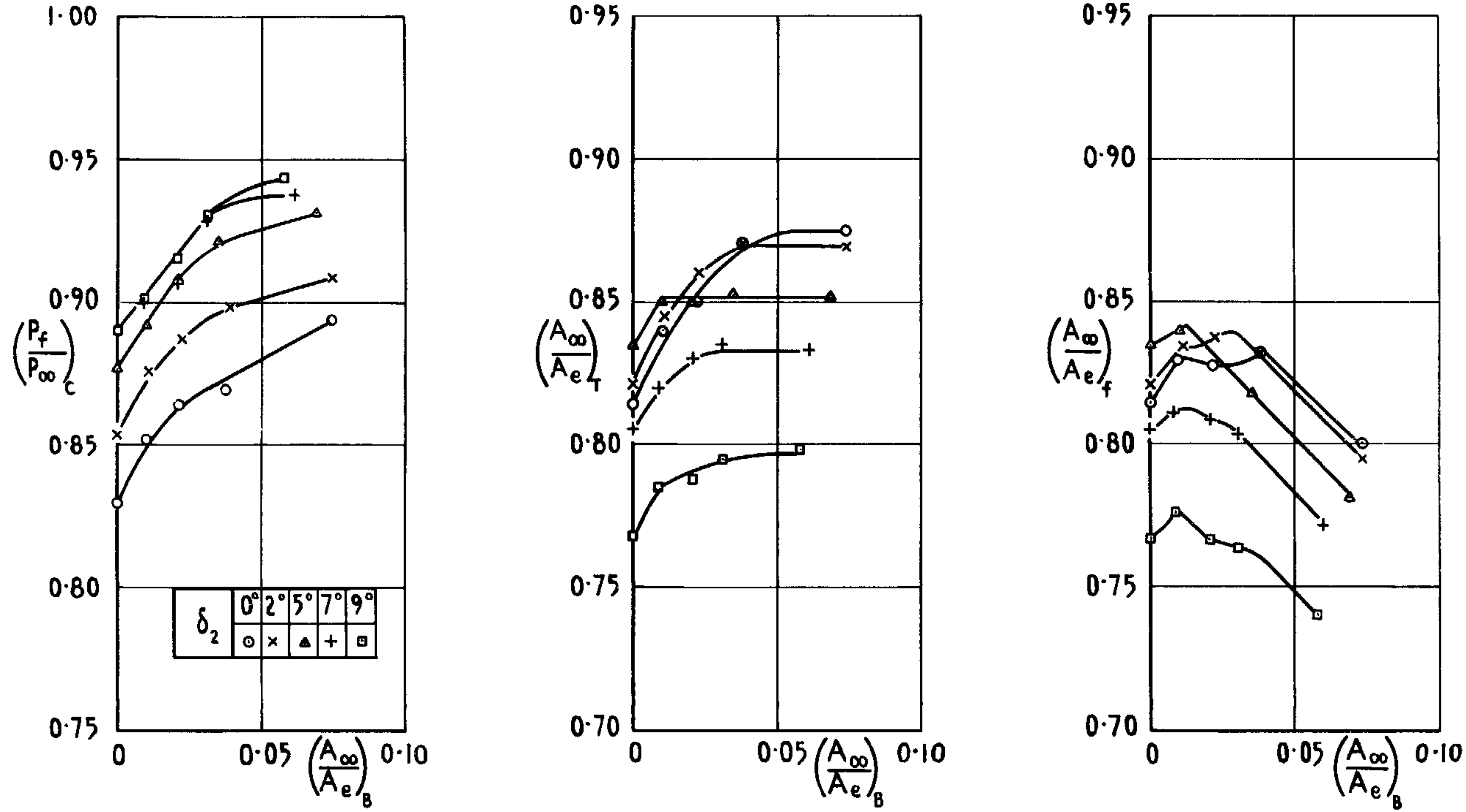

Fig. 30 Effect of bleed on critical pressure recovery, total mass flow and mass flow at engine face. M_∞ 1·90

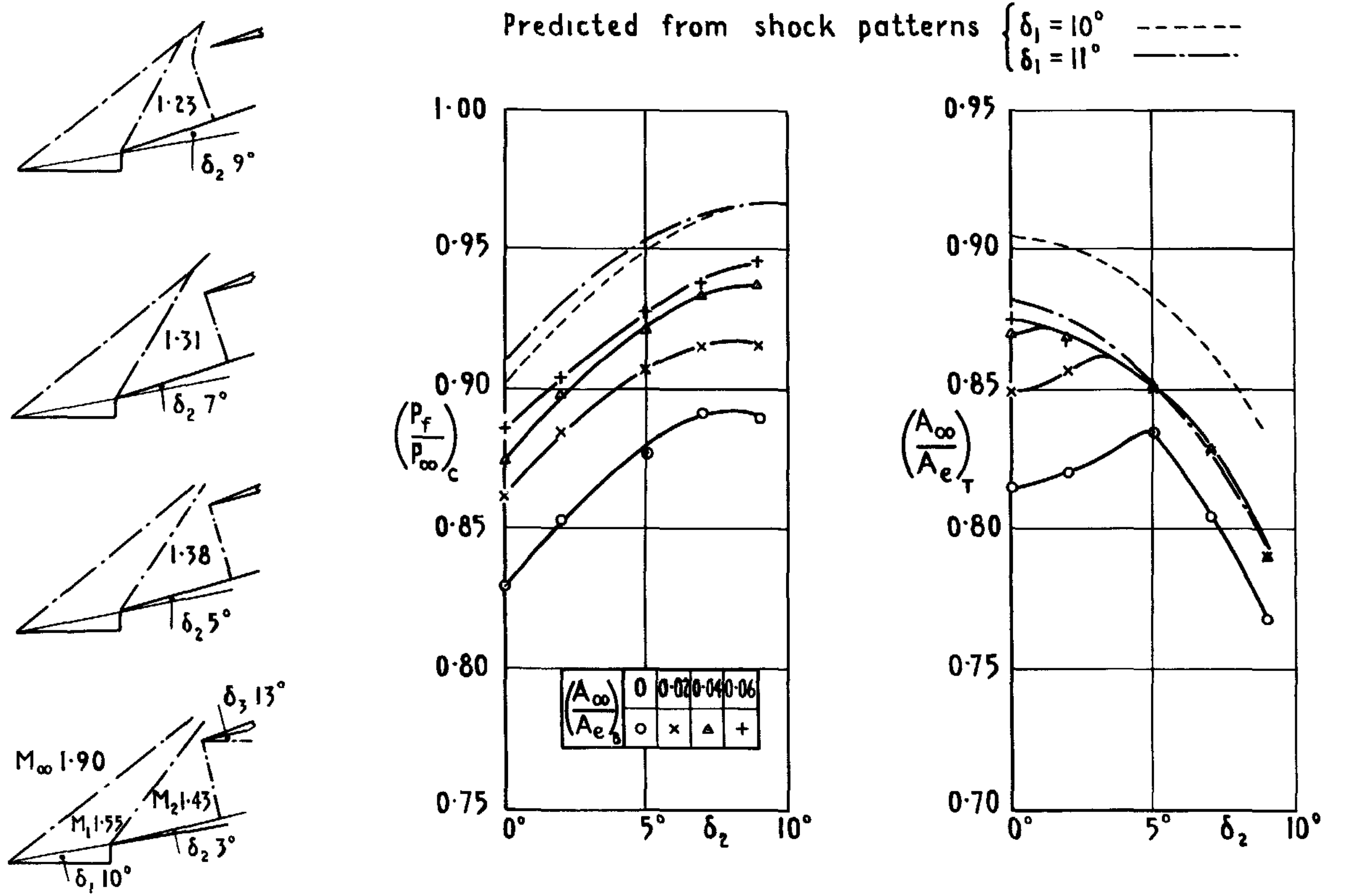

Fig 31 Variation of critical pressure recovery and maximum mass flow with δ_2 at constant bleed flow. M_∞ 1·90

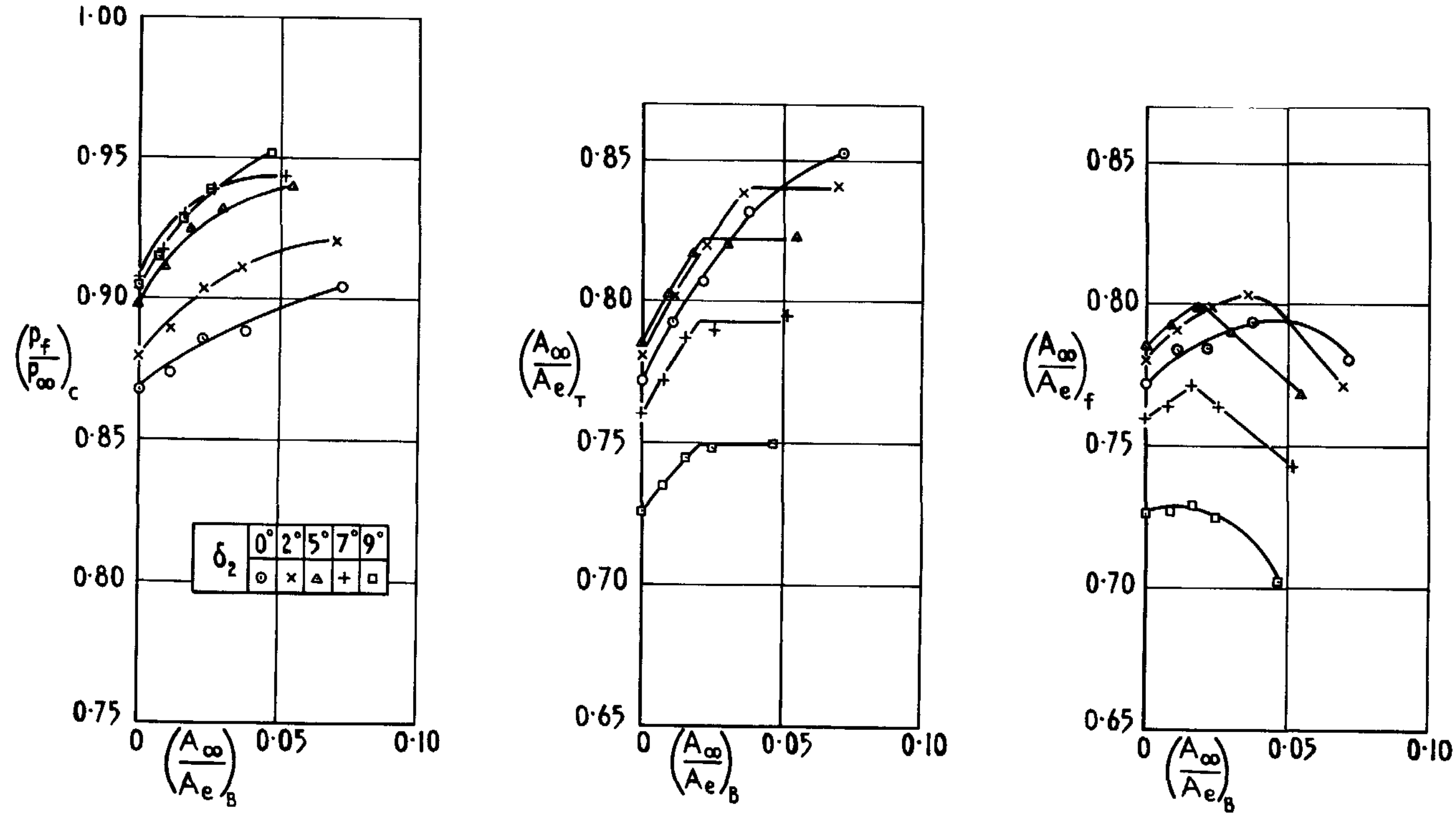

Fig 32 Effect of bleed on critical pressure recovery, total mass flow and mass flow at engine face. M_∞ 1·80

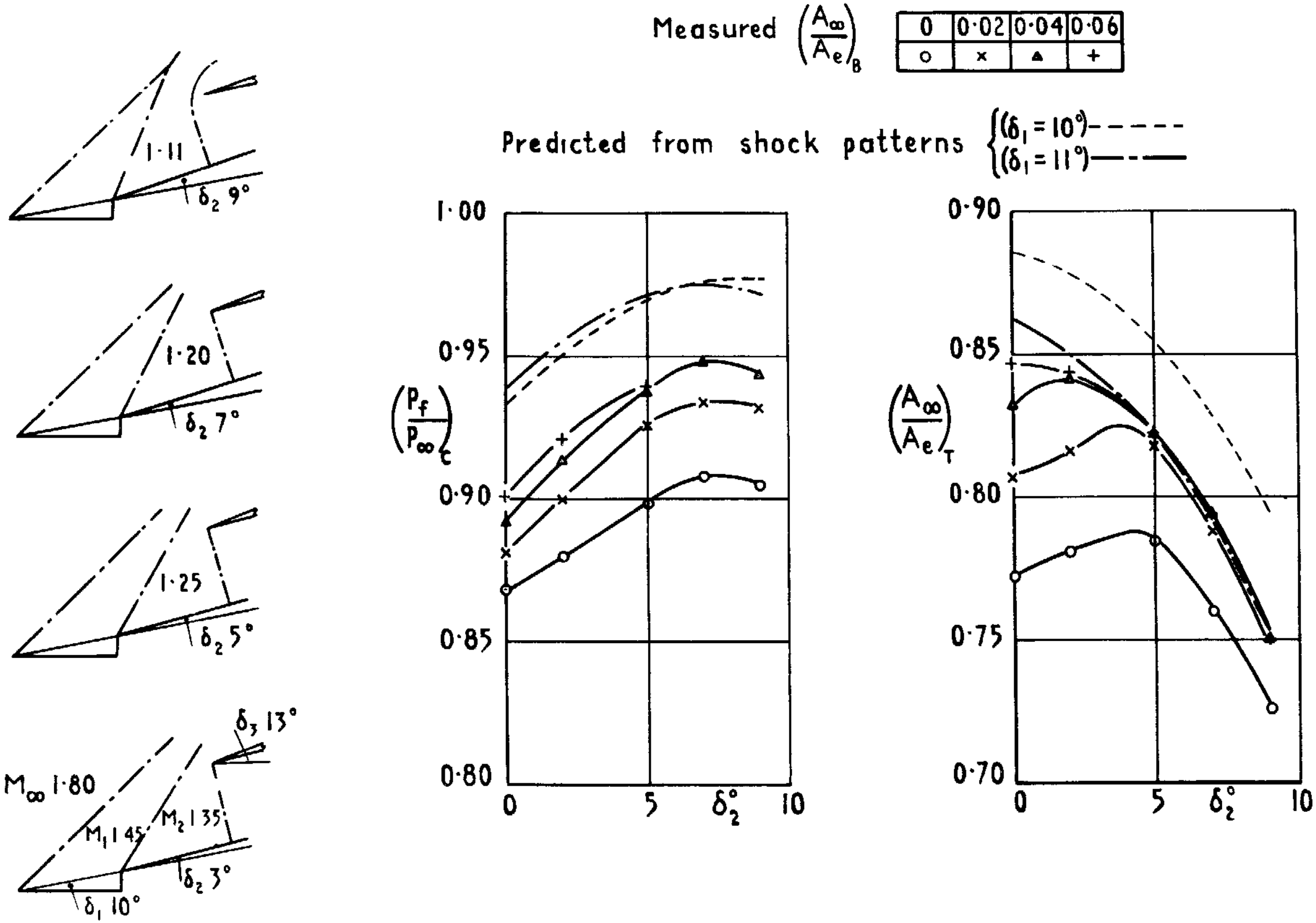

Fig 33 Variation of critical pressure recovery and maximum mass flow with δ_2 at constant bleed flow. M_∞ 1·80

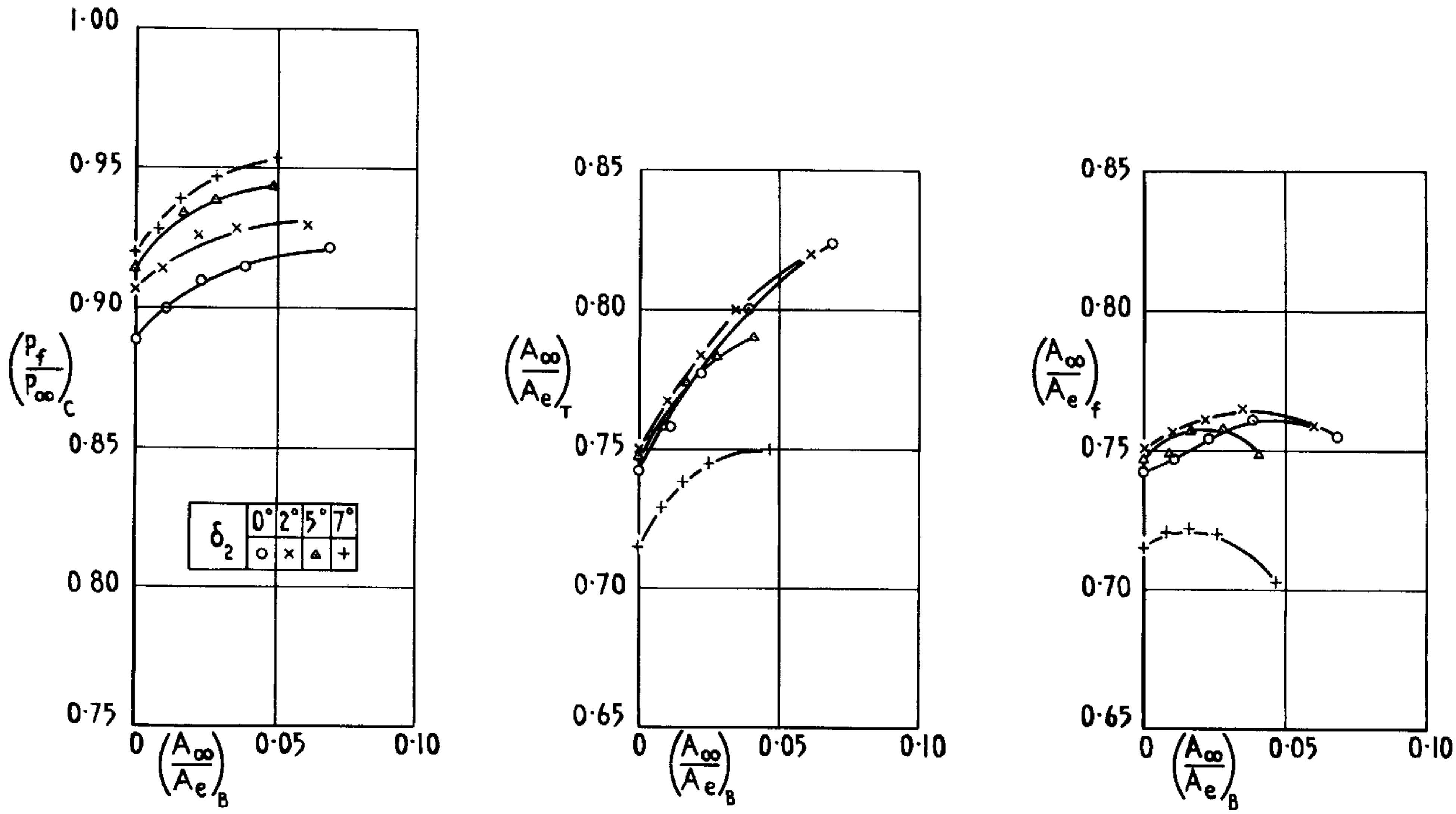

Fig.34 Effect of bleed on critical pressure recovery, total mass flow and mass flow at engine face. M_∞ 1·70

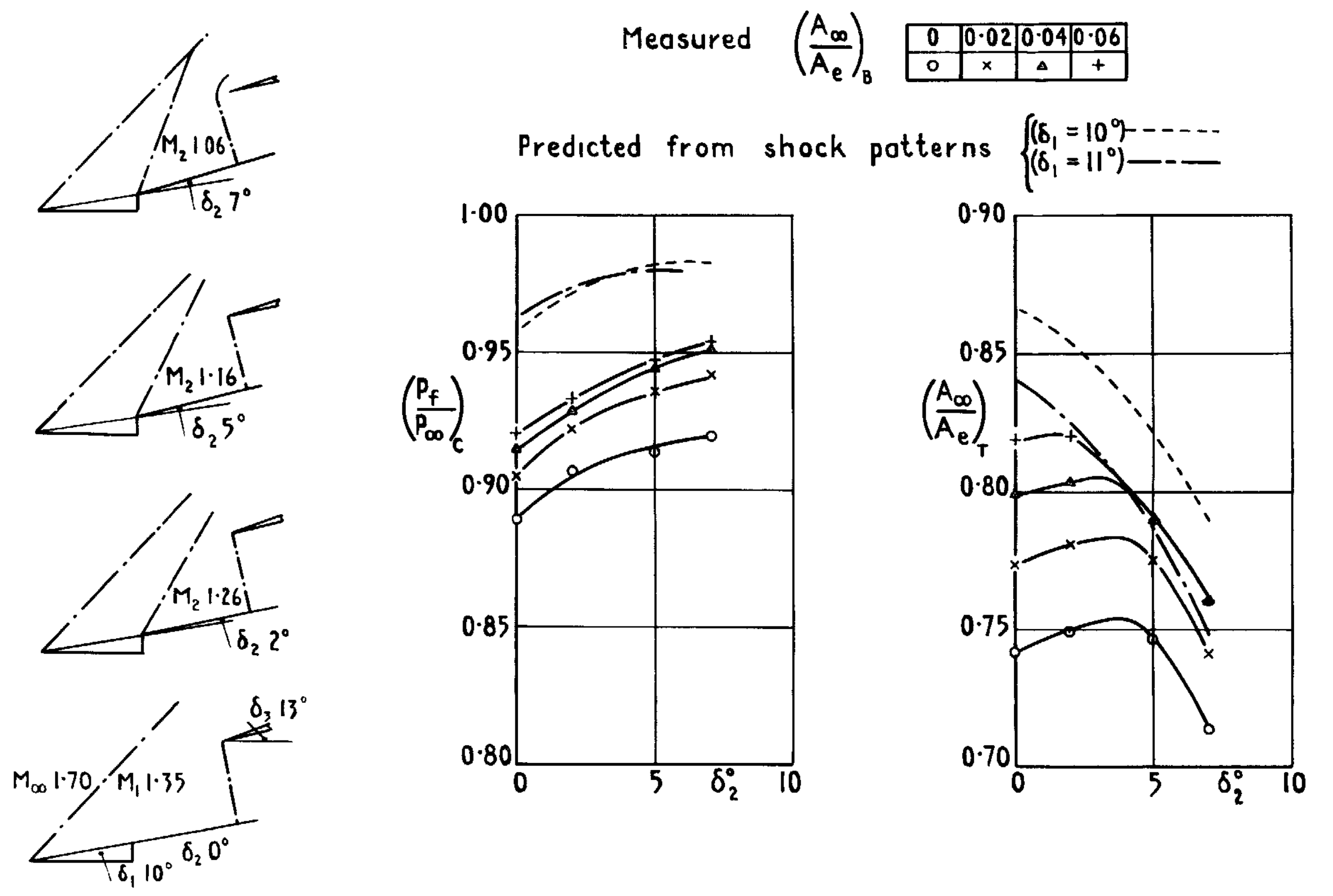

Fig. 35 Variation of critical pressure recovery and maximum mass flow with δ_2 at constant bleed flow. M_∞ 1·70

Curve A:- Ratio of minimum geometric internal area to A_l
Curve B:- Minimum internal contraction required for 'starting' with 0·98 full capture flow—B_1
0·96 full capture flow—B_2
0·94 full capture flow—B_3
Curve C:- Apparent internal contraction at zero bleed

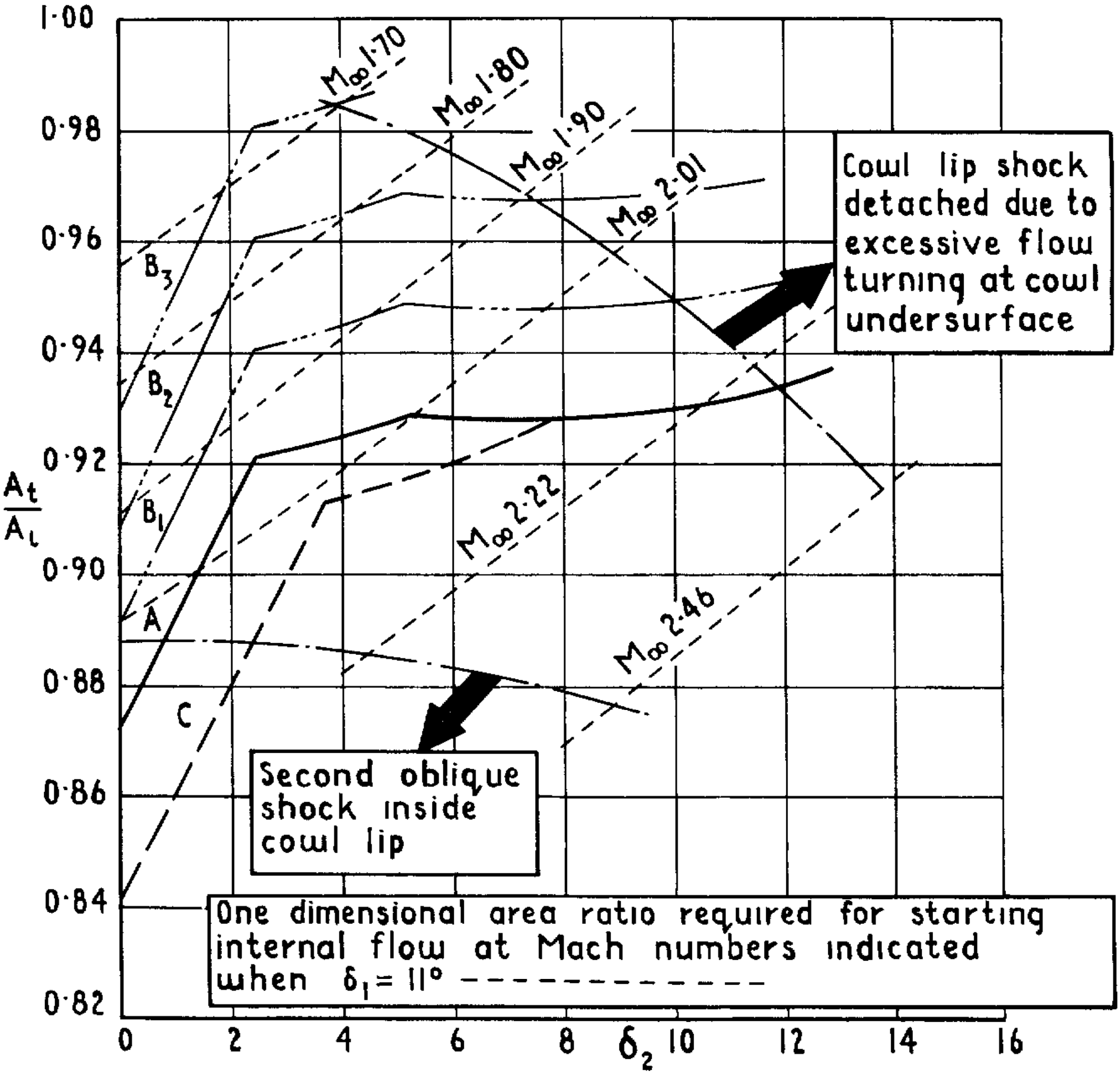

Fig 36 Comparison of the internal contraction of the intake with the one dimensional area ratio required for starting the internal flow

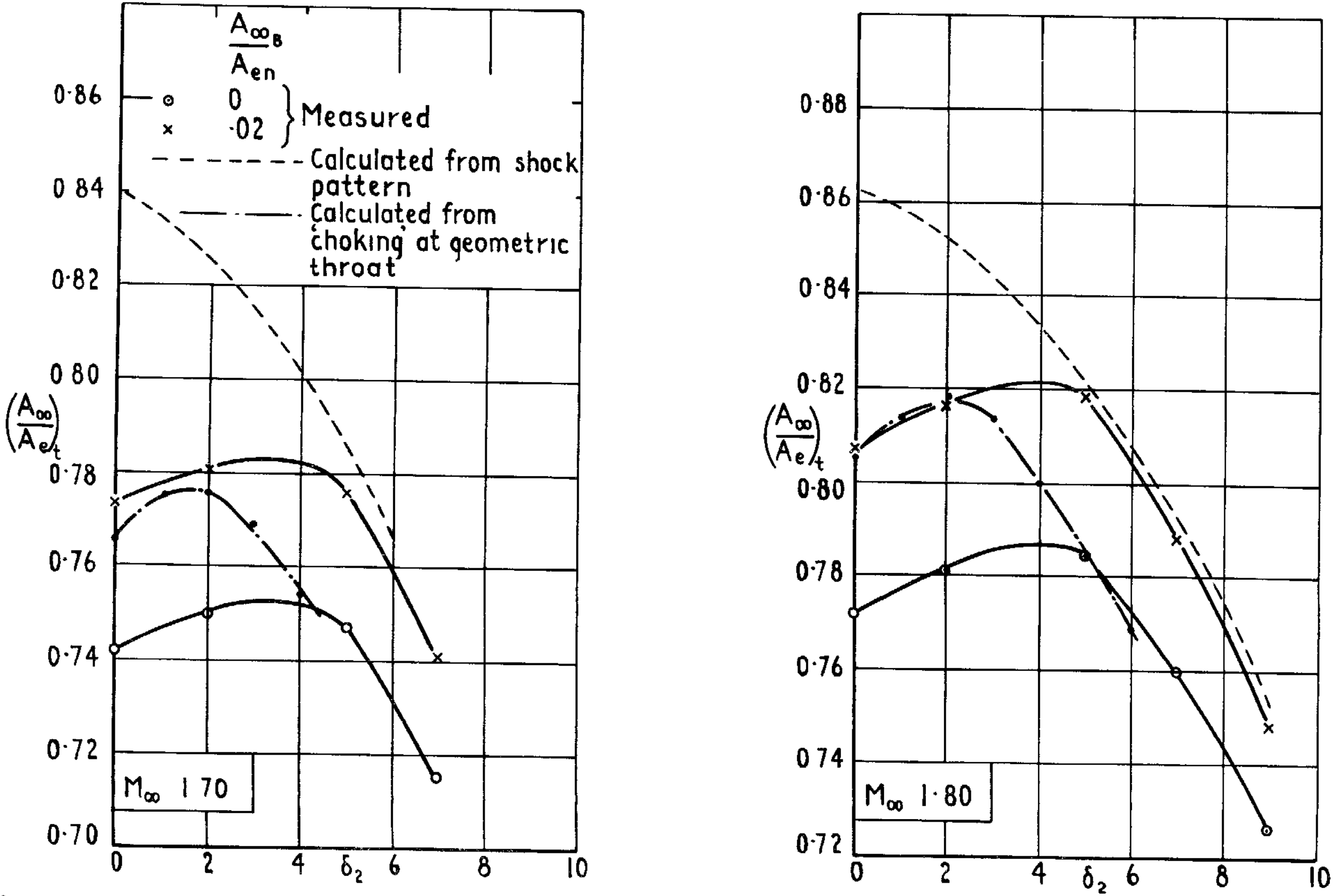

Fig 37a Comparison of measured and calculated mass flows M_∞ 1·70 and 1·80

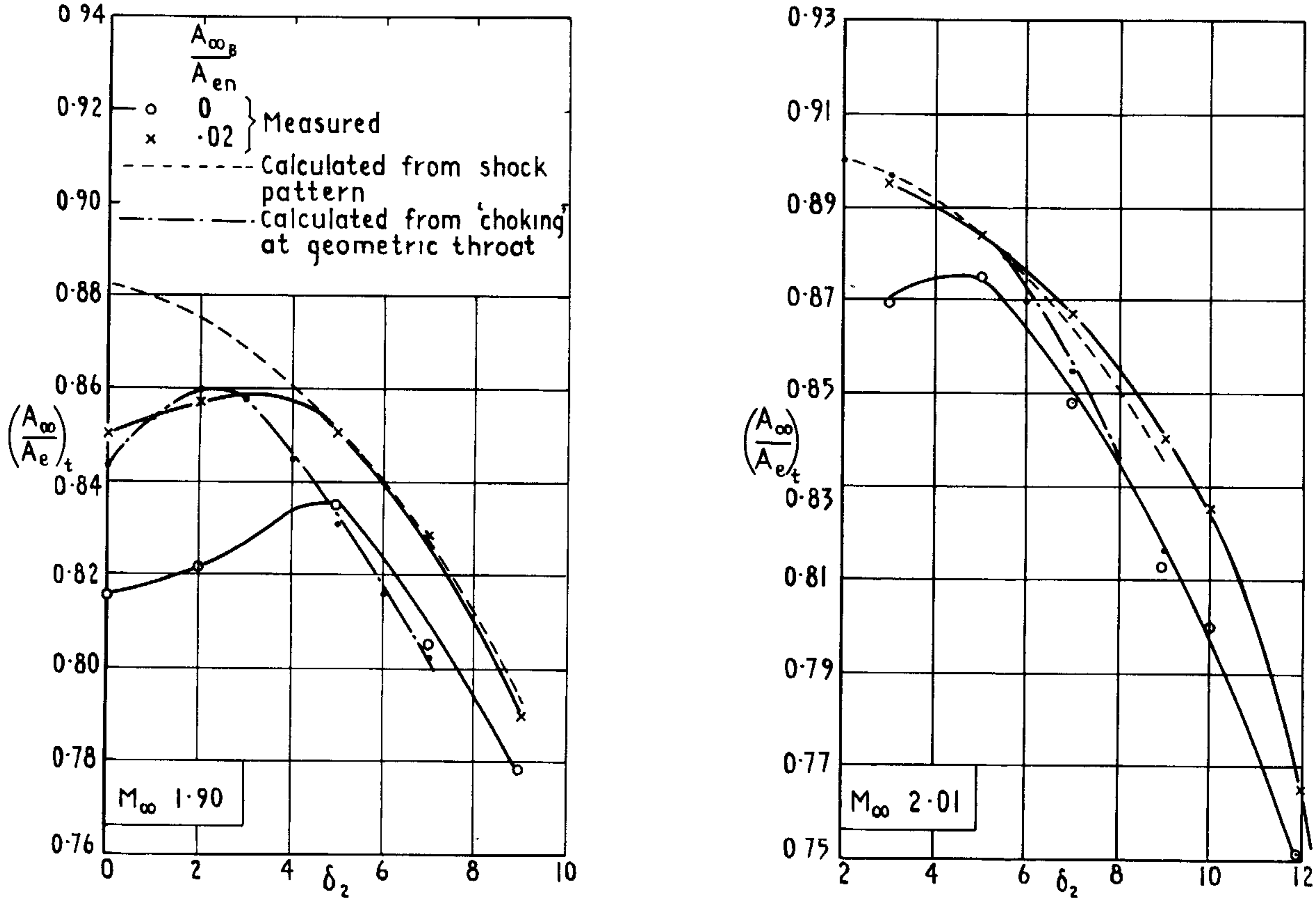

Fig.37b Comparison of measured and calculated mass flows M_∞ 1 90 and 2·01

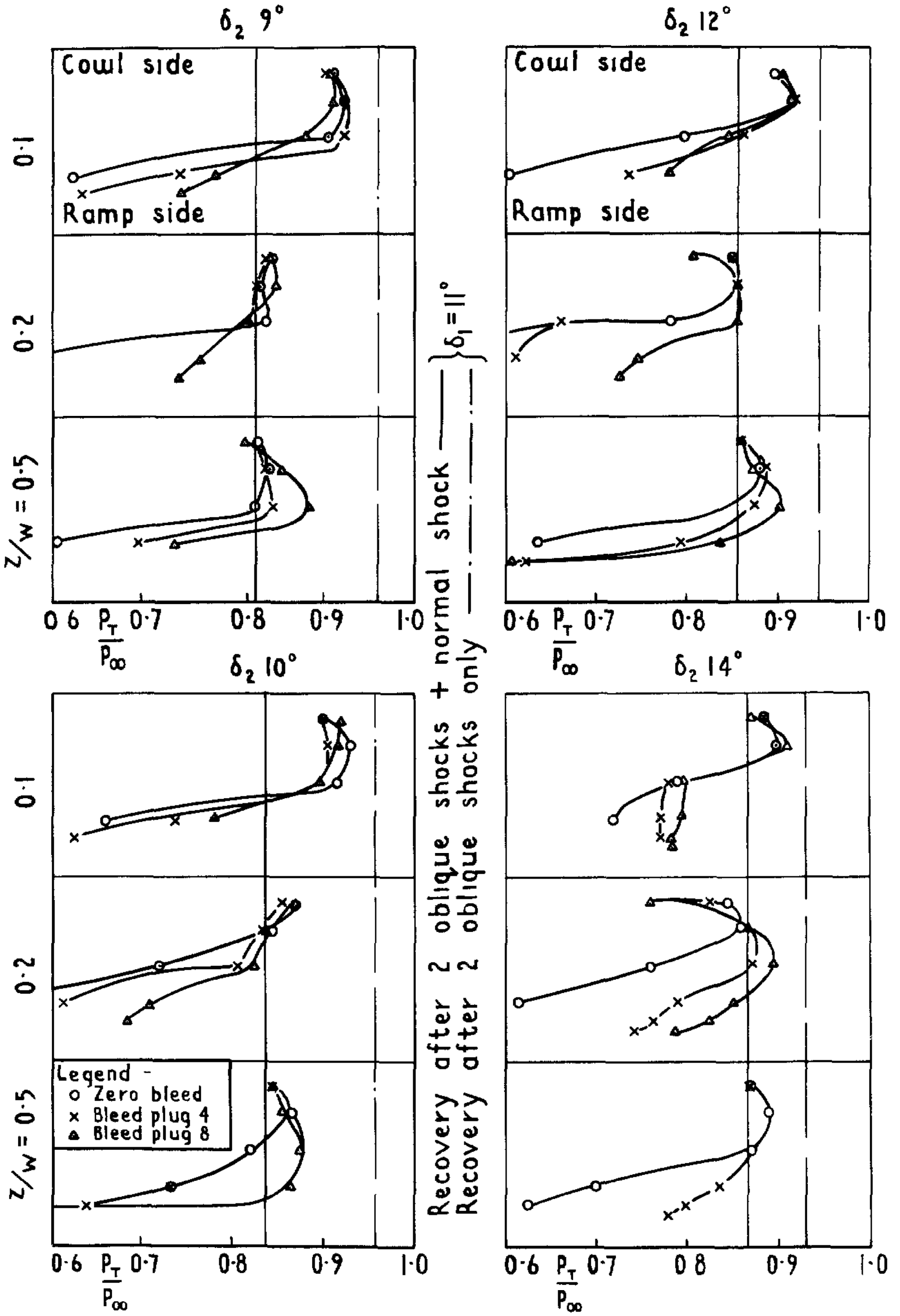

Fig 38 Pressure distribution at rear hinge position M_∞ 2 46

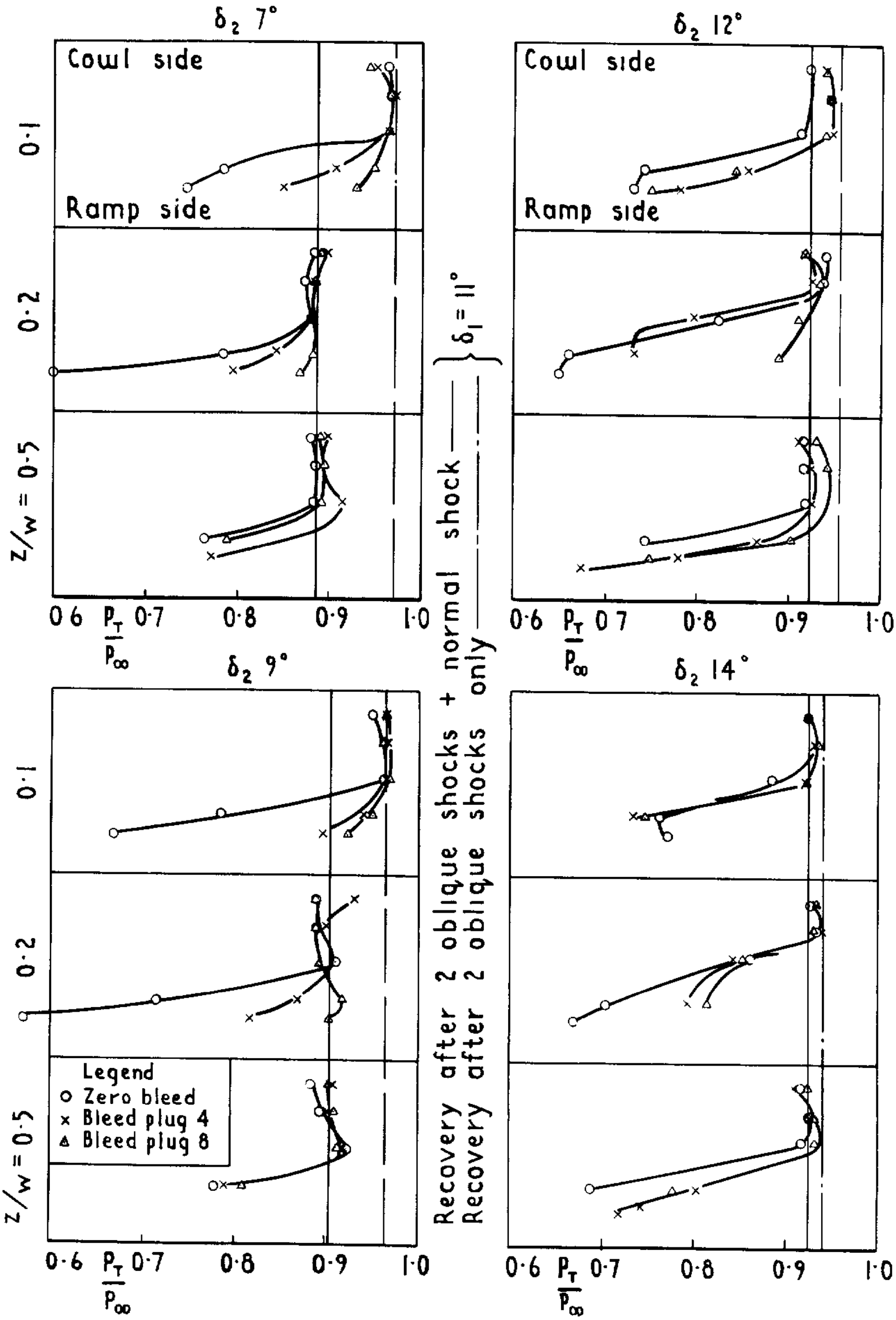

Fig 39 Pressure distribution at rear hinge position M_∞ 2·22

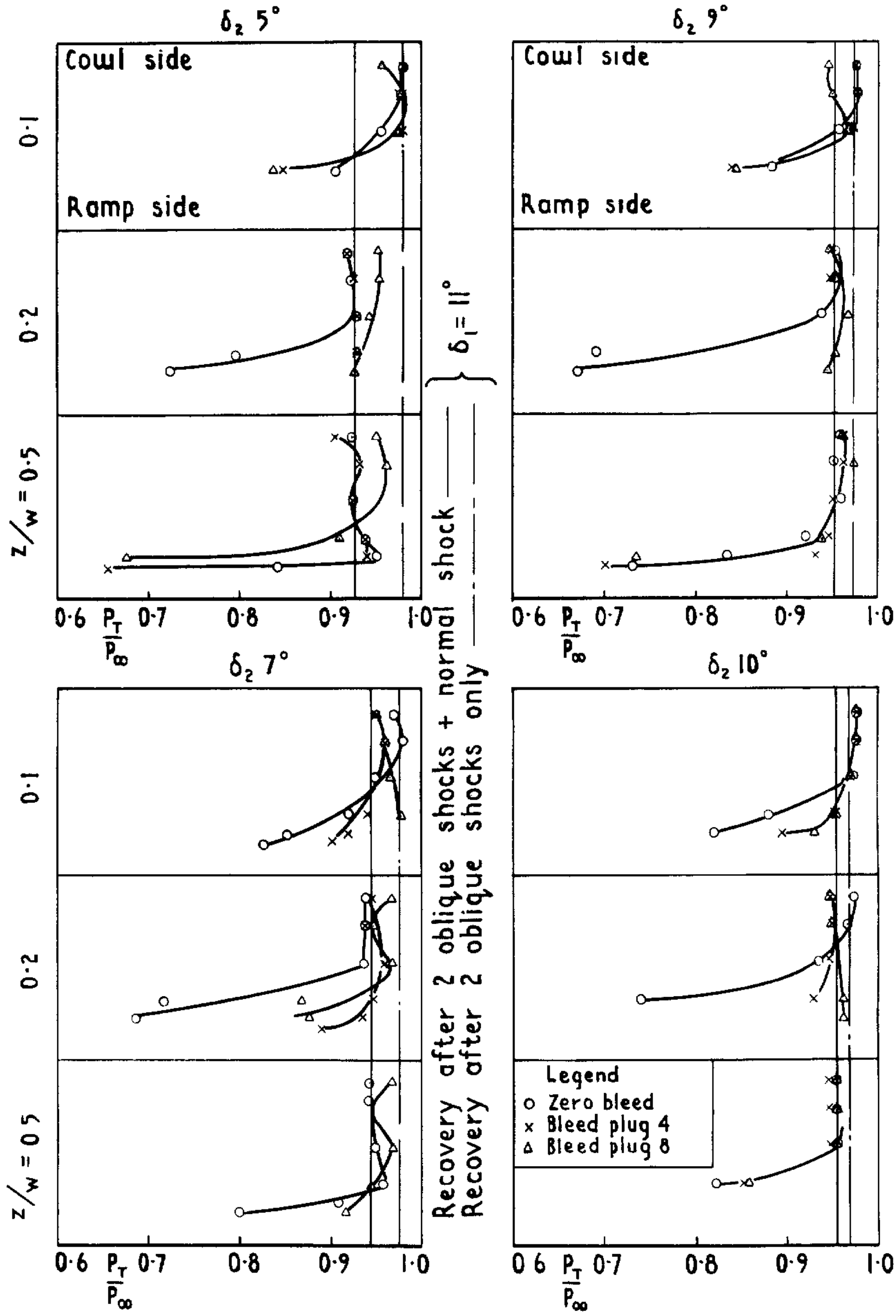

Fig. 40 Pressure distribution at rear hinge position M_∞ 2·01

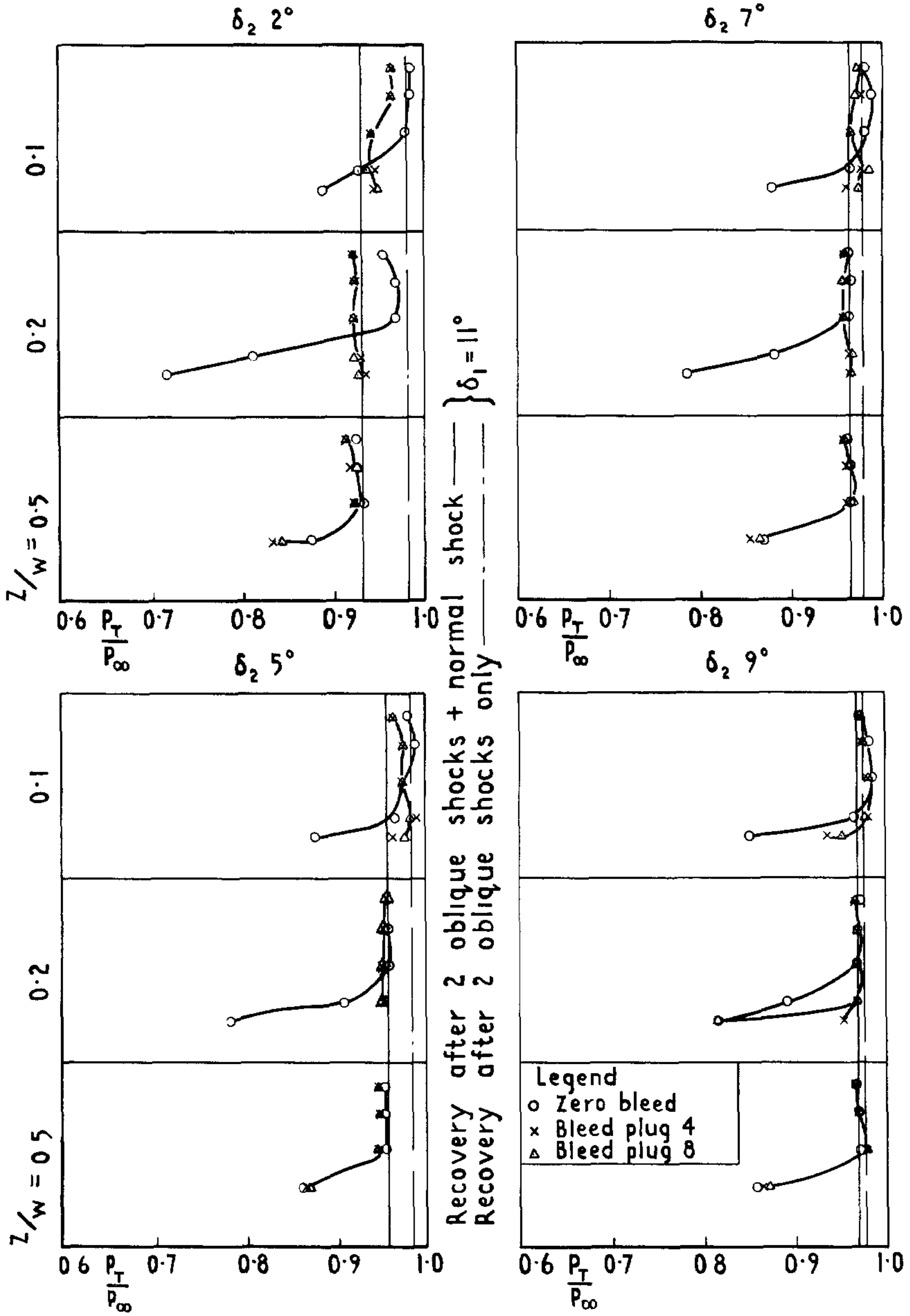

Fig.41 Pressure distribution at rear hinge position

M_∞ 1·90

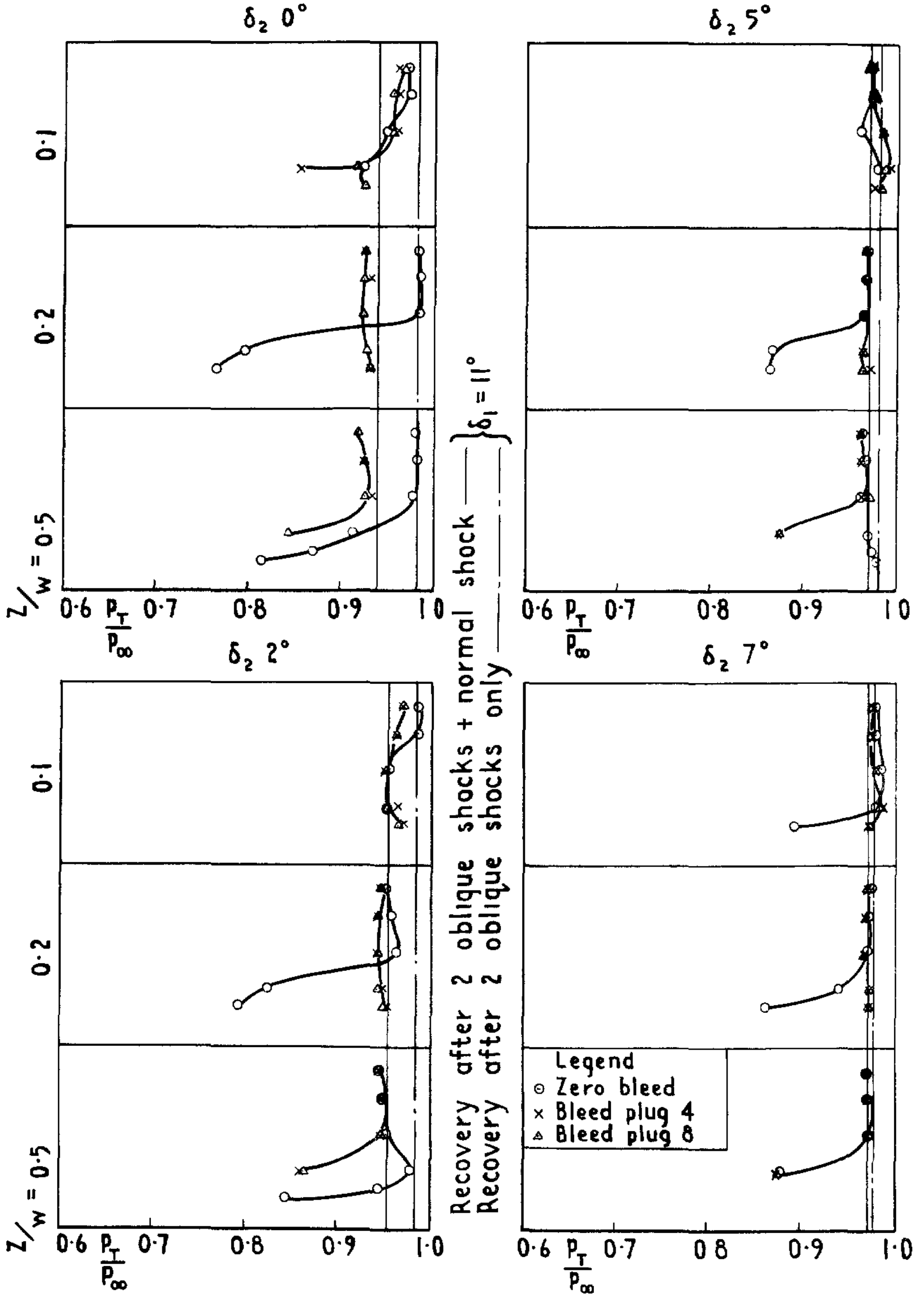

Fig.42 Pressure distribution at rear hinge position

M_∞ 1·80

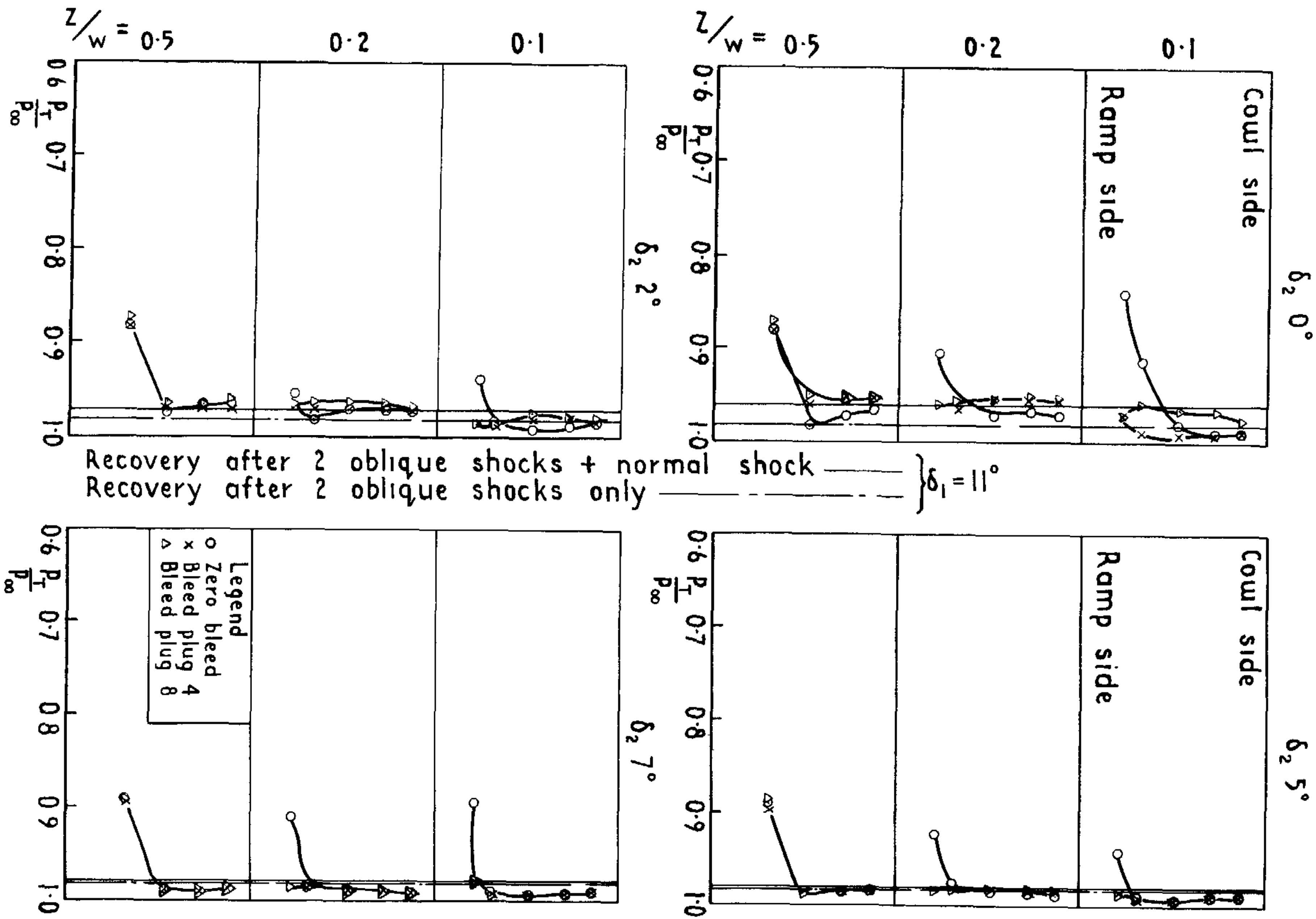

Fig.43 Pressure distribution at rear hinge position M_∞ 1·70

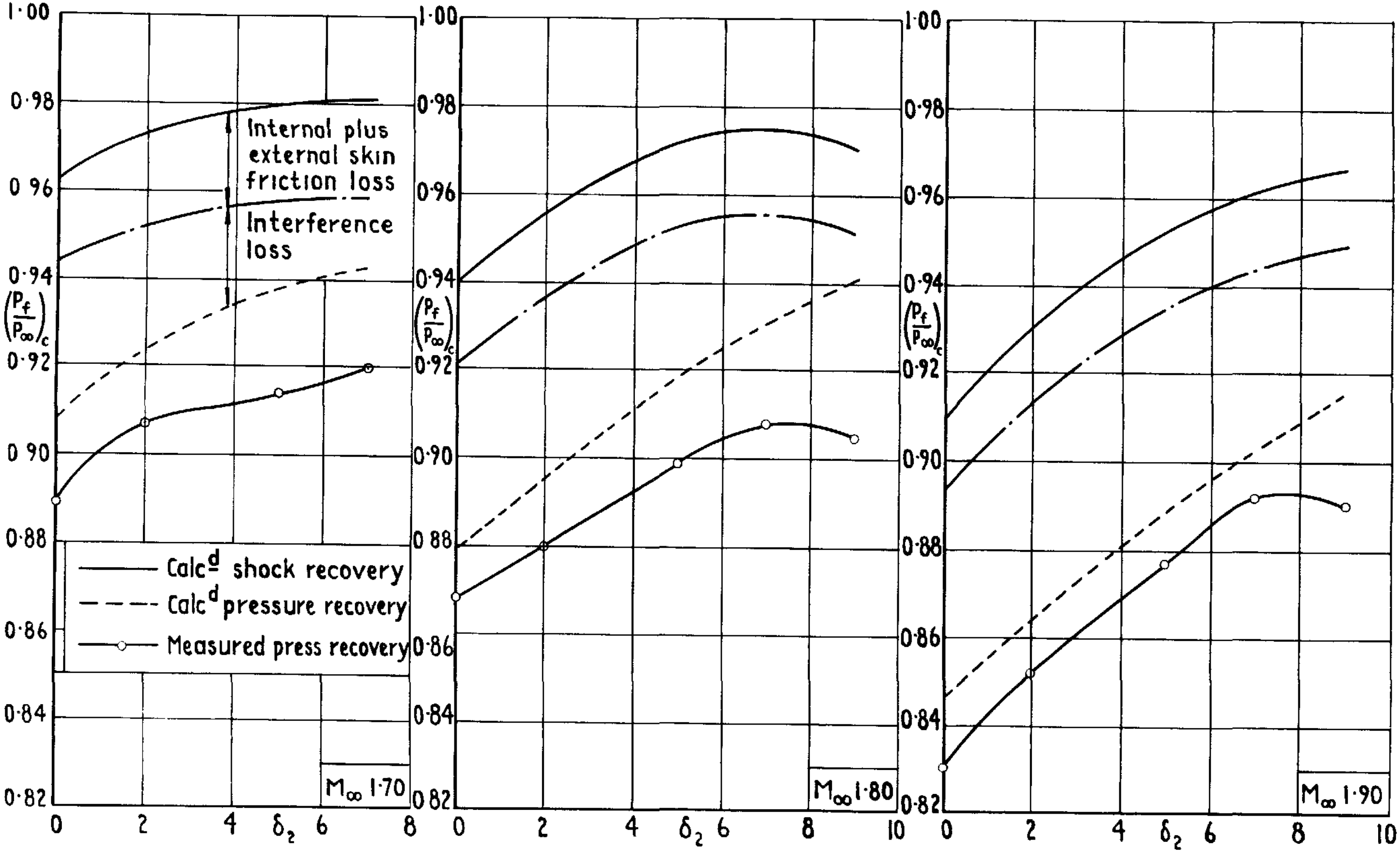

Fig 44a Comparison of measured and calculated pressure recovery at zero bleed flow

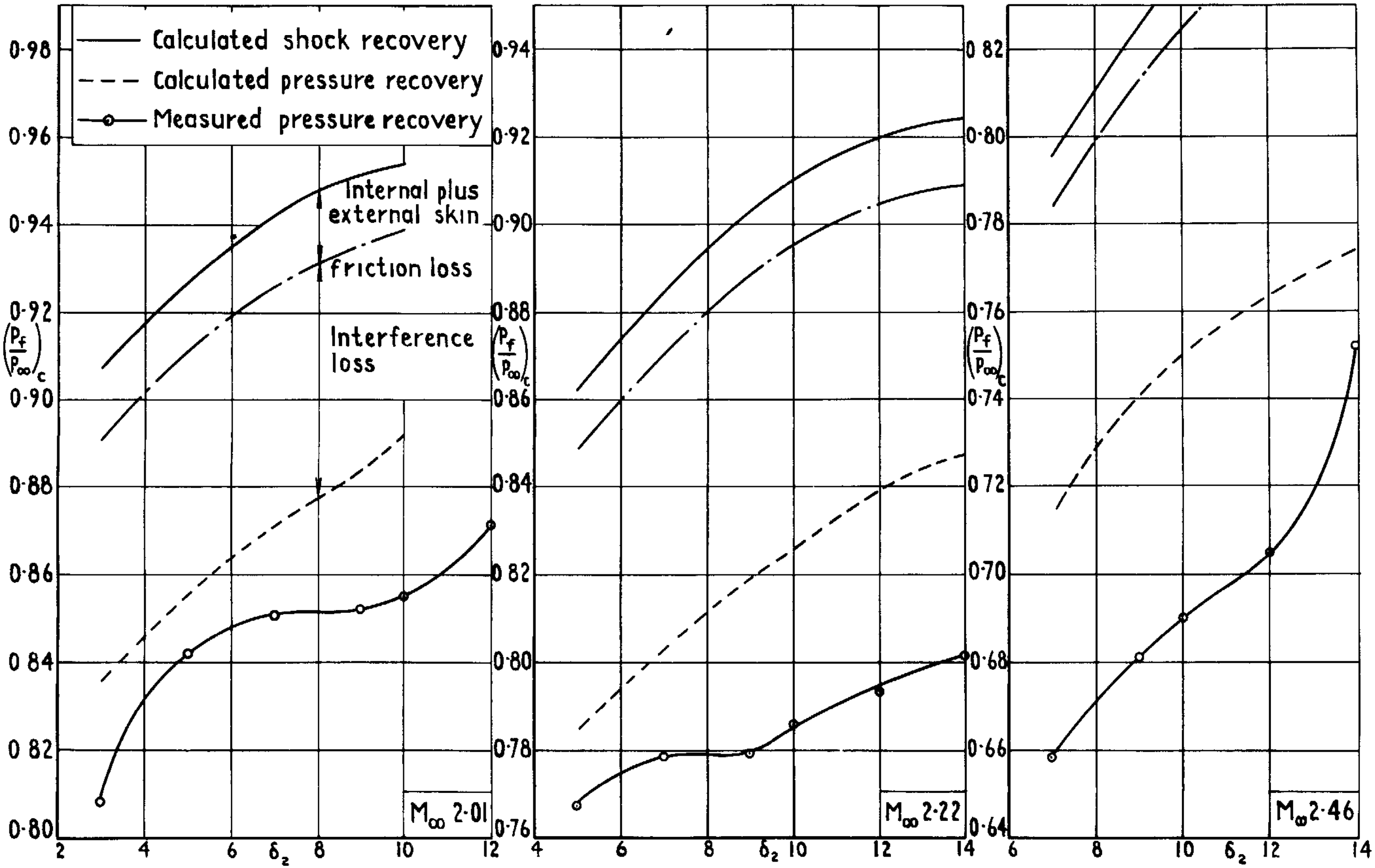

Fig. 44b Comparison of measured and calculated pressure recovery at zero bleed flow

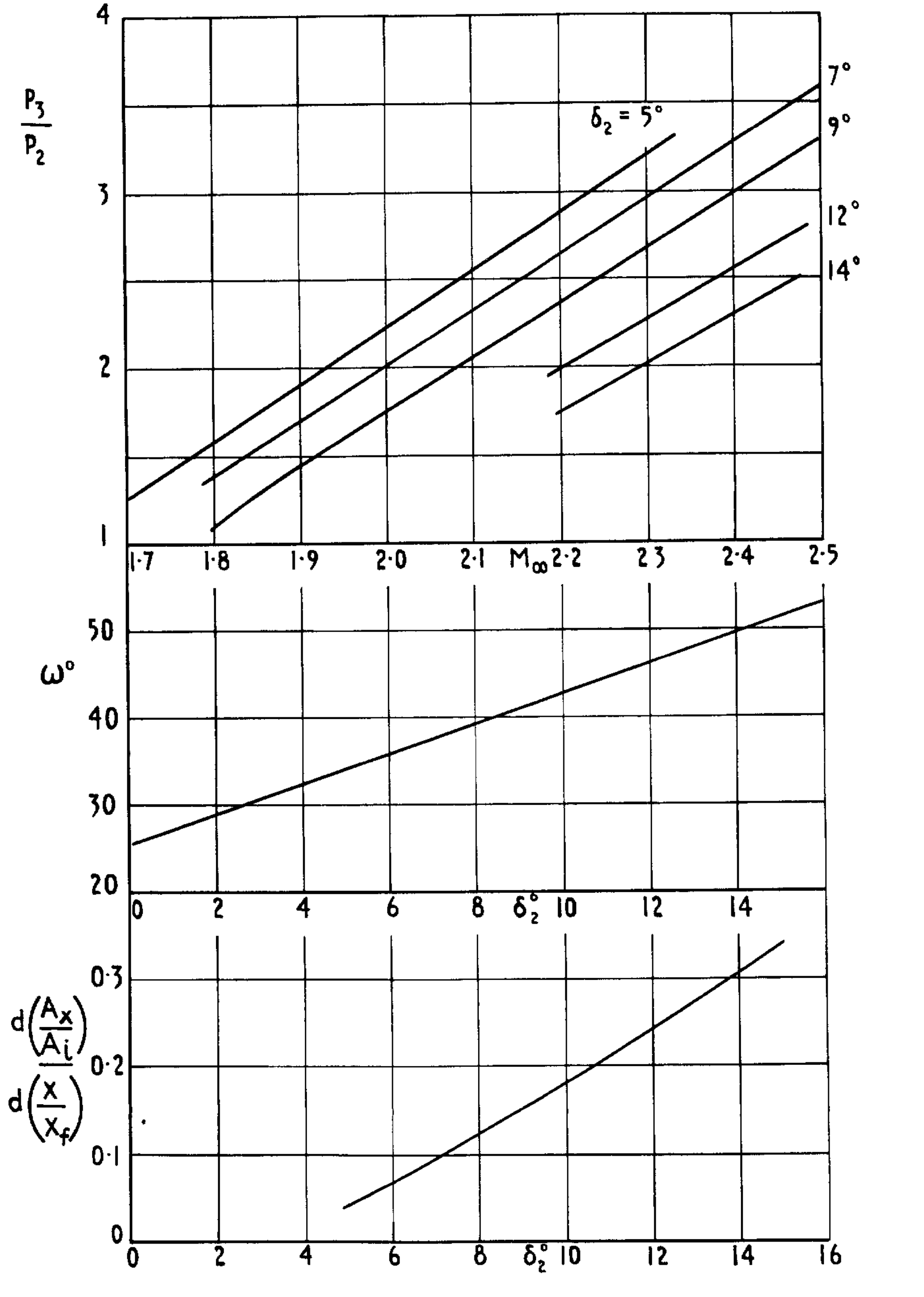

Fig.45 Variation of geometric and flow conditions with second ramp angle and free stream Mach number

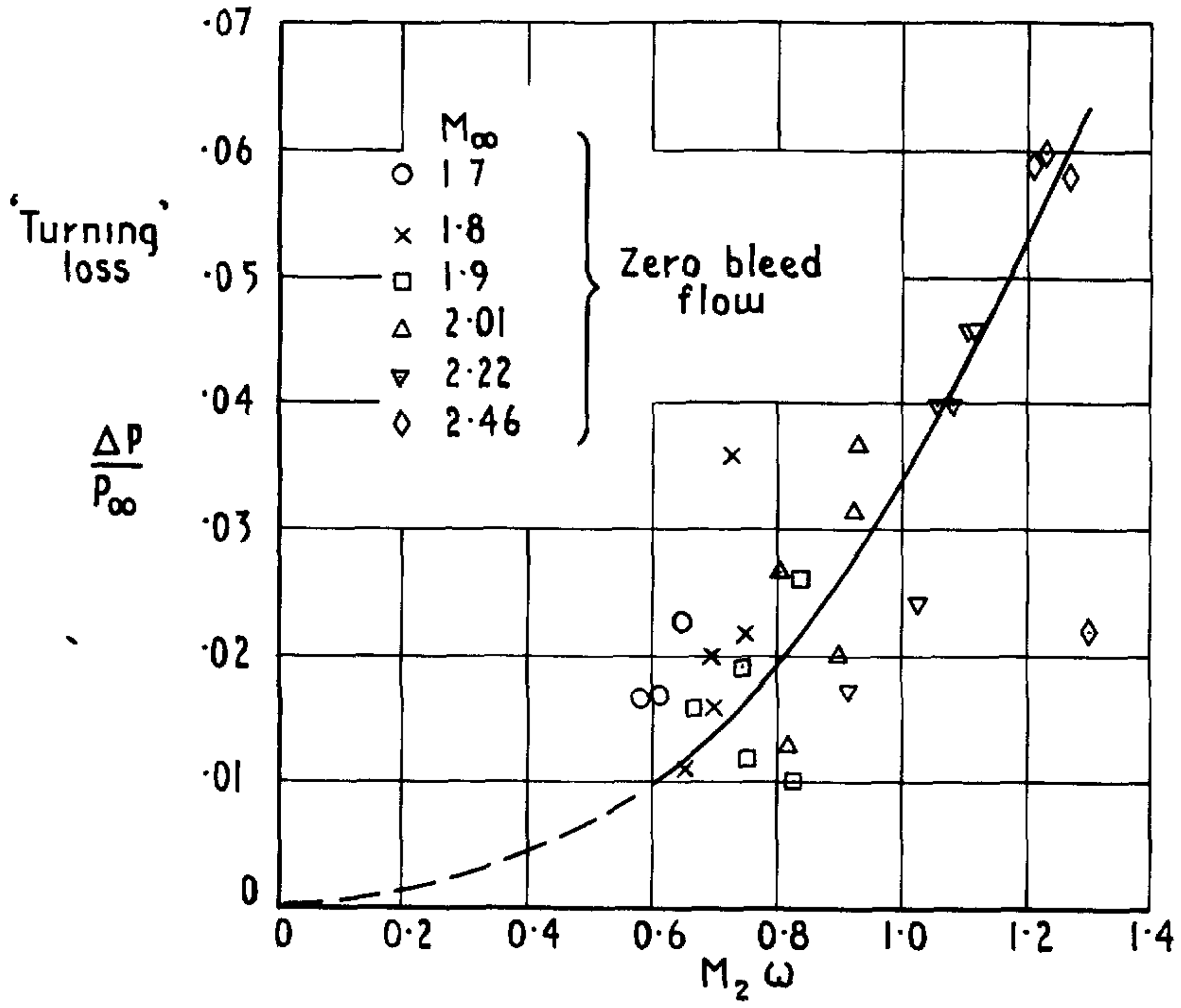

Fig. 46 Correlation of flow 'turning' loss with normal shock Mach number and angle between front and rear movable ramps

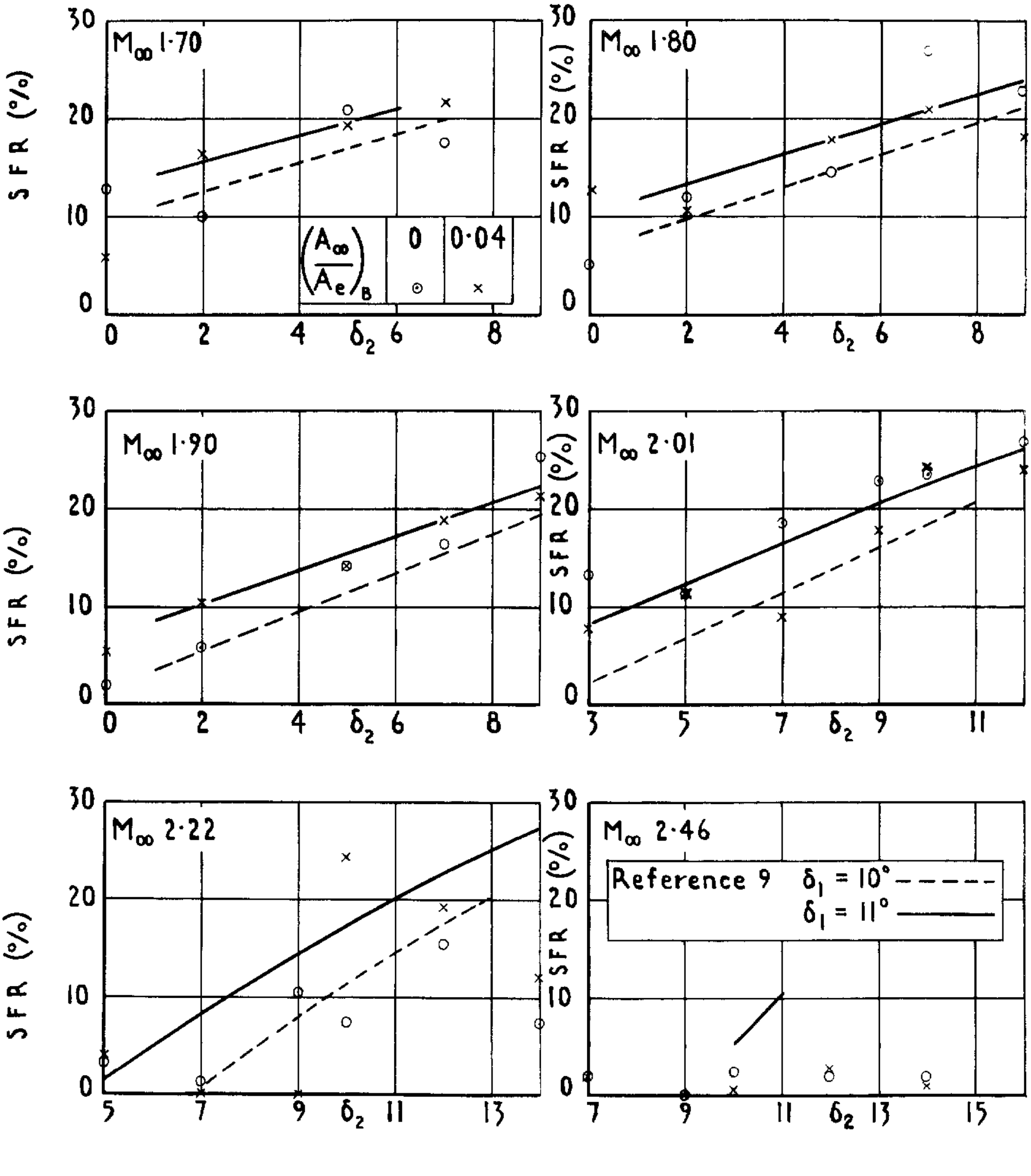

Fig 47 Variation of stable flow range with δ_2

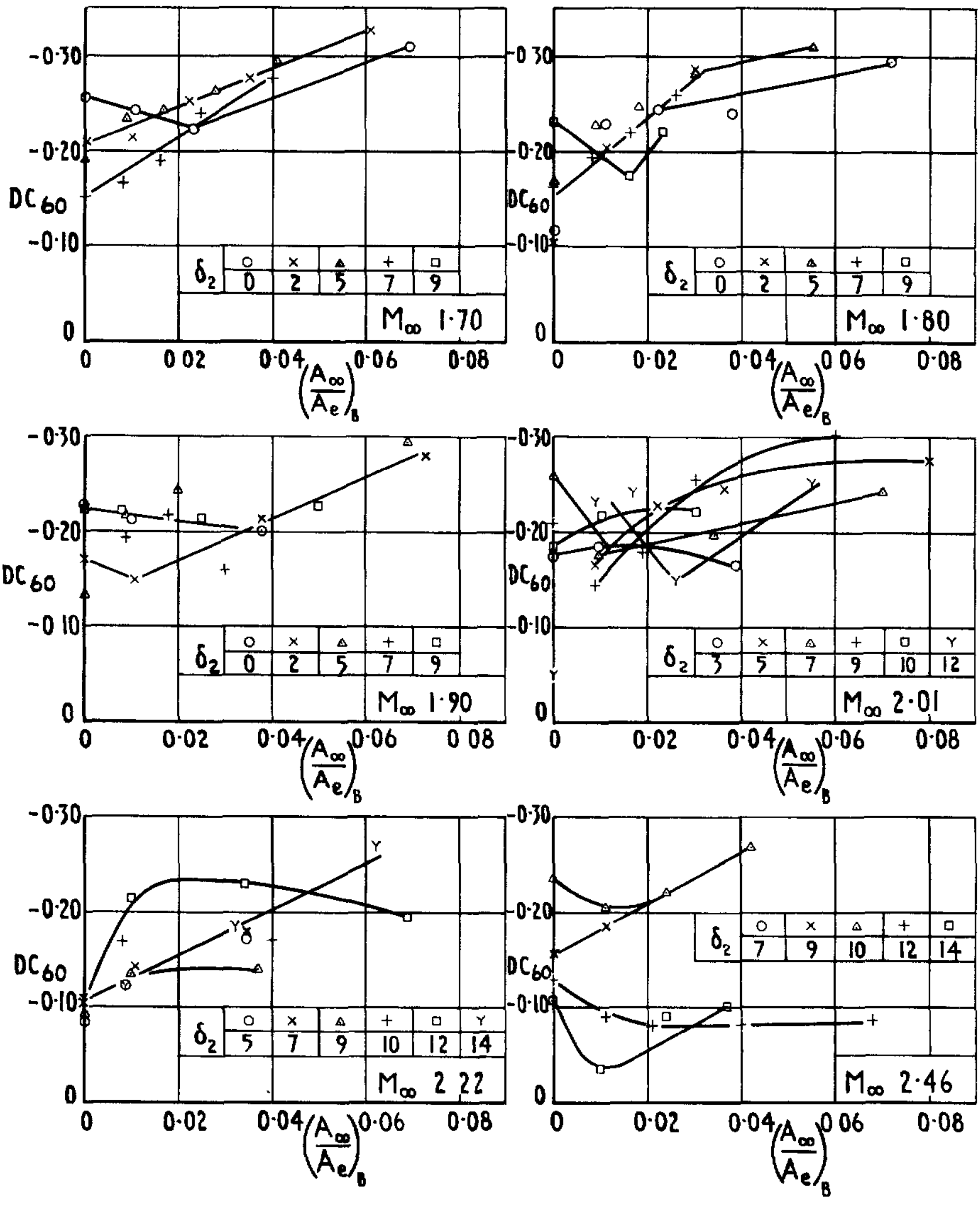

Fig.48 Effect of bleed on DC60 at critical point

Printed in England for Her Majesty's Stationery Office by the Royal Aircraft Establishment, Farnborough Dd 503427 K4 2/73

ARC CP No.1243
August 1971

533.697 2
533 6 015
533 6 011 5

Brown, C S
Goldsmith, E L

MEASUREMENT OF THE INTERNAL PERFORMANCE OF A RECTANGULAR AIR INTAKE WITH VARIABLE GEOMETRY AT MACH NUMBERS FROM 1 7 TO 2.5

Measurements have been made of the internal performance of a rectangular intake having variable geometry compression surfaces The measurements have been made over a range of Mach numbers from 1 70 to 2 46 The Reynolds number based on intake height was between 1.27 and 1 54 x 10^6 Pressure recoveries at zero bleed are well below those predicted from simple shock patterns, but there is a substantial gain with increase of bleed flow particularly at Mach numbers above 2 Subcritical stable flow range correlated quite well with the Ferri instability criterion

These abstract cards are inserted in Technical Reports for the convenience of Librarians and others who need to maintain an Information Index

Detached cards are subject to the same Security Regulations as the parent document, and a record of their location should be made on the inside of the back cover of the parent document

— Cut here —

ARC CP No 1243
August 1971

533 697 2
533 6 015
533 6 011 5

Brown, C.S
Goldsmith, E L

MEASUREMENT OF THE INTERNAL PERFORMANCE OF A RECTANGULAR AIR INTAKE WITH VARIABLE GEOMETRY AT MACH NUMBERS FROM 1 7 TO 2 5

Measurements have been made of the internal performance of a rectangular intake having variable geometry compression surfaces The measurements have been made over a range of Mach numbers from 1 70 to 2 46 The Reynolds number based on intake height was between 1 27 and 1 54 x 10^6 Pressure recoveries at zero bleed are well below those predicted from simple shock patterns, but there is a substantial gain with increase of bleed flow particularly at Mach numbers above 2 Subcritical stable flow range correlated quite well with the Ferri instability criterion

ARC CP No 1243
August 1971

533 697 2
533 6 015
533.6.011.5

Brown, C S
Goldsmith, E L

MEASUREMENT OF THE INTERNAL PERFORMANCE OF A RECTANGULAR AIR INTAKE WITH VARIABLE GEOMETRY AT MACH NUMBERS FROM 1 7 TO 2 5

Measurements have been made of the internal performance of a rectangular intake having variable geometry compression surfaces The measurements have been made over a range of Mach numbers from 1 70 to 2.46 The Reynolds number based on intake height was between 1 27 and 1 54 x 10^6 Pressure recoveries at zero bleed are well below those predicted from simple shock patterns, but there is a substantial gain with increase of bleed flow particularly at Mach numbers above 2 Subcritical stable flow range correlated quite well with the Ferri instability criterion

DETACHABLE ABSTRACT CARDS

— Cut here —

DETACHABLE ABSTRACT CARDS

C.P. No. 1243

Published by
HER MAJESTY'S STATIONERY OFFICE

To be purchased from
49 High Holborn, London WC1 V 6HB
13a Castle Street, Edinburgh EH2 3AR
109 St Mary Street, Cardiff CF1 1JW
Brazennose Street, Manchester M60 8AS
50 Fairfax Street, Bristol BS1 3DE
258 Broad Street, Birmingham B1 2HE
80 Chichester Street, Belfast BT1 4JY
or through booksellers

C.P. No. 1243

SBN 11 470801 0